Republic of Iraq
Ministry of Higher Education
and Scientific Research
University of Babylon
College of Engineering
Mechanical Engineering Department

FREE CONVETION HEAT TRANSFER FOR NON-NEWTONIAN FLUID IN RECTANGULAR ENCLOSURE CONTAINING A HOT OBSTACLE

A Thesis

Submitted to the College of Engineering, University of Babylon Partially fulfilling the requirements for the degree of Master in Engineering \Mechanical Engineerin \Power

By

Zainab Mahdi Agool Hassan

Supervised by

Asst. Prof. Dr. Rafel Hekmat Hameed

2021 A.D. *1442 A.H*

بِسْمِ اللَّهِ الرَّحْمَٰنِ الرَّحِيمِ

وَوَهَبْنَا لَهُمْ مِنْ رَحْمَتِنَا وَجَعَلْنَا لَهُمْ لِسَانَ صِدْقٍ عَلِيًّا

صدق الله العلي العظيم

سورة مريم آية ﴿50﴾

Certification

I certify that this thesis titled "FREE CONVETION HEAT TRANSFER FOR NON-NEWTONIAN FLUID IN RECTANGULAR ENCLOSURE CONTAINING A HOT OBSTACLE" was Prepared by Mrs. ***Zainab Mahdi Agool*** under my supervision at the University of Babylon as partial fulfillment of the requirements for the degree of Master of Science in Mechanical Engineering (Power Mechanics).

I recommend that this thesis be forwarded for examination in accordance with the regulation of the University of Babylon.

Signature

Asst. prof. Dr. Rafel Hekmat Hameed

Department of Mechanical Engineering

College of Engineering

University of Babylon

Data: / / 2021

Dedication

To those who gave me support, inspiration, courage,
and strength

Especially

My Dear Parents
Father and Mother

My dear husband, who accompanied me step by step
Ali
My children
Sara, Zaid and Hussain

My sisters and brothers

Zainab Mahdi

2021

Acknowledgements

No project can be fully accomplished without thanking those who made it possible. First and foremost, I thank God for my place and for giving me the strength to go on.

I would like to express my deepest appreciation to my supervisor Asst. prof. Dr. Rafel Hekmat Hameed for her dedicated sharing, assistance, and guidance that helped me while researching and writing this thesis, I could not have done without her help.

I would like to take this opportunity to thank the staff of the Mechanical Engineering Department at Babylon University for their support.

Much thanks and gratitude goes out to all my friends for their help during this work.

Lastly but first in mind, I would like to express my gratitude to my family for their unconditional love and support.

I am also grateful to everyone who directly or indirectly helped me complete this work.

Zainab Mahdi

2021

Abstract

In the present work, the experimental and numerical realization has been achieved to study the heat transfer by natural convection in an enclosure with a hot obstacle at the base wall filled with non- Newtonian fluid.

Carboxymethylcellulose CMC with distilled water was used as a non-Newtonian fluid with a three-volume concentration of [1%, 0.5%, and 0%]. The power-law index values for the three concentrations are 0.59,0.72, and 1, respectively. Two values are used for aspect ratios AR, 0.75 and 0.5. Also, two shapes of hot obstacles are used cylindrical and cuboid. The value of the Rayleigh number for the base fluid where AR is 0.75 are 8.73E+06 ≤ Ra ≤ 4.36E+07, and when the value of AR is 0.5 are 2.36E+08 ≤ Ra ≤ 9.76E+08. Twenty four of thermocouples are used to measure the temperature of the working fluid inside the enclosure at different places of the hot and cold walls of the enclosure at the two values of AR 0.75 and 0.5.

Theoretical work was represented by using the CFD COMSOL program in 3-D to predict the fluid temperature distribution inside the enclosure.

Temperature measured from the experimental work was analyzed to calculate Rayleiegh number (Ra), Prandtl number (Pr), convective heat transfer coefficient (h), and Nusselt number (Nu). The value of $\overline{Nu}$ increases with increasing the concentration of the CMC and the Rayleigh number, which is affected by the properties of the fluid and the hot temperature of the obstacle, as well as the aspect ratio. The Nusselt number improves from 40.46% at n =1 to 50.79% at n =0.59, which means that the heat transfer improves by decreasing the value of the power-law index for non-Newtonian fluid.

The experimental work agreed well with the theoretical work with a mean deviation of about 8.9 %.

Nomenclature

Symbols	Notations	Units
h	heat transfer coefficient	$W/m^2.K$
$\overline{Nu}$	Nusselt number	-
T	temperature	◦C
q	heat flux	W/m^2
A	surface area	m^2
cp	heat capacity	J/ kg. K
k	thermal conductivity	W/ m. K
g	gravity acceleration	m/s^2
Gr	Grashof number	-
Ra	Rayleigh number	-
Pr	Prandtl number	-
AR	aspect ratio	-
L	the characteristic length which length between hot and cold walls	m
H	height of the enclosure	m
u, v, w	velocity components in the x- ,y- and z-direction, respectively	m/s
n	a dimensionless constant called the power-law index	
m	the consistency factor, which is an indicator of the degree of the fluid viscosity.	

T_{calib}	calibrated temperature value	^oC
T_{re}	temperature recorded by the temperature recorder	^oC
Q_{calib}	calibrated discharge value,	L/min
Q_{re}	the flow meter measurement	L/min

Greek letters

Symbols	**Notations**	**Units**
μ	dynamic viscosity	kg/m. s
μ_O	zero shear viscosity	kg/m.s
μ_∞	infinite shear viscosity	kg/m.s
β	thermal expansively	K^{-1}
ρ	density	kg/m^3
$\dot{\gamma}$	shear rate	1/s
τ	shear stress	Pa
α	thermal diffusivity	m^2/s

Subscribes

h	hot
c	cold
f	fluid

Abbreviations

CFD	Computational Fluid Dynamic
CMC	Carboxymethylcellulose
CPV	Concentrating photovoltaic

Contents

CHAPTER ONE

INTRODUCTION

Introduction

1.1 Natural Convection in Enclosures

Natural convection is a heat transport mechanism in which the fluid motion is generated by the buoyancy force arising from the change in the density of the fluid due to the rise in the temperature rather than by any external source (like a pump, fan, suction device, etc.) [1]. The laminar boundary layer development on a heated vertical plate in figure (1.1) can be taken as a classic example of buoyant flow induced by the temperature difference between a fluid and a surface immersed in it.

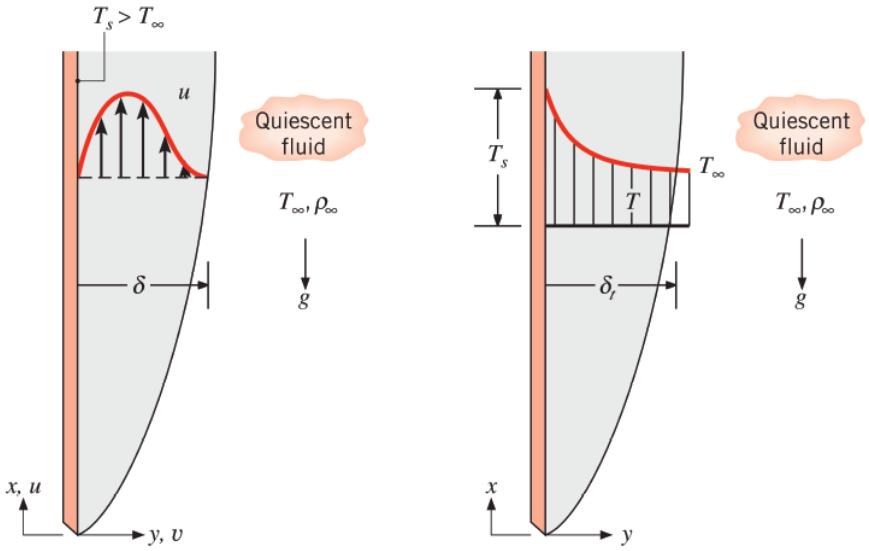

(a)velocity boundary layer ***(b)thermal boundary layer***

Figure (1- 1) laminar boundary layer development on a heated vertical plate [1].

As it can be seen from the figure (1-1), the thickness of the velocity boundary layer increases in the vertical direction where the fluid velocity increases as the normal distance from the surface increases, eventually reaching a maximum value within the boundary layer, then gradually decreases to zero again. Accordingly, the temperature of the fluid in the

vicinity of the surface increases due to heat transfer from the plate to the fluid. Consequently, the warmer fluid in the vicinity of the surface moves upwards along the vertical plate under the action of buoyancy forces arising from density variation of the fluid in response to temperature change.

Natural convection can be subdivided into two major categories. The first category deals with buoyant flows induced by temperature differences between a fluid and a surface immersed in it, which is called the external natural convection as shown in figure (1-1). The second category deals with buoyant flows which occur inside enclosures confined by surfaces at different temperatures and this category is referred to as the internal natural convection.

1.1.1 Differentially heated side walls configuration

Natural convection in containers with the sidewalls that are differentially heated is one of the most extensively analyzed natural convection problem. Classical examples of two-dimensional rectangular enclosures are shown schematically in figure (1-2) where the vertical walls of rectangular enclosures are kept at various temperatures, while the other walls are adiabatic, as illustrated by Yigit [2].

The fluid flow generated by the buoyancy force inside the enclosure is usually a recirculating vertical motion in the core region, in addition to the boundary layers on the top of the no-slip impenetrable walls see figure (1-2a). This type of natural convection in the rectangular enclosures has two characteristic dimensions, H is an enclosure height and L is an enclosure width (length between hot and cold walls). The enclosure is referred to as shallow when the aspect ratio ($AR = L/H$) is smaller than unity, while it is termed as a tall enclosure for AR greater than unity.

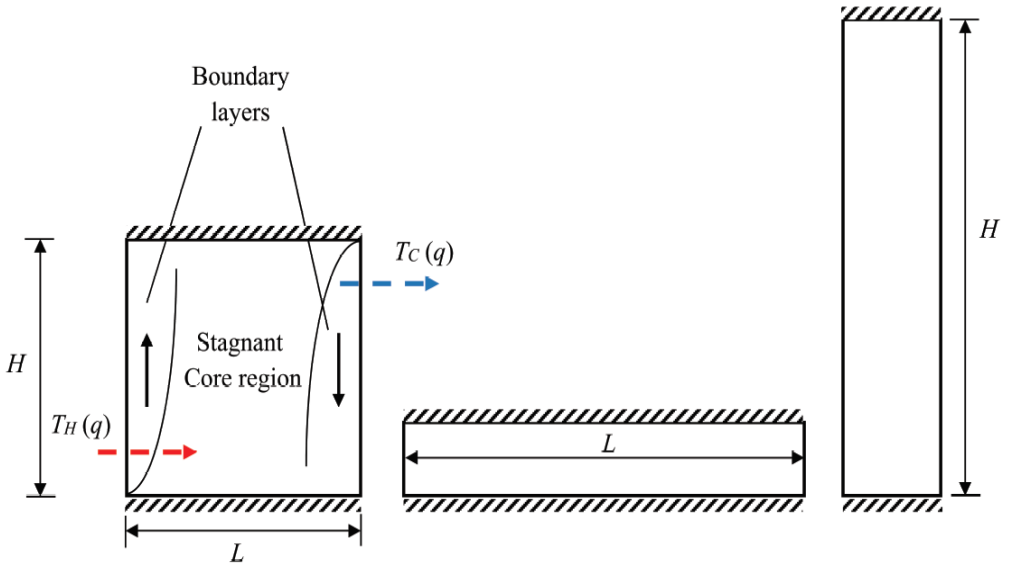

(a) square enclosure (b)shallow enclosures (c)tall enclosures

Figure (1- 2) classical examples of two-dimensional rectangular enclosures with deferentially heated from sidewalls [2].

1.1.2 Differentially heated horizontal walls configuration

The second most extensively studied natural convection in enclosures problem is called as Rayleigh-Bénard convection configuration or natural convection in an enclosure with differentially heated horizontal walls. Figure (1-3) explains the horizontal walls that are differentially heated in which the fluid is enclosed between two large horizontal plates of varying temperatures ($T_1 \neq T_2$). In case (a), the bottom plate's temperature is higher than the upper plate's temperature ($T_1 < T_2$). In the direction of the gravitational force, the density decreases. If the temperature difference is greater than a critical value, the fluid density distribution becomes unstable and buoyancy force overcomes viscous forces to initiate the flow. As a result, the denser fluid descends under the action of gravity, while lighter fluid rises and gets colder as it moves. However, this condition does not hold for in case (b), when ($T_1 > T_2$) and the density no longer drops in the direction of the gravitional force. As a result, lighter fluid lies on top of the heavier fluid, forming a stable stratified state with no bulk fluid movement.

In case (a), heat is transferred from the bottom to the top surface by natural convection, but in case (b), heat is transferred only through thermal conduction from the top to the bottom as mentioned by Bergman et al.[1].

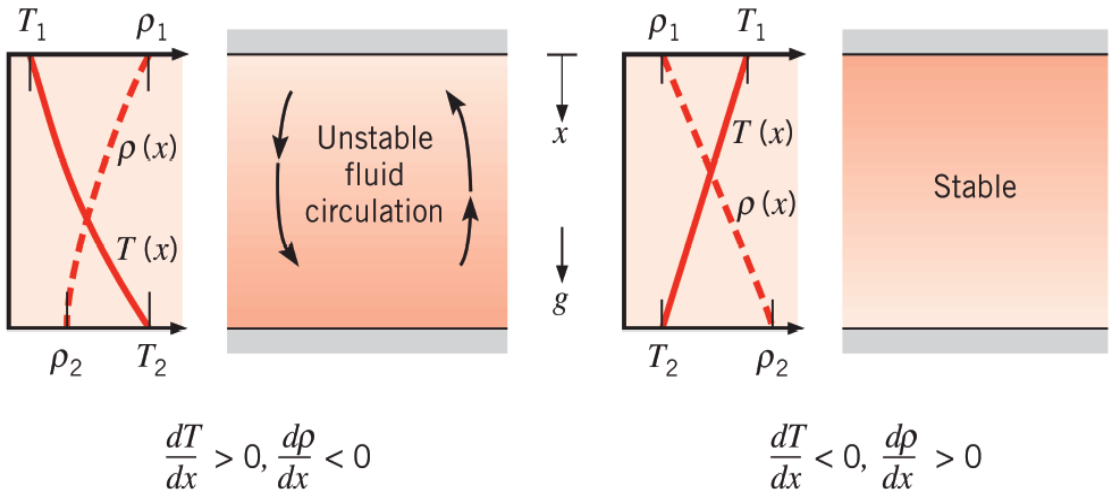

(a) unstable temperature gradient ***(b) stable temperature gradient***

Figure (1- 3) conditions in a fluid between large horizontal plates at different temperatures [1].

The configuration (a), in figure (1-3) is called Rayleigh-Bénard convection in the heat transfer literature which is briefly explained by Yigit [2].

1.2 Non-Newtonian Fluid Behavior

Graebel [3] classified fluids in two ways by their response to externally applied forces like pressure, temperature, and shear stress. The first classification distinguishes between "compressible" and "incompressible" fluids, based on whether or not the volume of a fluid element changes when exposed to external force, or change of pressure or temperture. The second classification divides the fluids into "Newtonian" and "non-Newtonian" fluids, depending on the shear rate dependence of the viscosity of the fluid. A Newtonian fluid in which its viscosity is constant and independent of shear rate ($\dot{\gamma}$). On the other hand, if the viscosity can

change with the change of shear rate , the fluid is charactrized as a non-Newtonian fluid. The thin layer of a Newtonian fluid is divided by two parallel planes by a distance (dy) as illustrated in figure (1-4). The fluid is sheared when a force F is applied to the top surface of the fluid with area A, as shown in figure (1-4, a), and this force must be matched by an equal and opposite internal frictional force in the fluids. For the incompressible Newtonian fluid in a laminar flow, the resultant shear stress follows Newton's law, that is equal to the product of the shear rate and viscosity. The slope of the linear relationship between shear stress and shear rate in figure(1-4b) provides the measurement of viscosity [4].

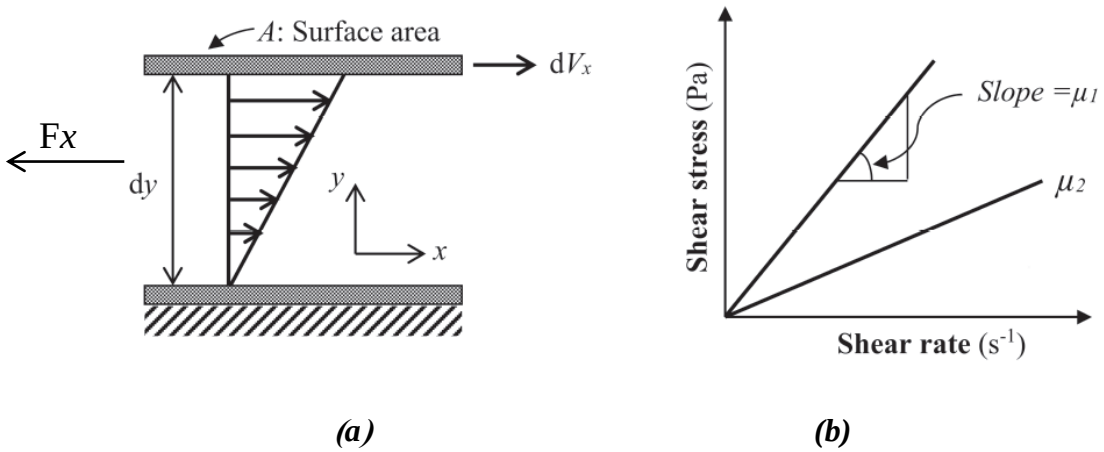

Figure (1- 4) a- is a schematic representation of the unidirectional shearing flow, and b- is a typical shear stress vs. shear rate behavior for Newtonian fluids.

The shear rate for Newtonian fluids can be expressed as velocity gradient in a direction perpendicular to it:

$$\frac{F_x}{A_{xz}} = \tau_{yx} = \mu\left(-\frac{dV_x}{dy}\right) = \mu\,\dot{\gamma}_{yx} \qquad \text{..... (1.1)}$$

The viscosity, μ of Newtonian fluid is constant and independent of shear stress or shear rate and is completely dependent on the material, its temperature, and pressure. For non-Newtonian fluids, however, the relationship between shear stress and shear rate is non-linear. This means

that non-Newtonian fluid viscosity is influenced not only by temperature and pressure but also by flow conditions such as shear rate [5].

1.2.1 Applications of non-Newtonian fluid

These fluids have been utilized for numerous purposes in daily life and industry for many applications such as cooling of electronics, thermal energy storage systems, and solar collectors, as presented by Sharma et al.[6]. They can be used for designing new thermal management systems or improving existing ones for many applications.

For example non-Newtonian liquid-induced cooling has been investigated to improve the electric performance of solar cells. It has been found that cooling and electrical performance increases with decreasing liquid layer thickness which covers solar cells due to augmentation of convection as a result of shear-thinning features of dielectric liquid. Accordingly, the direct liquid immersion cooling of the solar cell was proposed as a solution for thermal management of concentrating photovoltaic (CPV) systems as described by Han et al. [7].

1.2.2 Classification and type of non-Newtonian fluids

There are several types of non-Newtonian flow behavior, which are characterized by the way that the fluid viscosity changes in response to the changes in the shear rate. Chhabra and Richardson [8] explained how to classify fluids with the shear stress as a function of shear rate.

1.2.2.1 Non–Newtonian fluids – time independent

1. Pseudo plastic (shear – thinning) behavior

The shear-thinning fluid is one of the most common types of time-independent non-Newtonian fluid behavior. It is characterized by an apparent viscosity that decreases with increasing shear rate hence it is

called shear thinning, as shown in figure (1-5). The most of shear-thinning or power law fluids exhibit Newtonian behavior at very low and at very high shear rates. The resulting values of the apparent viscosity at very low and high shear rates are known as the zero shear viscosity(μ_o) and the infinite shear viscosity (μ_∞) respectively. Thus, the apparent viscosity of a shear-thinning fluid decreases from μ_o to μ_∞ with increasing shear rate [8]. The majority of synthetic and biological fluids exhibit shear-thinning behaviors as blood, silicone oils, ketchup, and coatings.

2. Dilatants (Shear – Thickening) behavior

The shear-thickening fluid is also another common type of time-independent non-Newtonian fluid behavior. It is characterized by an apparent viscosity that increases with the increasing of the shear rate, thus they are called shear-thickening fluids as shown in figure (1-5). Originally this type of behavior was observed in concentrated suspensions; at low shearing levels, the liquid lubricates the motion of each particle past another to minimize solid-solid friction as illustrated by Chhabra and Richardson [8]. The most well-known examples of shear thickening fluids are The mixtures of corn starch and water, so-called “bullet-proof” custard.

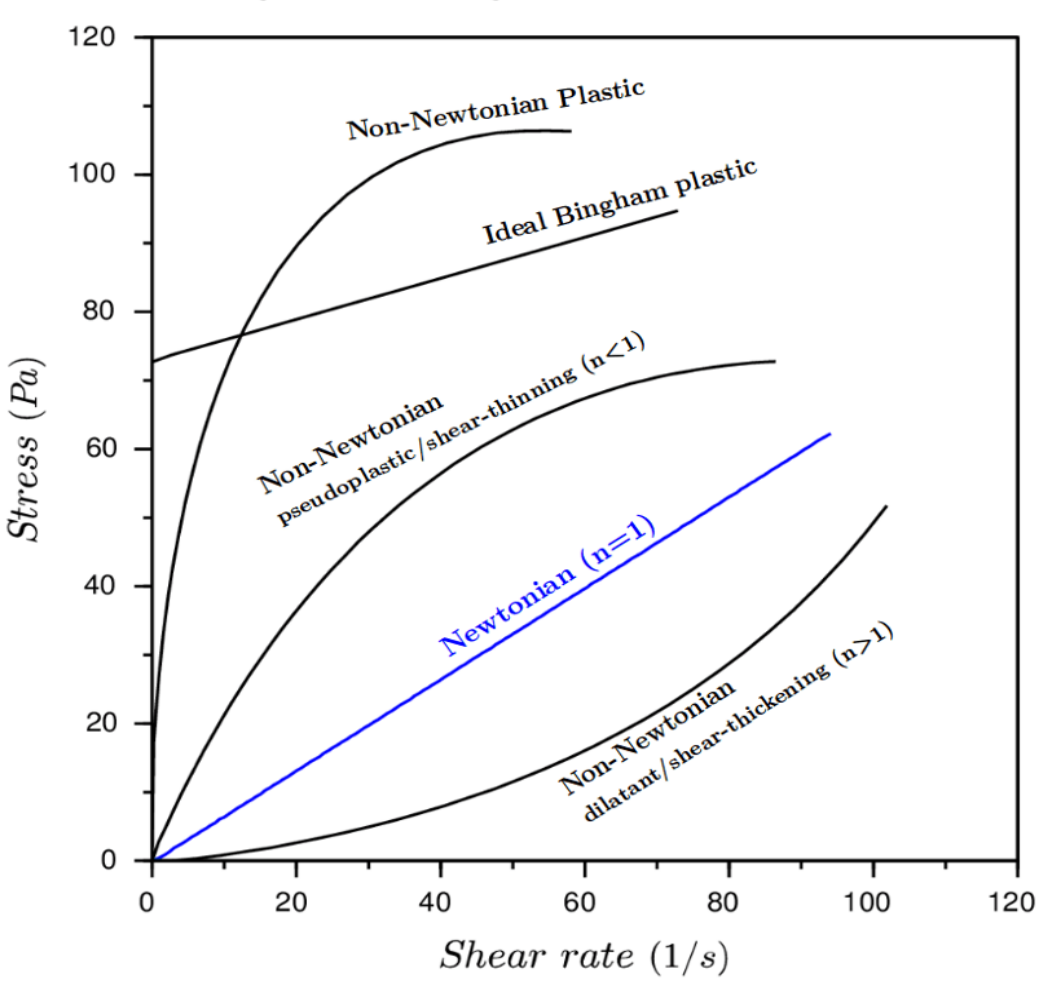

Figure (1- 5) types of time-independent flow behavior [8].

1.2.2.2 Power law

The relationship between shear stress and shear rate (plotted on double logarithmic coordinates) for both shear thinning and thickening fluid can often be approximated by a straight line over a limited range of shear rate. For this part of the flow curve, an expression of the following form is applicable:

$$\tau_{yx} = m\,(\dot{\gamma}_{yx})^{n} \qquad \text{……..…(1.2)}$$

the apparent viscosity for the so-called power-law or Ostwald de Waele fluid is given by:

$$\mu = \tau_{yx}/\dot{\gamma}_{yx} = m(\dot{\gamma})^{n-1} \qquad \text{……..(1.3)}$$

where, the fluid exhibits shear-thinning properties at $n < 1$, while at $n = 1$, shows a Newtonian behavior and at $n > 1$, shows a shear-thickening behavior.

In these equations, m and n are two empirical curve-fitting parameters and are known as the fluid consistency coefficient and the flow behavior index respectively. For a shear-thinning fluid, the index may have any value between 0 and 1. The smaller the value of n, the greater is the degree of shear-thinning. For a shear-thickening fluid, the index n will be greater than unity. When $n = 1$, equations (1.2) and (1.3) reduce to equation (1.1) which describes Newtonian fluid behavior.

3. Bingham behavior

Fluids that have a linear shear stress/shear strain rate relationship but require a finite yield stress before they begin to flow as shown in figure (1-5) (the plot of shear stress against shear strain rate does not pass through the origin) are called Bingham plastics. There are several examples of the Bingham plastics, such as clay suspensions, drilling mud, toothpaste, mayonnaise, chocolate, and mustard.

1.2.2.3 Non –Newtonian fluids – time dependent

Some fluids display a change in viscosity with time, under conditions of constant shear rate. Time-dependent fluid behavior may be further subdivided into two categories thixotropy and rheopex or negative thixotropy [8], as noted in figure (1-6).

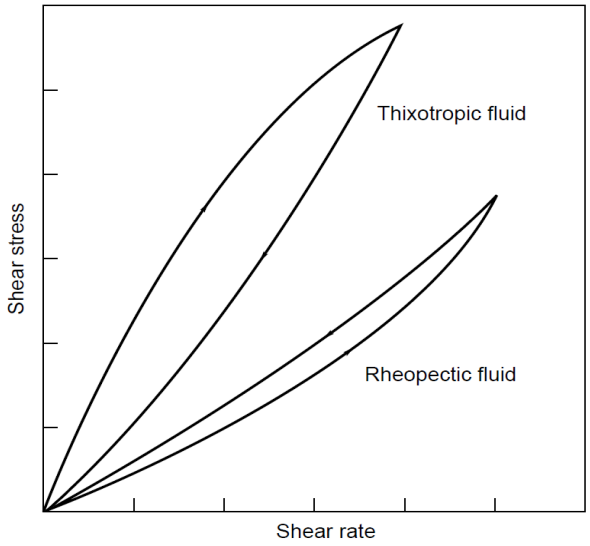

Figure (1- 6) schematic shear stress–shear rate behavior for time-dependent fluid behavior [8].

1. Thixotropic fluids

In this case, the fluid undergoes a decrease in viscosity over time while undergoing continuous shearing as shown in figure (1-6) [8]. For example, a non-drip paint can flow with a lower viscosity when stirred in the paint vessel, such behavior where systems that appear rather solid but on stirring become liquid like, with lower viscosity, is called thixotropic. At rest, the viscosity increases again, so the paint does not form drops on the wall.

2. Rheopectic fluids

The fluid viscosity increases with time as it sheared at a constant rate as shown in figure (1-6). The apparent viscosity increases with increasing shear rate, the effect is called rheopecty, if time-dependent, and dilatancy, if time-independent. Gypsum pastes and printer inks are a well-known example of rheopectic fluids as described by Chhabra and Richardson [8].

In this study, it will be concentrated on the natural convection characteristic of the incompressible time-independent as shown in the flow

chart given in figure (1-7). The scope of this study is to investigate the natural convection of power-law fluids (shear-thinning fluids) in enclosed spaces with a hot obstacle.

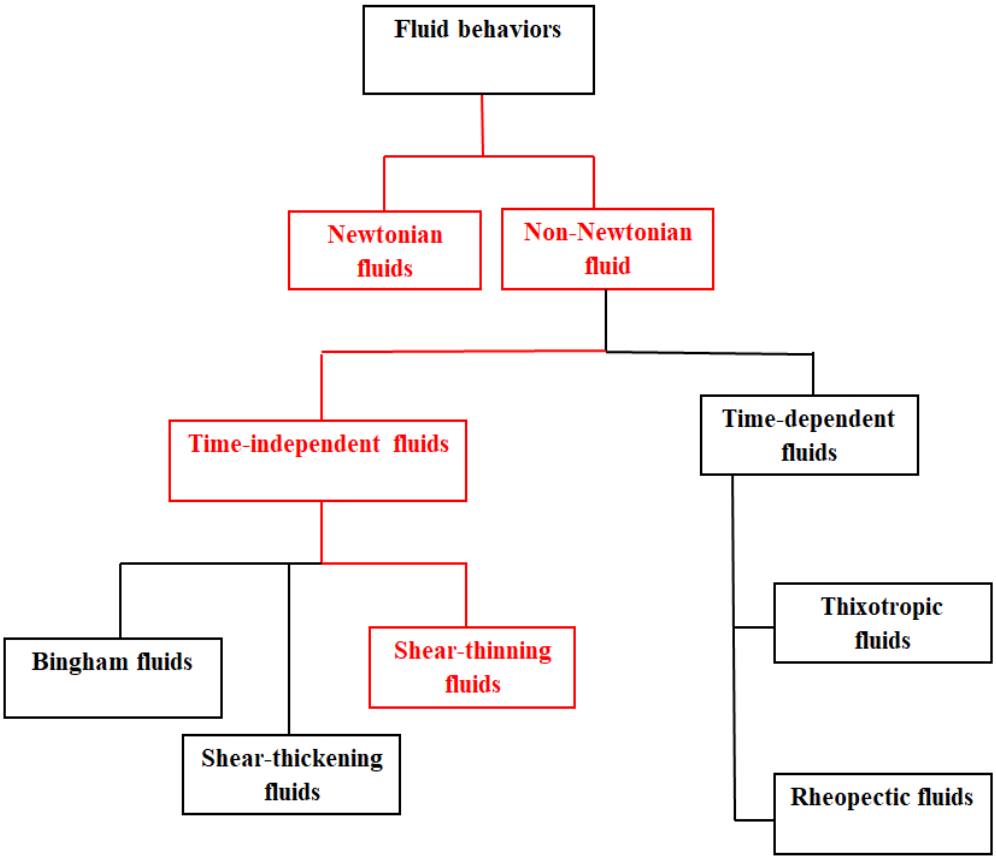

Figure (1-7) the classification of fluid behaviors, where the red color represents the scope of this study.

1.3 Objective of the present work

This study aims to investigate the mechanism of heat transfer by natural convection practically and theoretically for the working fluid in a closed rectangular enclosure containing a hot obstacle. The specific objectives are:

1- Comparing the change in the heat transfer process when using a Newtonian and non-Newtonian fluid.

2- Studying the effects of the controlling parameter Rayleigh number, the power-lawn index, aspect ratio, and change the obstacle shape .

1.4 Outline of the thesis

Basically, this thesis involves six chapters and each chapter will be briefly introduced as follows :

- Chapter one : deals with an introduction and outline the aims.
- Chapter two : is concerned reviews and the previous related literature, which presents the contributions and work.
- Chapter three : accounts of details of experimental apparatus , setup, and procedur.
- Chapter four : displays the theoretical explains of the mathematical model to analyze the temperature distribution inside the enclosure.
- Chapter five : introduces the results and discusses the experimental and theoretical work.
- Chapter six : sums up the conclusions arrived at the end and the suggestions for future works.

CHAPTER TWO

LITERATURE REVIEW

Literature Review

Convective heat transfer in cavities filled with non-Newtonian fluids has attracted great interest from researchers because this technique is simple, low-noise, low-cost, small in size, and has a wide range of practical applications such as cooling components of electrical and electronic refrigeration systems. Several theoretical and experimental investigations have been carried out regarding the effects of geometry on containers filled with the non-Newtonian fluids.

2.1 Theortical Studies

Kim et al. [9] presented numerically the transient convection for a non-Newtonian liquid model of power law in a closed square cavity where the heating occurs by raising the temperature of the sidewall and cooling takes place by reducing the temperature of the opposite wall. They explained the effect of the Rayleigh number, index power law (n), and Prandtl number on Nusselt number. The numerical results of this study showed that the average Nusselt number rises as the power-law index is reduced for a certain set of values of Ra and Pr, that is used at an aspect ratio of the enclosure AR = 1, $10^5 \leq Ra \leq 10^7$, $10^2 \leq Pr \leq 10^4$, $0.6 \leq n \leq 1$.

Lamsaadi et al. [10] performed a two-dimensional analytical simulation of a shallow rectangular container, its long horizontal walls were insulated, and short vertical walls have been subjected to a uniform heat flow. It is filled with a non-Newtonian fluids power law model that proposed by Oswald-de Weil. The behavior and the effects of flow and heat transfer of the non-Newtonian fluid. The different values were presented for Rayleigh number (10^3-10^5), index power law (0.6 - 1.4), Prandtl number (1, 100, 1000), and aspect ratio (AR = 8). They found that the rate of heat transfear in shallow cavities can be mainly controlled by an index power

law and Rayleigh number, where the shear thinning behavior fluid circulation and heat transfer is enhanced by convection while thickening shear behavior produces the opposite effect. The non-Newtonian fluids are not effected by changing the value of AR and Pr when their values are large.

Lamsaadi et al. [11] examined the natural convection numerically in the rectangular vertical-shaped containers. The container is filled with non-Newtonian fluid (power law model). It was cooled and heated from the vertical sidewalls by exposing them to a uniform heat flux, while the horizontal walls remain adiabatic. Several variables were used to present results in terms of flow function, velocity, temperature, and rate of heat transfer for different values of AR (1 - 12), Ra (10^3 - 10^5), and n (0.6 - 1.4). The results include that at the high values of Prandtl number and aspect ratio no effect on natural convection in tall cavities where the main controller is the Rayleigh number and flow behavior index. The rate of heat transfer and fluid flow increase in the case of non-Newtonian fluids, compared to Newtonian fluid especially in the case of shear-thinning. In contrast, the shear thickening reduces the rate of transmission and flow.

Lamsaadi et al. [12] studied numerically natural convection in a tall sloping rectangular container that filled with a non-Newtonian fluid (power-law). Its short walls were subjected to a uniform heat flux while other walls were adiabatic. The governing parameters were the power law index n (0.6 -1.4), Rayleigh number (10^3-10^5), and the angle of inclination Ø (-180^o -180^o). Their results showed that at the high values of the aspect ratio and Prandtl number there is no effect on heat transfer rate or fluid flow. The non-Newtonian heat transfer rate increases in the case of pseudo-plastic fluids, while the expanded fluid has the opposite effect, compared to Newtonian fluids.

Muhadi [13] demonstrated uniform convection in an isosceles triangular container filled by Newtonian and non-Newtonian fluids theoretically. The range of Rayleigh numbers was (10^3-10^5), the modified Prandtl number was in the range of (Pr = 1, 10, 100), and the dimensionless parameter (NE) of the Prandtl - Eyring model has a range (0 - 10). Two types of boundary conditions were used, the first was to heat one of the inclined walls and cool the second wall while the base is insulated, and the second was to heat the base by using a uniform heat flux and cool the inclined walls. The results displayed the effect of a variable NE on velocity and temperature properties, the streamlines to present the behavior of the fluid flow, the temperature ranges, and the isotherms. They showed that average number of Nusselt is a strong function of the modified Rayleigh number.

Turan et al. [14] numerically showed laminar natural convection in a square container with the differentially heated vertical walls filled with a non-Newtonian Bingham fluid. The effect of the heat and the momentum transfer for the variables values of Rayleigh number with the range of (10^3-10^6), Prandtl number (0.1 - 100), and different ranges of Bingham number were examined. They discovered that the raising of Rayleigh number for Newtonian and non-Newtonian fluids causes the mean Nusselt number to rise. The resulting values of a Nu in the case of Bingham fluids are less than that for the Newtonian fluids at the same Ra value due to the poor convection transfer. An increase in the Bingham number leads to a decrease in the mean Nusselt number relative to the non-Newtonian fluids of the model used. For the large values of Bingham number, the Nusselt number stabilizes into unity and the thermal transfer occurs using conduction.

Turan et al. [15] performed a two-dimensional simulation of a stratified heat load in the square-shaped container with a non-Newtonian power-law model. Lateral heating at a constant temperature for vertical walls with isolated horizontal wallswas used. They studied the effect of index power law in the range of (0.6 - 1.4) on heat and momentum transfer. The applied Rayleigh number was in the range of 10^3-10^6 and the Prandtl number was in the range of 10-10^5. The mean of the Nu was improved as the Ra increased for the both the power-law and the Newtonian fluids. With the increase of shear thickness, the mean Nusselt number settles into unity where the heat transfer occurs mainly due to the thermal conductivity.

Turan et al. [16] theoretically illustrated a 2-D stratified natural convection in a square container filled with Power-law fluids. vertical walls differentially heated by the constant wall heat flux. They showed that the effect of Ra, Pr, and n on Nu within the ranges of ($10^3 \leq Ra \leq 10^6$), ($10 \leq pr \leq 10^5$), and ($0.6 \leq n \leq 1.8$). The findings were compared to a constant wall temperature, the results were found to be significantly different from constant wall temperature. It was observed that the Nusselt number rises as the Rayleigh number and index power-law rise for both kinds, the constant wall heat flux and the constant wall temperature. They showed that the values of the Nusselt number for Newtonian fluids were smaller /greater than that for power-law fluids with $n < 1/n > 1$, at the same Rayleigh number value due to the strength and the weakness of the thermal transfer. When the power-law index exceeds 1, the thickness of the shear rises, the Nusselt number settles into unity, the heat is transferred by conduction. the effect of the Prandtl number is negligible within the mentioned range.

Ternik and Rudolf [17] numerically examined the natural convection in a square container. The sidewalls of the container are

differentially heated by subjecting them to constant temperatures. The container filled with an aqueous solution of carboxymethyl cellulose (CMC) base of 0.4 % in weight, with the nanoparticles Au, Al_2O_3, Cu, and TiO_2, which all obeyed to the power-law model. The effect of the nanoparticle size fraction ($0\% \leq \varphi \leq 10\%$) on the heat transfer properties based on CMC over a wide range of Ra ($10^3 \leq Ra_{nf} \leq 10^6$) was investigated. The results were obtained in the form of the dimensionless temperature and velocity variables, the isothermal, and the mean Nusselt number. It showed that the properties of the heat transfer and the momentum are only effected by the Rayleigh number of the Nanofluid, while the type of the nanoparticles and their volumetric fraction have only an effect on the improving of heat transfer.

Sojoudi et al. [18] investigated theoretically a free convection in a trapezoidal cavity filled with a non-Newtonian fluid. The right inclined surface was uniformly cooled while the left inclined surface was uniformly heated. The upper and the lower surfaces were adiabatic. Heat transfer coefficients and fluid flow were characterized using Ra with a range of (10^5 - 10^7), n (0.6 - 1.4), and Pr (10^2 – 10^4). The results were collected that in the isotherm, the streamlines, and the local Nusselt number forms for different inclined angles, Ra, n, and Pr. They were found that the reduction of the maximum Nusselt number at the left hot wall can be obtained by the increasing of the trapezoidal angle. The value of the Nusselt number for the type of shear-thinning behavior was higher than that of the shear thickening due to the lower maximum stream function. Increasing the Rayleigh number enhances the local Nusselt number. The variation of the Prandtl number has no significant effect on the Nu as most of the non-Newtonian fluids have higher values than Pr.

Ternik et al. [19] demonstrated theoretically natural convection in a cubic cavity filled with a homogeneous aqueous solution of (CMC) gold-based (Au) nanoparticles according to a power-law model. The vertical wall of the cavity was heated and the opposite wall was cold, while the other walls are adiabatic. They showed the effect of the fraction nanoparticle size on the heat transfer properties of the CMC-based (Au) Nanofluid over a wide range of Rayleigh number. Their results are presented in the form of the dimensionless changes in temperature and velocity, heat transfer rate, and Nusselt number. The addition of the nanoparticles to the CMC solution delays the onset of natural convection. The addition of particles after the onset of convection reduces the average value of the Nusselt number for any Rayleigh number for the base fluid.

Yigit et al. [20] analyzed numerically the Rayleigh–Bénard convection and the effect of the aspect ratio on it, for non-Newtonian fluids which were represented by the power-law model in a rectangular container. The container has horizontal walls that heated at constant temperatures, where a bottom wall has a higher temperature. They indicated in their results that the convection was weak with an increase in aspect ratio. Heat transfers only due to the thermal conductivity when AR > 2, ($10^3 \leq Ra \leq 10^5$), ($0.25 \leq AR \leq 4$), $Pr = 10^3$, and ($0.6 \leq n \leq 1.8$). The flow pattern for $AR \leq 2$ has been found to be dependent not only on Ra and n. The viscous resistance weakens with decreasing power-law index for a given set of values of Ra, AR, and Pr. The mean Nusselt number Nu does not exhibit a monotonic increase with decreasing n for $AR \leq 2$ because of the change in flow pattern (number of convection rolls/cells) within the enclosure.

Raisi [21] explained numerically the natural convection of a cavity at its base as a heat source that produced a uniform flow of heat, while the

rest of the base was isolated. The sidewalls of the container are insulated and the top wall is at low temperature. The cavity filled with a non-Newtonian fluid (power-law model).He studied the effect of some variables such as index power law (0.6 - 1.8), position and length of heat source ($0.2 \leq S \leq 0.5$), ($0.2 \leq W \leq 0.8$) respectively, and Rayleigh number Ra (10^3 - 10^6) on the thermal performance of the system. He showed that when increasing the Rayleigh number, thermal performance increases, especially when n is less than 1, meaning that when using shear-thinning fluids for large Rayleigh numbers, the cooling performance of the heat source improves. He also showed the length and location of the thermal source, depending on Ra and n, were important in influencing the thermal performance of the system.

Gangawane and Manikandan [22] demonstrated theoretically the steady-state natural heat transfer and flow, in a square container containing a heated hexagonal block. They were kept either at uniform heat flow (UHF) or constant wall temperature (CWT) thermal conditions. They also relied on a simple set of related parameters such as Grashof number ($10^3 \leq Gr \leq 10^6$), index power law ($0.5 \leq n \leq 1.5$), and Prandtl number ($1 \leq Pr \leq 100$). Momentum analysis and heat transfer properties were determined by, isotherms, streamlines, mean change value of Nusselt number, and Colborne's natural convection factor (jnH). It was observed that heat flow and fluid flow change with the distribution pattern in the cavity for both thermal conditions. Nusselt number between linear variance with Grashof and Prandtl numbers. The highest rate of heat transfer is by using a uniform heat flow condition.

Alsabery et al. [23] studied numirecally natural transient convection in a trapezoidal cavity filled with a nonNewtonian nanofluid with sinusoidal boundary conditions on both sidewalls. The sloping walls

for cavity are heated by sinusoidal temperature distributions, while the horizontal walls do not allow heat to transfer to surroundings. Water-based Nano fluids with Cu, Ag, TiO_2, or $Al2O_3$ Nanofluids were taken for investigation. The governing parameters for this study were ($10^4 \leq Ra \leq 10^6$), ($0.6 \leq n \leq 1.4$), phase deflection ($0 \leq \gamma \leq \pi$), sidewall angle slope ($0^\circ \leq \phi \leq 21.8^\circ$), amplitude ratio ($0 \leq \varepsilon \leq 1$), timeless ($0 \leq \tau \leq 0.2$), and nanoparticle size fraction ($0 \leq \varphi \leq 0.2$). They observed that the rate of heat transfer increases significantly by adding phase deflection. Good improvements in heat transfer was achieved by using a higher wall tilt angle. However, for square cavity heat transfer approaches the steady-state with increasing dimensionless time.

Hasan et al. [24] investigated the convective steady-state of a non-Newtonian laminar fluid flow in an elliptical container numerically. Two types for boundary conditions are considered, firstly at inner holes it was under a constant heat flux, and the second was when the inner holes were heated to a constant temperature. The walls of the enclosure is isolated in all cases. Wide ranges of Rayleigh numbers(1.34×10^3, 1.34×10^4 and 1.34×10^5), power law index (0.1, 0.5,1 and 5) with Prandtl number(1.37, 6.37 and 15.37) are implemented. The results presented in terms of isotherms to present the temperature field, it showd that the Nusselt number is strongly influenced by Rayleigh numbers, Prandtl number, and power-law indicator. The effect of changing the power-law index of the non-Newtonian fluid on the temperature distribution is explained. Further increasing the number of Prandtl leads to an increase in the rate of heat transfer.

Thohura et al. [25] conducted a study numerical of laminar convection within a two-dimensional skewed cavity filled with shear-thinning or pseudoplastic fluid where the horizontal walls are adiabatic, and

the temperature difference resulting in the convection comes from the vertical sidewalls using the finite volume method. The study has been conducted for a wide range of Ra (10^3-10^5), index power law (n = 0.5), and Pr = 10. The obtained results were presented regarding isotherms, streamlines, velocity, and temperature profiles as well as the rate of heat transfer for shear-thinning fluids. They showed the rate of heat transfer in shear-thinning fluids within the cavity is highly dependent on Ra, Pr, and n. Rayleigh number increasing leads to convective strength and leads to increasing average Nusselt number.

Pishkar et al. [26] presented a numerical study on the unsteady natural convective flow of Newtonian and non-Newtonian fluids in a square enclosure. The bottom wall of the enclosure contained a heat source with oscillating heat flux. The top wall was thermally insulated and the other walls were at a relatively low temperature. The flow and temperature fields and the heat transfer performance are examined for different non-Newtonian fluids and heat source locations. The results were presented for different values of the power-law index (0.6, 1, 1.4), Rayleigh number (10^4 to 10^5), and the fluctuation period. It was found that the flow and temperature fields vary as the oscillating heat flux was changed. The pseudoplastic non-Newtonian fluid was associated with a higher heat transfer, and the dilatant non-Newtonian fluid was associated with a lower heat transfer with respect to the Newtonian fluid. The heat source oscillation period significantly affected the maximum flow temperature in the enclosure.

Khan et al. [27] demonstrated numerically the natural convection of a non-Newtonian fluid Casson type inside the square container with the Y-shaped fin at the bottom. Its purpose of which was to increase the surface area of heat transfer by convection. The sidewalls of the cavity are kept at

cold temperature, the bottom surface at a hot temperature, and the top surface as adiabatic. The effects of radiation and magnetic field were included in the governing equations. They take into account the effect of Rayleigh number ($10^4 \leq Ra \leq 10^6$), Hartmann number ($0 \leq Ha \leq 10^3$), and radiation coefficient ($0 \leq Rd \leq 10^3$) on the streamlines, dimensionless velocity components, Temperature isothermal, and Nusselt number along heated fin and the bottom wall. The results showed that a higher value of the Rayleigh and Hartmann number as a result of an increase in the rate of heat transfer along the fin surface. The dimensional temperature in the upper wall decreases with increasing radiation coefficient and Hartmann number.

Li et al. [28] displayed the natural entropy generation and convection for a non-Newtonian fluid (power-law) in an inclined triangular enclosure exposed to a magnetic field, theoretically. The upper wall was cold while part of the left or right wall of the container was at a high temperature. The remainder of the walls is insulated. The results reveal that when the hot wall is on the left and the Rayleigh number is increased from 10^3 to 10^5. The heat transfer rate increases 1.50 times for shear-thinning fluids, while the rate of entropy generation increases more than 2 times. These modifications result in a 71 percent increase in heat transmission and an 80 percent increase in entropy production for Newtonian fluids. The Bejan number decreases as the Rayleigh number increases. The mean Nusselt number decreases as a result of the rise in the Hartmann number.

Pandey et al. [29] studied the laminar unsteady natural convection in a square enclosure with an internal circular cylinder containing non-Newtonian fluid. The results illustrated the effect of vertical movement of an internal circular cylinder on the flow and heat transfer mechanism within a square enclosure for Rayleigh numbers ranging from 10^3 to 10^6,

power-law index from 0.6 to 1.6 with a step size of 0.2, and Pr = 10. The internal cylinder was positioned at three different locations along the vertical centerline near the isothermal bottom wall, at the center, and near the isothermal top wall. The temperature and velocity fields were affected by the location of the cylinder inside the container, as well as the Nusselt number was a decreasing function of the power-law index.

Pandey et al. [30] investigated the buoyancy-driven flows inside an enclosure with an inner cylinder embedded within it. The square enclosure contains the power-law fluids. The enclosure's lower and top walls are both isothermal. They illustrated the vertical movement of the inner cylinder and its impact on the heat transfer and flow mechanism within the container at three different points along the diagonal (the center, at the lower wall, and near the top wall). Rayleigh number ranges ($10^3 \leq Ra \leq 10^6$), power-law index ranges ($0.6 \leq n \leq 1.6$). The Prandtl number remains fixed (10). The results showed that at the enclosure is filled with a plastic pseudo-fluid the rate of heat transfers around the cylinder increases. Nu decreases with increasing n due to the active shear stress around the cylinder surface and especially in higher Rayleigh numbers. Nusselt number was lower when the cylinder is in the center and higher when the cylinder is near the bottom wall.

Zhang et al. [31] presented a numerically the free heat convection and entropy generation of non-Newtonian fluids, power-law model, inside an L-shaped cavity subjected to a magnetic field. The bottom and left walls of the cavity have been kept at a uniform high temperature. Internal walls were also kept cold. The remaining walls have been insulated. The effects of Hartmann number (Ha), aspect ratio, power-law index (n), and Rayleigh number (Ra), on the flow field, temperature distribution, and entropy distributions were studied. The results showed that the magnetic field and n

have an ever-decreasing effect on the heat transfer rate and the entropy generation, while the Ra has an ever-increasing effect. The maximum heat transfer enhancement of 71% happens at the lowest and the highest values of n and Ra, respectively, for the case with no magnetic field. The maximum heat transfer deterioration of 77% happens at the highest and lowest values of n and Ra, respectively, in the presence of the highest magnetic field strength. The heat transfer rate and the total entropy generation for the Newtonian and shear-thinning fluids increase, by raising the aspect ratio, while the figure for the shear-thickening case is different. It is decreased first and then increased.

Khan et al. [32] developed a mathematical model of a non-Newtonian fluid in parallel heated plates. He reduced entropy within the system and pressure gradient as means of maximizing the heat transfer capacity. They noted in their results that flow velocity and temperature of fluid are functions of the non-Newtonian coefficient (power-law indicator). The pressure gradient parameter increases the volume and heat flux fields. There is a decreasing characteristic of the wall shear stress occurring in the bottom plate versus the time parameter.

Ali et al. [33] examined numerically the impact of an external magnetic field on the hydrothermal aspects of natural convection of a power-law non-Newtonian nanofluid inside a baffled U-shape enclosure. The enclosure is heated from the bottom and cooled from the baffles while the other walls are thermally insulated. Rayleigh number (Ra), Hartmann number (Ha), nanoparticle volume fraction (ϕ), the aspect ratio of cold baffles (AR), inclination angle, and power-law index (n) on the flow and heat transfer characteristics were studied effected. The results showed that the impact of n on the Nusselt number (Nu) was considerable for $Ra=10^6$. The influence of n and Ha on the heat transfer was significant when Ha is

smaller than 30. For Ha<30, there was a threshold value of nanoparticle after which the rise of n augments heat transfer, which is 5% for AR=0.4 and 7% for AR=0.6.

Rostami et al. [34] examined the flow of Newtonian magnetohydrodynamic fluid and compared it with two different non-Newtonian power-law fluids within a square container. The enclosure with horizontal insulated walls has two constant-temperature obstacles, while two sidewalls were differentially heated with the sinusoidal pattern. the effects of Rayleigh's number, an aspect ratio of constant temperature barriers, Hartmann number, and a case study of the sinusoidal limitations were examined. The findings revealed that as the Rayleigh number rises, so does the Nusselt number, but as the power-law index and Hartmann number increase, decreases the Nusselt number. In the case of shear-thinning and Newtonian shear condensing fluids, the Nusselt number drops. additionally, The Nusselt number was increased as the aspect ratio of barriers was increased. The number of Newtonian dilution fluids and shear fluids rises as the sinusoidal state's frequency increases from 2π to 4π, whereas it reduces as the sinusoidal state's periodicity lowers.

Ye et al. [35] studied the effects of a centered conducting body on natural convection of non-Newtonian fluid in a square cavity with time-periodic temperature distribution. The effects of the power-law index, Rayleigh number, heat capacity ratio, thermal conductivity ratio, body size, temperature pulsating period, and the temperature pulsating amplitude on fluid flow and heat transfer were analyzed. The results showed that the increase of Rayleigh number and thermal conductivity ratio, as well as the decrease of the power-law index, can strengthen both transient and global heat transfer. The increase in body size will reduce both the transient heat transfer ratio and the overall heat transfer ratio. In addition, the decrease of

temperature pulsating period can enhance the transient heat transfer, but it will slightly weaken the overall heat transfer.

Shahabadi et al. [36] showed theoretically, the heat transfer by natural convection and flow of a non-Newtonian fluid (power-law) in a square cavity. The container's horizontal walls are insulated, the right vertical wall is cold, and the left wall is heated. A flexible fin is connected to the heated wall of the container. The interaction of flow with the fin causes the fin to deform, and the resulting change in shape causes a change in heat transfer and flow. The finite element approach was utilized to solve the governing equations. They noticed that the fin deflection for expanding non-Newtonian fluids is higher than for pseudo-plastic and Newtonian fluids. The rate of heat transmission is little affected by non-Newtonian behavior. The pseudoplastic to Newtonian and expanding effects limit the rate of heat transfer with increase the internal pressures in fin.

2.2 Experimental Studies

Khalili et al. [37] investigated experimentally the non-homogenous distribution of nanoparticles in the nanofluid by natural convection heat transfer inside a square enclosure. An experimental set-up was built to carefully take micro-litter samples of nanofluid from a 8×8×18 (cm^3) square cavity. The nanofluid was prepared using 20 nm-gamma type Al_2O_3 nanoparticles dispersed in deionized distilled water. The experiments were done for three Rayleigh numbers 0.992×10^7, 0.51×10^8 and 1.53×10^8. The result showed that the differences between maximum and minimum volume fraction in the whole cavity increases from 18% at Ra = 0.992×10^7 to 28.74% at Ra = 1.51×10^8. It was observed also that the average nanoparticle volume fraction along cold wall is 3.10% greater than that

along hot wall for minimum Ra however at higher Ra this difference would weaken.

Abou-Ziyan et al. [38] practically predicted of free convection from electrically-heated short horizontal circular cylinder of small aspect ratio (L/d=8) to five fluids with high Prandtl numbers.Three of these fluids are Newtonian and two are weakly power-law shear thinning fluids. Experiments were conducted, under constant heat flux, at various bulk temperatures (40-175^{o}C) and heat fluxes (0.66-104 kW/m^{2}) that correspond to heat generation from about 0.7 to 113 MW/m^{3}. Effects of oil bulk temperatures, oil properties and heat generation parameter, on the free convection results, were investigated.The results indicated that Newtonian fluids attain higher free convection heat transfer coefficient than the power-law fluids by 16% or more. The Nusselt number for free laminar convection is related to the power-law index.

Giwa et al. [39] studied experimentally, the natural convection of hybrid nanofluids of Al_2O_3–MWCNT/water nanofluids at various bi-nano particles percent weights (Al_2O_3:MWCNT;80:20, 60:40, 40:60, and 20:80) in a square cavity(length 96, width 96, and height 105) mm. The corresponding vertical sidewalls were heated differently. The rest of the cavity walls were well insulated. The Nuav, hav, Ra and Qav at varying temperature gradients (20°C–50°C) were considered. The range of Ra (1.65×10^{8}– 3.8×10^{8}). A direct relationship was noticed between Ra and Nuav. Temperature gradient and percent weight of bi-nanoparticles in the nanofluids were observed to augment Nuav, hav, and Qav. The hybrid nanofluid with 60:40 wt% of Al_2O_3 and MWCNT nanoparticles was identified to have the highest value for Ra, Nuav, hav, and Qav at various temperature gradient maximum enhancements of 16.2%, 20.5%, and 19.4% were recorded for Nuav, hav, and Qav, respectively, at T=50°C, in relation

to the base fluid. The engagement of Al_2O_3−MWCNT/water nanofluids in a square cavity has shown improved natural convection performance.

Hassan et al. [40] demonstrated natural convection in the heated enclosure investigated both computationally and experimentally. The enclosure was heated partially at the bottom wall at its center. The side walls were isothermally cooled. In addition, an experimental investigation on the viscoplastic test fluids, prepared from Carbopol Ultrez 20 polymer, has also been carried out. The proposed computational model has been validated with our own experimental results. The results in terms of flow and thermal characteristics of Bingham number (0-30), the hot length of the bottom wall (ε), Ra (10^4-10^6), and Pr (1-100) were checked. In a constant heat flux, It was discovered that local heating of the bottom surface and cooling of the side walls have a substantial impact on fluid circulation with heat transfer as compared to isothermal conditions. It was also discovered that owing to the symmetric cooling of the walls, heat transfer at the margins of heated bottom lengths rises.

2.3 Summary

Most of the researchers were reviewed theoretically the non-Newtonian fluid behavior and it is effect on heat transfer inside the different shapes of the enclosure with different boundary conditions. The impact of heating on the characteristics of the non-Newtonian fluid inside the container was the subject of a few experiments.

In the present work, the influence of heat transfer on the non-Newtonian fluid inside a rectangular enclosure was investigated experimentally and numerically. It was building a rectangular enclosure with insulated vertical wall and base, while the upper wall kept as a constant cold temperature. Two types of obstacle shapes were used in this

work as a hot source. Carboxymethylcellulose (CMC) with two concentrations were used as a working fluid. Water was also used in this study to compare the effect of the heat transfer mechanism between both Newtonian and non-Newtonian fluids. The effect of changing the aspect ratio (AR) two values was elaborated. COMSOL software was used to analyze the heat transfer between the Newtonian and non-Newtonian fluid with the boundary conditions were assumed. Table (2-1) shows the summary of all researches works were reviewed in this chapter.

Table (2- 1) summery table

Ref. No.	**Authors**	**Year of the study**	**Main conclusion and result**
9	Kim et al.	2003	The Nu increases with decreasing n.
10	Lamsaadi et al.	2006	The heat load values controlled mainly by the n and Ra because the shear thinning behavior circulation and heat transfer are enhanced by convection, while the shear thickening produces the opposite effect. Non-Newtonian fluids are not affected by the change of the AR & Pr value when they have large values.
11	Lamsaadi et al.	2006	Pr and AR when having high values do not affect natural convection in tall cavities as the main controller is the Ra and n. The Nu increases in the case of non-Newtonian fluids and especially in the case ($n < 1$) compared to ($n = 1$), in contrast to the behavior of ($n > 1$),
12	Lamsaadi et al.	2006	AR and Pr when having large numbers it did not affect the heat transfer rate or the fluid flow. Ra and n in addition ∅, main controller. The behavior of the non-Newtonian fluid in the case of n >1

Ref. No.	Authors	Year of the study	Main conclusion and result
			decreasing the rate of heat transfer, while the behavior of n < 1 has the opposite effect compared to n=1
13	Muhadi	2007	Nu is a strong function of the modified Rayleigh number, boundary conditions, and modified Prandtl number when used triangular enclosure.
14	Turan et al.	2010	Nu increased with increasing Ra for non-Newtonian and Newtonian fluids. At the large numbers of Bingham, Nu=1and the thermal transfer occurs using conduction.
15	Turan et al.	2011	Nu increased with an increase in the Ra for both Newtonian fluids and power-law fluids. With the increase in the shear thickness, Nu=1
16	Turan et al.	2012	Nu increases with the increase Ra and n for both types (the constant wall heat flux (CHWF) and the constant wall temperature (CWT)). Nu for Newtonian fluids was smaller (greater) than power-law fluids with n < 1 (n > 1), for the same Ra value due to strength and weakness of the thermal transfer.
17	Ternik & Rudolf	2013	Ra of the Nanofluid, while the type of nanoparticles and their volumetric fraction have only an effect on improving heat transfer.
18	Sojoudi et al.	2013	Nu for the type of shear-thinning behavior was higher than that of the shear thickness due to the lower maximum stream function. Increasing Ra reinforces the local Nu.

Ref. No.	Authors	Year of the study	Main conclusion and result
19	Ternik et al.	2015	The addition of nanoparticles to the CMC solution delays the onset of natural convection.
20	Yigit et al.	2015	The convection was weak with increase AR. Nu does not show a decrease (increase) with increasing n (Ra), When AR ≤ 2, changes occur in the flow pattern inside the enclosure.
21	Raisi	2016	Ra increasing the lead to increases the thermal performance, especially when the $n < 1$, and the length and location of the thermal source, depending on Ra, n.
22	Gangawane & Manikandan	2017	The convective heat transfer rate decreased to the power-law index value. The highest rate of heat transfer is by using a uniform heat flow condition.
23	Alsabery et al.	2017	Strong improvements in heat transfer through higher wall tilt angles.
24	Hasan et al.	2018	Nu is strongly influenced by Ra, Pr, and n. The effect of changing n of the non-Newtonian fluid on the temperature distribution is explained.
25	Thohura et al.	2019	The rate of heat transfers in shear-thinning fluids within the cavity is highly dependent on Ra, Pr, and n. Increasing Ra leads to convective strength and leads to increasing Nu
26	Bashkar et al.	2019	The heat transfer is high for a non-Newtonian pseudo-plastic and low for the dilatant non-Newtonian fluid, to the Newtonian fluid.
27	Khan et al.	2020	The higher value of Ra and Ha leads to an increase in the rate of heat transfer along the fin

Ref. No.	Authors	Year of the study	Main conclusion and result
			surface.
28	Li et al.	2020	The heat transfer rate of the shear-thinning fluid rises 1.5 times at Ra increase from 10^3 to 10^5, and the entropy generation rate increases more than 2 times. For the Newtonian fluid, these changes mean a 71% increase in heat transfer and a surge of 80% in entropy generation.
29	Pandey et al.	2020a	The rate of heat transfer increase by using pseudo-plastic fluids, as for the use of dilatant fluids in applications that need a decrease in the rate of heat transfer.
30	Pandey et al.	2020b	Nu decreases with an increasing n.
31	Zhang et al.	2020	The heat transfer rate and total entropy increased production of Newtonian and shear-diluting fluids, monotonously, by lifting the aspect ratio are different.
32	Khan et al.	2020	The flow velocity and temperature of the fluid are functions n. The pressure gradient parameter increases the volume and heat flux fields.
33	Ali et al.	2020	The effect of n on Nu is considerable for Ra = 10^6 and inappreciable below this value. The effect of n and Ha on heat transfer is dominant when Ha is less than 30.
34	Rostami et al.	2020	Nu rises due to the increase in the Ra but decrease as n and Ha rise so does the Nusselt number. Nu is increased as the AR of obsticales is increased.

Ref. No.	Authors	Year of the study	Main conclusion and result
35	Ye et al.	2021	An increase in Ra as well as a decrease in n, leads to an increase in transient heat transfer. Increasing body size leads to a decrease in both the transient heat transfer ratio and the total heat transfer ratio.
36	Shahabadi et al.	2021	The fin deflection is higher for n<1, compared to n>1 and n=1. Non-Newtonian effects have few effects on the rate of heat transfer. The pseudoplastic to Newtonian and expanding effects also reduce the rate of heat transfer and increase the internal pressures in the fin.
37	Khalili et al.	2017	Ra increasing, the flow due to convection, thermophoresis phenomenon, gravity, and Brownian motion.
38	Abou-Ziyan et al.	2017	Newtonian fluids have a higher coefficient of free heat transfer than power-law fluids of 16% or more. The Nusselt number is related to n
39	Giwa et al.	2020	There is a direct relationship between Ra and Nu. The use of hybrid Nanofluids improves the thermal and flow properties of the primary fluid resulting in an improvement in the natural convection behavior.
40	Hassan et al.	2020	Local heating have significant effects on fluid circulation and heat transfer. Increase in heat transfer was observed at the edges of the hot bottom length due to the symmetrical cooling of the walls.

CHAPTER THREE

EXPERIMENTAL WORK

Experimental Work

3.1 Introduction

Natural convection in enclosures supplied with non-Newtonian fluids has gotten a lot of attention in recent years because of its utility as a heat transfer mechanism in a range of energy systems. Mahrood et al.[41] were conducted an experiment work to improve the natural convective heat transfer of a non-Newtonian fluid in a closed vertical cylindrical container made of PTFE, which is uniformly heated from the bottom and cooled from the top. It is filled with two different types of non-Newtonian nanofluids. The fluid was prepared from dispersing aluminum oxide (Al_2O_3) and titanium oxide (TiO_2) in a carboxy methyl cellulose (CMC) at a concentration of 0.5 %. They compared the efficiency of the two heat transfer fluids and verified the different aspect ratios and their effect on heat transfer. They found that the convective heat transfer of the non-Newtonian liquids increases when the concentration of the nanoparticles is low, as the increasing of concentration has an opposite effect on enhancing heat transfer of the nanofluids, but at a certain concentration the heat transfer is maximum. They also discovered that the raising of the length ratio decreases heat transfer.

In the present work, experimental investigations of natural convection heat transfer are done using carboxymethylcellulose as a non-Newtonian fluid. An experimental rig is built to obtain the experimental realization by using two concentrations of carboxymethylcellulose. Two different values of aspect ratio and two forms of obstacles shapes are used.

3.2 Test Equipment

3.2.1 Enclosure

The main part of the rig design in the experimental work is an enclosure in the form of a rectangular box. It made of galvanized alloy steel with ASTM A653 specifications and coating G90.The dimensions of the enclosure are length (L = 40 cm), width (W = 30 cm), and height (H = 30 cm). The vertical walls are made of a double sheet of galvanized steel (0.15 cm) thick, and the space between them is filled with foam to ensure insulation. The lower wall of the enclosure makes of PTFE (poly tetra fluoro ethylene), the PTFE plate acts as an insulating material. A hole of 13 cm in diameter is perforated in the lower wall of the enclosure to insert the heat source into the obstacle. The upper wall of the enclosure is cooled at a constant temperature. The aspect ratio of the enclosure is controlled by using a screw jack. Figures (3-1) and (3-2) show the photograph of the enclosure that adopted in the experiment and its schematic diagram respectively.

Figure (3- 1) enclosure (40×30×30)cm.

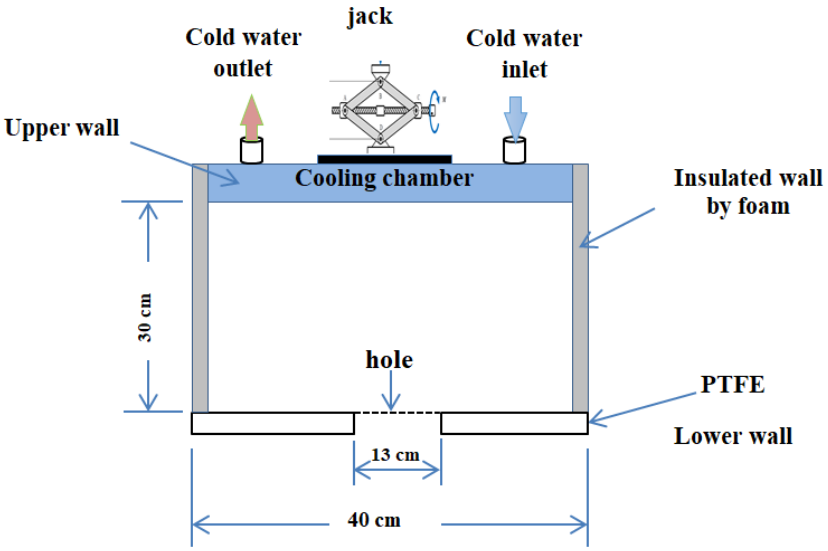

Figure (3- 2) schematic diagram of the enclosure.

3.2.2 Obstacle

Two different shapes of obstacles made of galvanized alloy steel with ASTM A653 specifications and coating G90 are involved. The first one is a hollow cuboid with dimensions (20 cm ×15 cm ×15 cm), The other is a hollow cylinder with a diameter of (20 cm) and a height of (15 cm). These two obstacles are shown in figure (3-3).

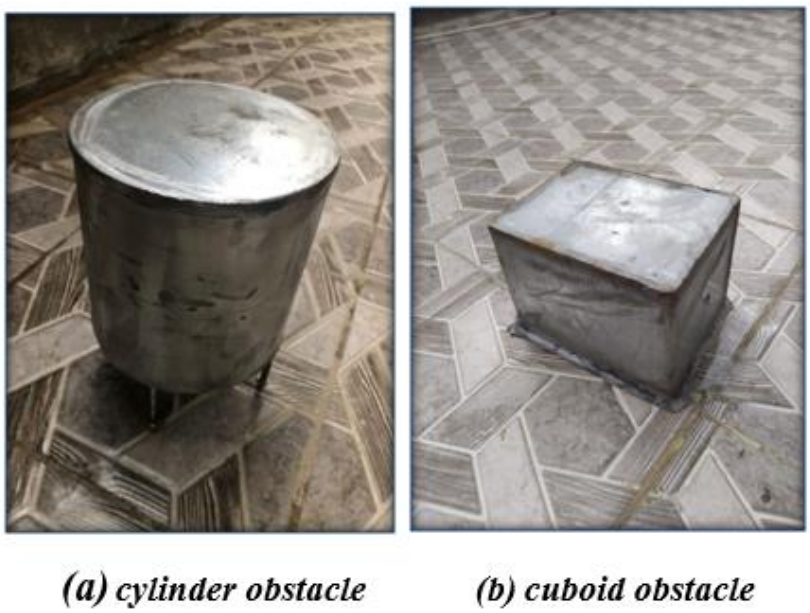

Figure (3- 3) shapes of obstacles.

3.2.3 Heater

The heater is placed inside the obstacles to heat its walls at a constant heat temperature. It is insulated by glass wool. The specifications of the heater are (HP-1010A), with voltage range from (220 to 240 volts), electrical power (1000 watts), and with a frequency of (50-60 Hz). Figure (3-4) shows a photograph of the heater.

Figure (3- 4) heater.

3.2.4 Voltage Variation Device

The electric current value of the heater is controlled by using a variable voltage device as shown in figure (3-5). This device can provide different values of voltage in the range (0-260 volts). The required value of the voltage is reached by changing the internal resistance.

Figure (3- 5) voltage variation.

3.2.5 Power analyzer Device

The value of the power generated in the heater is determined by using a power analyzer. Digital power analyzer type LUTRON model (Dw – 6091) with a maximum current (10 A) and maximum voltage (600 V) is used to convert an analog voltage signal from a power supply into digital data that it is possible to read, as shown in figure (3-6).

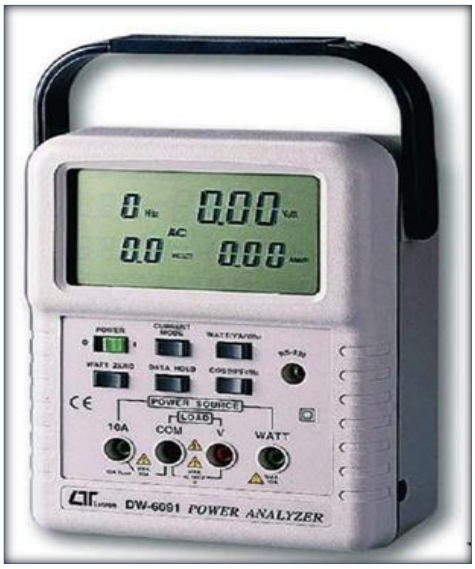

Figure (3- 6) power analyzer device.

3.2.6 Cooling System

The cooling system consists of a cold water tank, cooling chamber, and water pump. Tank with volume (25 L) is supplied cold water to the cooling chamber. It is made from galvanized alloy steel with ASTM A653 specifications and coating G90. It is fixed at the upper wall of the enclosure. The shape of the cooling chamber is rectangular with dimension (7 cm ×40 cm ×30 cm) is used to keep the upper wall of the enclosure at constant cold temperature as a boundary condition. The cold water flows from the cold water tank to the cooling chamber as a circulation cycle by using a water pump. The flow meter controls the flow rate of cold water. This cooling system is illustrated in figure (3-7).

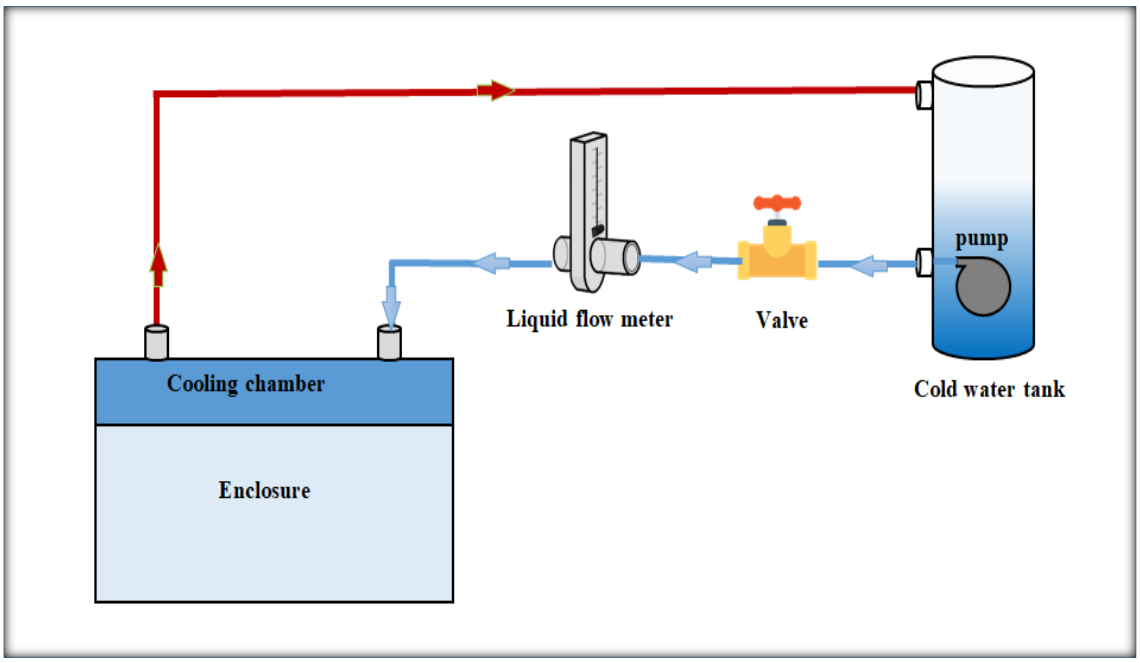

Figure (3- 7) schematic diagram of cooling.

3.3 Measuring Devices

3.3.1 Temperature Recorder Device

Temperature recorder device type LUTRON and model BTM-4208SD of accuracy (±0.4%) °C with 12 channels is displayed in figure (3-8). The temperature reading data are stored in the S.D card, these data are recorded with time and can be loaded as an excel software. It uses many different types of thermocouples such as T, S, R, K, and J. It is working as a data logger on a manual basis, or data logger (automatic) with time range (1 to 3600) seconds.

In the present work, two devices of temperature recorder are used to measure the temperature inside the enclosure, and twenty four thermocouples type (K) are used to measure the temperature, with a range of (-50 ^{o}C to 1000 ^{o}C), as shown in figure (3-9).

Figures (3-10) and (3-11) represent the position of thermocouples inside the enclosure for two shapes of obstacles.

Figure (3- 8) temperature recorder device.

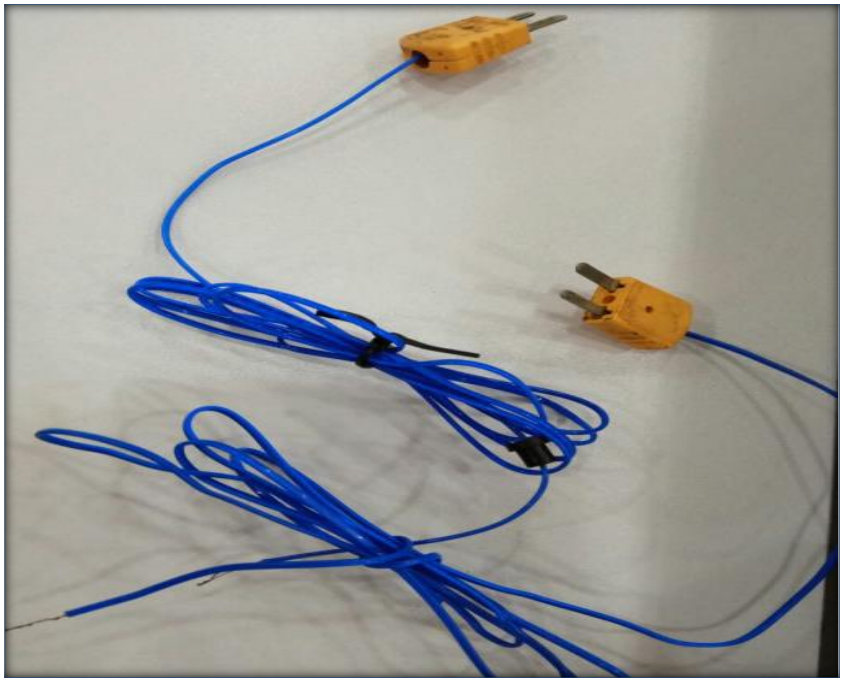

Figure (3- 9) thermocouples type (K).

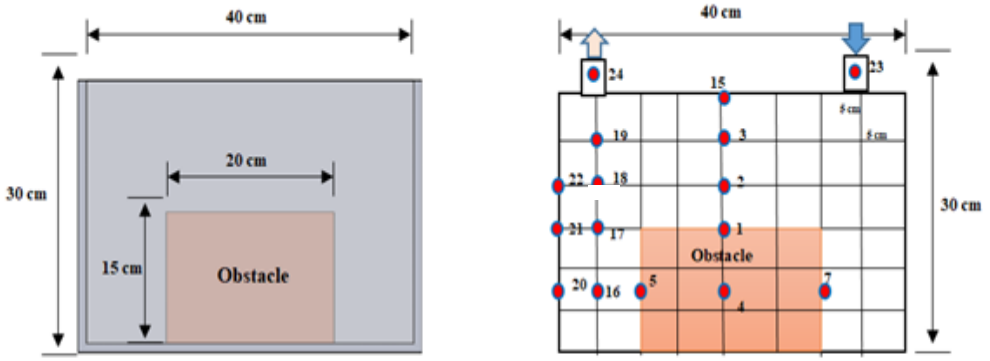

a- Front View

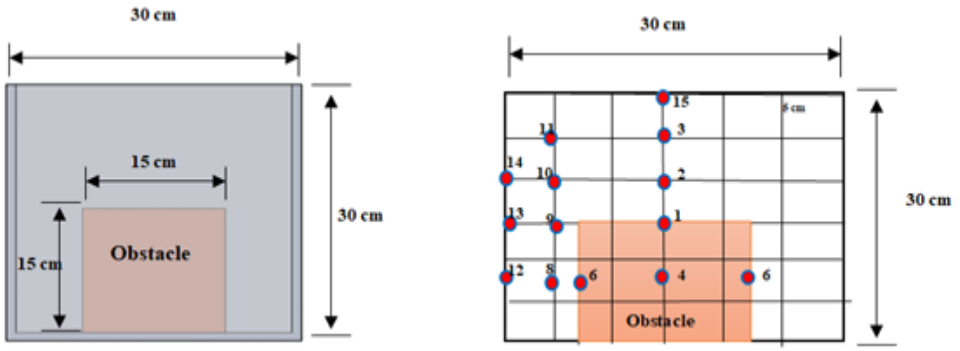

b- side View

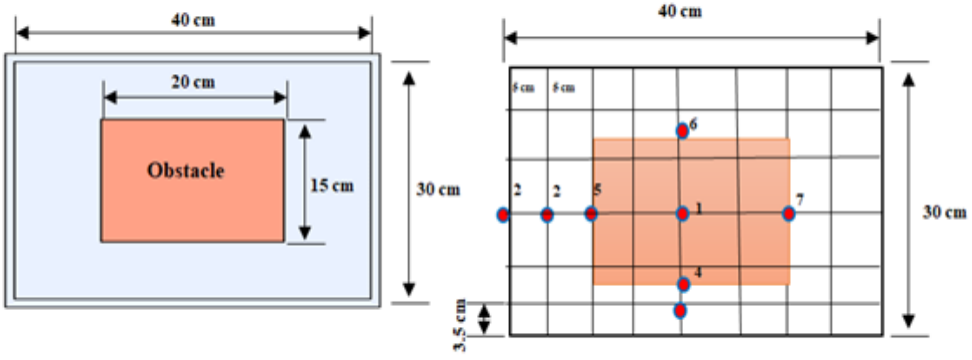

c- top View

Figure (3- 10) thermocouples location in the enclosure with cuboid obstacle.

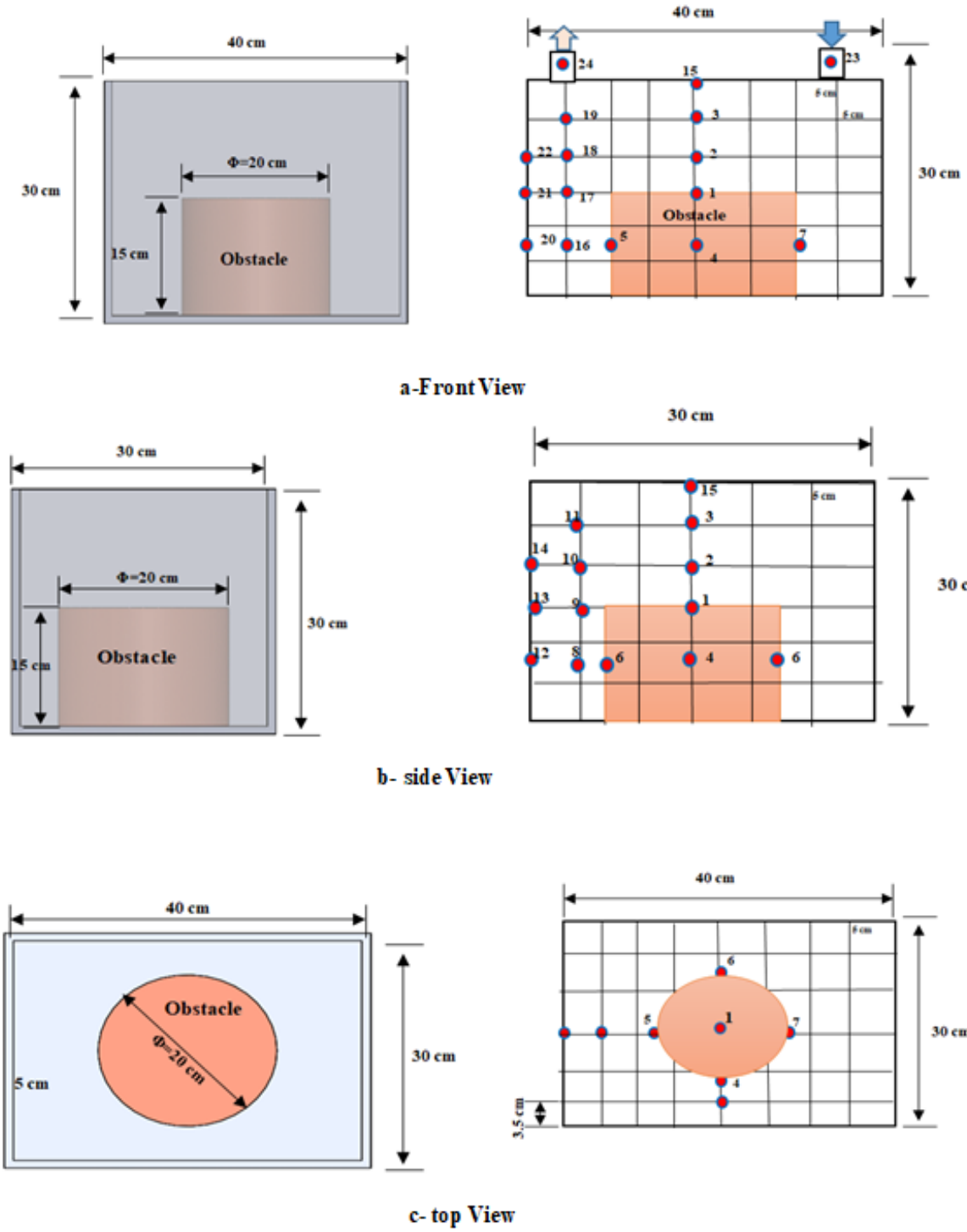

Figure (3- 11) thermocouples location in the enclosure with cylindrical obstacle.

3.3.1.1 Temperature reading calibration

A digital calibration device (PROVA MODEL 123) is used to calibrate temperature readings of the 24 thermocouples, as shown in figure (3-12). The calibration signal of the device is determined by The signal being converted into a temperature reading by the device, which is powered by the batteries. Next, the calibration signal of the device is transmitted to the thermometer through a thermocouple wire. The following points summarize the device calibration steps:

1. Turn on the electricity for about 1 minute, till the sign vanishes.
2. For calibration, connect the thermocouple connectors, corresponding K-type connections to the calibration device's terminals. The sliding switch should be set to positions C and F.
3. Press any key on the keypad (including the minus button) to directly enter the temperature value.
4. Enter a temperature value between (10 and 50) ^{o}C as shown schematicly in figure (3-13).
5. Figure (3-14) depicts the relationship between the temperature measurements of the two devices. For adjusting the measured temperature measurements, a polynomial equation is derived:

$$T_{re} = 4E\text{-}5T^{3}_{calib} - 0.0044\ T^{2}_{calib} + 1.1499T_{calib} - 1.1594 \quad \text{……..…} \quad (3.1)$$

Figure (3- 12) calibration temperature reading device (PROVA MODEL 123).

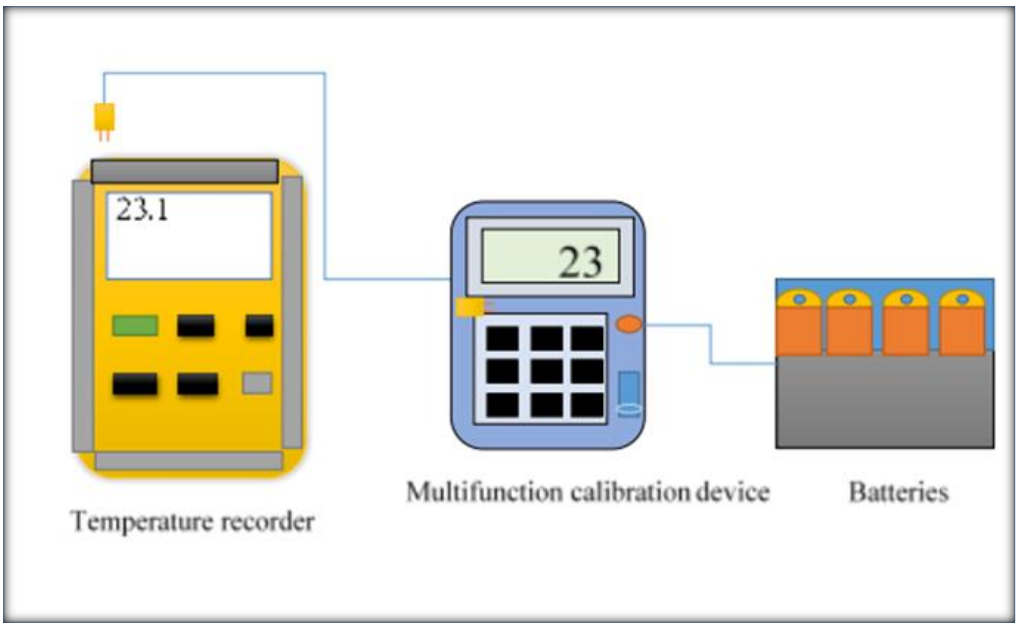

Figure (3- 13) schematic diagram of calibration of the temperature recorder.

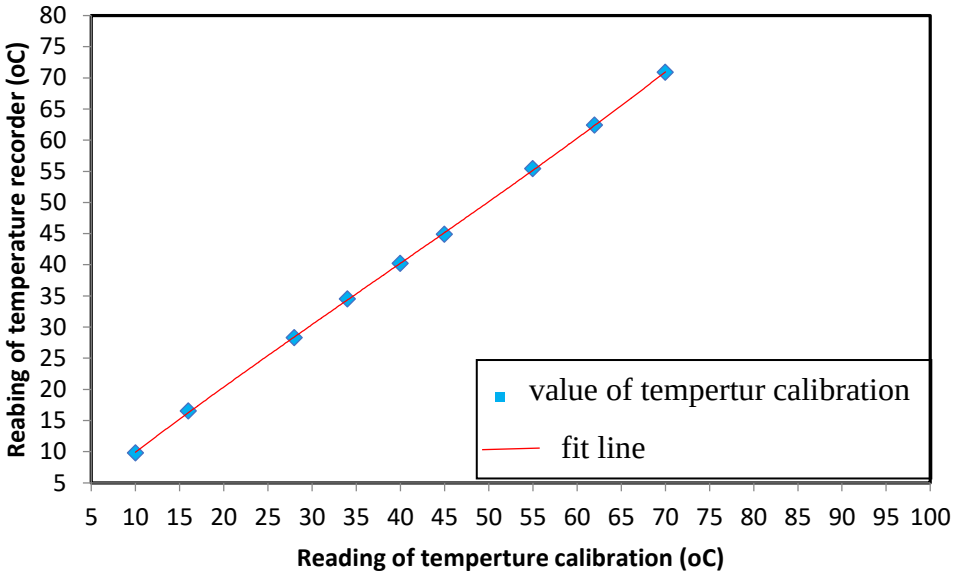

Figure (3- 14) curve of temperature calibration.

3.3.2 Flowmeter

The flowmeter model ZYIA is used to measure the flow rate of cold water. The flow enters the bottom of the vertical tapered tube and causes the float to move upward. Weight and buoyancy forces are balanced with an increase in floatation to a point in the tube, and a pull force ranging from (0.5 to 4) litters/minute as shown in figure (3-15) can be controlled by a valve attached to it. The flowmeter is vertically connected to measure the flow rate of the cold water that present from the cold water tank before entering the cooling system.

Figure (3- 15) flow meter.

3.3.2.1 Calibration of the liquid Flow Meter

The flowmeter is calibrated by using a volume-scaled tank and a stopwatch to clock the time it takes to fill a specific volume of the tank. Calibrations are performed with distilled water. The findings are close, as presented in figure (3-16).

$$Q_{re} = 0.106\ Q^3_{calib} - 0.737\ Q^2_{calib} + 2.561\ Q_{calib} - 0.744 \qquad \text{.....(3.2)}$$

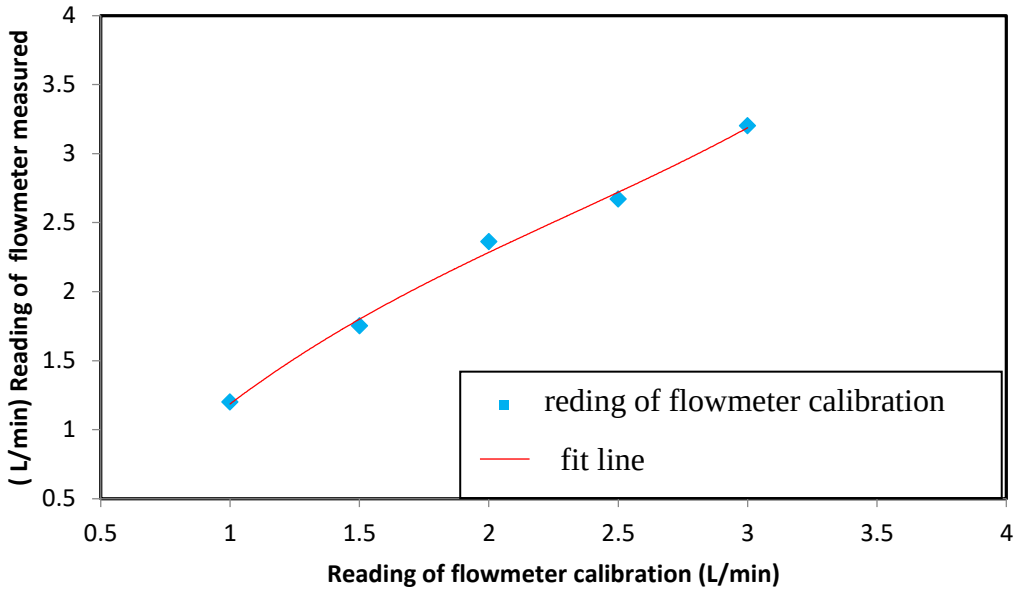

Figure (3- 16) flow meter calibration.

3.4 Equipment Assembly

The photograph of a rig of the equipment used in this experimental work is shown in figure (3-17). The schematic diagram rig of this equipment is seen in figure (3-18).

1	Enclosure	5	Valve	9	Power analyzer (Wattmeter)
2	Thermocouple's wire	6	pump	10	Power supply
3	Temperature recorder	7	Constant temperature bath	11	Cooling chamber
4	Liquid flow meter	8	jack		

Figure (3- 17) photograph rig of equipment.

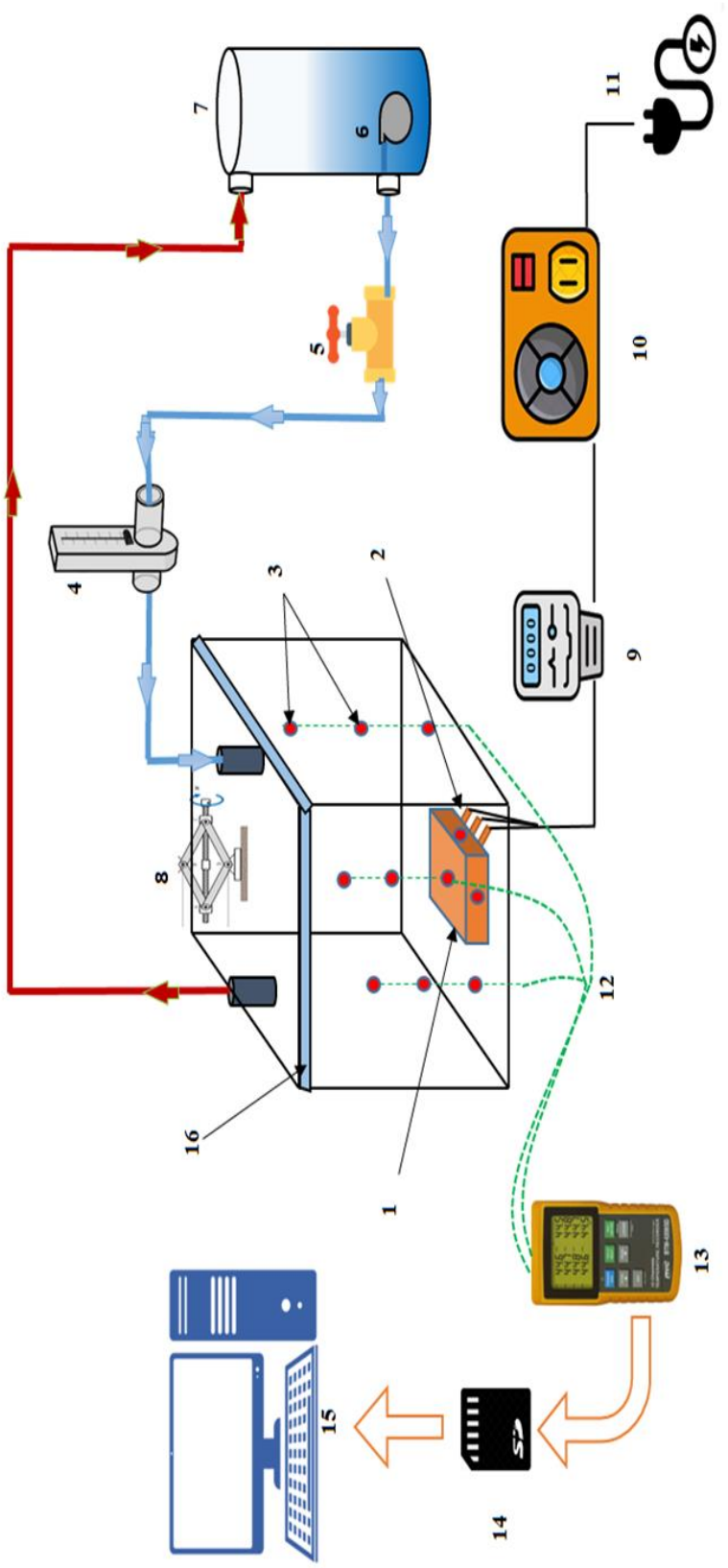

1	Obstacle	5	Valve	9	Power analyzer (Wattmeter)	13	Temperature recorder
2	Electrical heater	6	pump	10	Power supply	14	Memory card
3	Temperature measuring points	7	Constant temperature bath	11	Electrical source	15	Personal computer
4	Liquid flow meter	8	jack	12	Thermocouple's wire	16	Cooling chamber

Figure (3- 18) schematic diagram of rig

3.5 Working fluid

A Carboxymethylcellulose (CMC) with two concentrations 0.5 % and 1 % is used as a non-Newtonian working fluid. Also, water is used as a Newtonian fluid.

3.5.1 Carboxymethylcellulose

The reaction of cellulose with chloroacetic acid in the presence of sodium hydroxide gives carboxy methyl cellulose (CMC). It is outfitted from SINOCMC CO., LTD - China as a powder with cas.NO.9000-11-7, viscosity at 20 ^{0}C (250 Cp). Figure (3-19) shows a powder of CMC.

Figure (3- 19) powder of Carboxy methyl cellulose(CMC).

3.5.1.1 Preparation of CMC

Two different concentrations of CMC are prepared at 17 °C using the same prosedure of proportion that mentioned by Maiti and Bidinger [42]:

$$percentage\ concentration = \frac{\frac{m\ of\ CMC}{\rho\ of\ CMC}}{\frac{m\ of\ CMC}{\rho\ of\ CMC} + \frac{m\ of\ water}{\rho\ of\ water}} \qquad \ldots\ldots\ldots\ldots\ldots\ldots (3.3)$$

The distilled water of (31.5 L) is taken into a volumetric flask and dry CMC powder is added with weights (318 g) and (156 g) corresponding to the two concentrations (1%) and (0.5%), respectively. For homogeneous mixing

quality and to avoid sedimentation problems use a Hamilton mixer which features a single spindle, 3 test speeds (13,000, 16,000, 18,000) rpm, and a power source (230 VAC / 50-60 Hz motor). Figure (3-20) presents a Hamilton mixer that is used in the Nano-fluids Laboratory of the Department of Polymer Engineering in the College of Materials Engineering at the University of Babylon.

Figure (3- 20) Hamilton mixer.

The mixing is continued for (1) hour to ensure complete dissolution of the CMC. The prepared solution is poured into a properly labeled container and closed. The prepared solution is kept at rest at room temperature for (24) hours before physical properties are measured.

3.5.1.2 Physical properties of CMC

1. Density

The sample size is weighted for different concentrations of CMC, and divided by the volume to calculate density. The measurements are repeated three times and then the average value is taken to obtain an accurate magnitude. Figure

(3-21) represents the measurement density device. The measurement is carried out in the Nano-fluids Laboratory in the Polymer Engineering Department of the College of Materials Engineering at the University of Babylon. The results of the experimental measurements of density for two concentrations of CMC are shown in table (3-1).

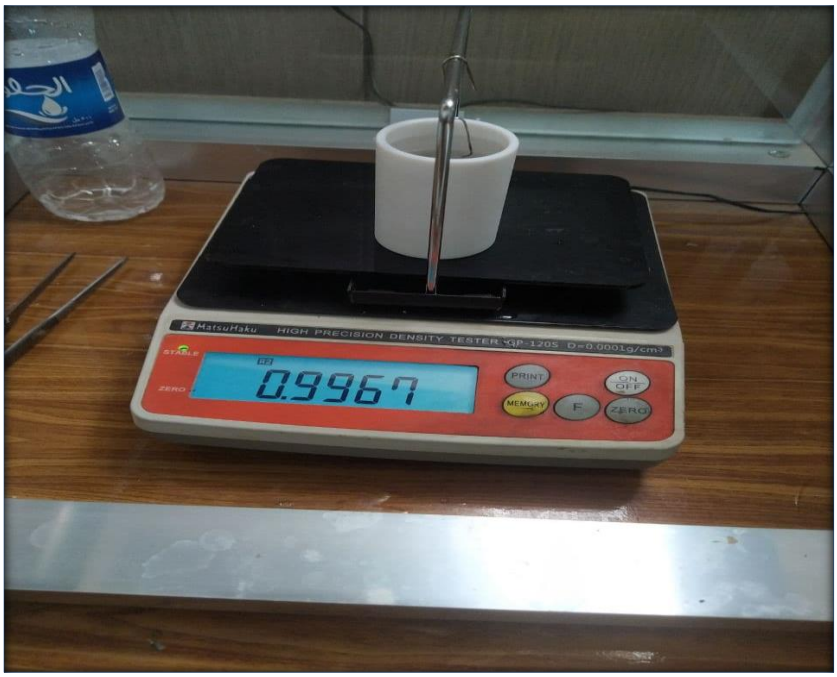

Figure (3- 21) measurement density device.

2. Specific Heat capacity

The specific heat capacity of CMC is determined by a Differential Scanning Calorimeter (DSC), which is a laboratory technique used to study the changes that occur in the polymer when heated. It consists of two vessels, the first container contains the tested sample, while the second contains the reference sample. The two bowls are placed in an oven set to a specified temperature, such as 10 degrees per minute. Each container has a thermal sensor that is connected to a computer and records the temperature change required to bring the sample to the same temperature as the reference sample. When the two vessels are heated the computer begins to draw the difference between their thermal energies as a function of the temperature. Temperatures are recorded and plotted on a graph.

Many properties are known from the graph including the specific heat capacity. The test is performed in the laboratories of the Polymer Department of the College of Materials at the University of Babylon. Figure (3-22) shows the device used with its accessories. The values of specific heat capacity for two concentrations of CMC are listed in the table (3-1).

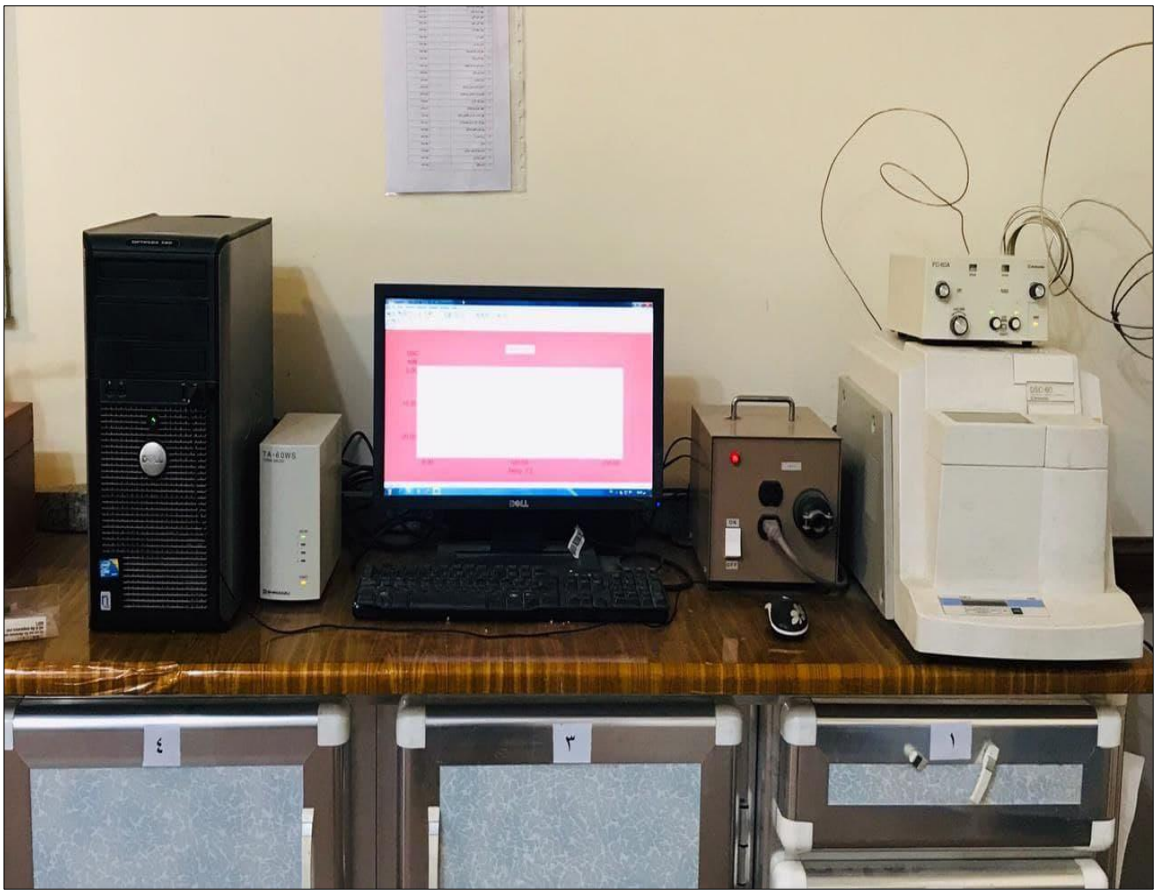

Figure (3- 22) Differential Scanning Calorimeter (DSC).

3. Viscosity

The digital viscometer model [CON-PLATE] is used to measure the viscosity of CMC, as shown in figure (3-23).

Figure (3- 23) viscometer.

A viscometer has rotated a spindle immersed in a CMC sample and connected to a calibrated spring. The deflection of the spring is used to determine the viscous force of the fluid against the spindle. A rotary transducer that provides a torque signal is used to measure spring deflection. Experimental measurements of viscosity for both concentrations of CMC are tableted in a table (3-1). The test is done in the Nano fluid laboratory of the Polymers Department, Faculty of Materials Engineering, University of Babylon.

4. Thermal Conductivity

The accurate and quick technology of the transient hot-wires (THW) method is used to evaluate the thermal conductivity of CMC. A KD2 pre thermal properties analyzer (Decagon Devices, Inc., USA) is used in this case, as illustrated in figure (3-24). Before starting any test, the thermal conductivity analyzer is calibrated using distilled water with a maximum inaccuracy of 5%. It should be noted that each measurement is repeated three times to ensure the

accuracy of the results, as the results showed that the thermal conductivity of water is greater than that of a carboxymethyl cellulose solution at both concentrations, as mentioned before [43], [44]. The test takes place in the Laboratory of Nanofluids Nanofluids, Department of Polymers, College of Materials Engineering, University of Babylon. The results of thermal conductivity measurements for CMC concentrations are shown in Table (1-3).

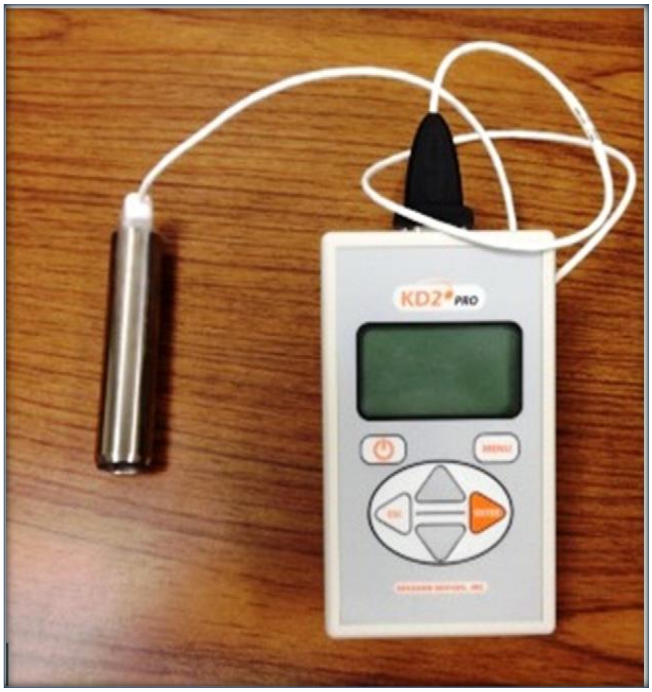

Figure (3- 24) KD2 pre thermal properties analyzer (Decagon Devices, Inc., USA).

Table (3- 1) experimental value of physical properties for CMC

Properties	**CMC/ Water Concentration 0.5 g/l**	**CMC/ Water Concentration 1 g/l**
Density [kg/m3]	998.1	1007.3
Specific heat [J/kg.K]	4203	4203
Viscosity [Pa.s]	0.001592	0.002856
Thermal Conductivity [W/m.K]	0.36	0.25

3.5.2 Water

The second fluid used in the experiment is pure water with a salt content of approximately 3%. It is a Newtonian fluid characterized which has density (997.1kg/m13), thermal conductivity (0.613W/m. k), and specific heat (4179 J/kg. k) as illustrated by Garbadeen et al.[45]. The fluid was prepared in the fluid laboratory of the Department of Mechanics, College of Engineering, University of Babylon.

3.6 Experimental Procedure

The experimental work is carried out in three cases:

1. Test One

In this case, a CMC of 0.5% concentration with a power-law index (0.72) at temperature of 15 ^{o}C is used as a working fluid. The experimental procedure consists of the following stages:

1. set the value of aspect ratio of enclosure to 0.5 and use the hollow cuboid obstacle. Fill the enclosure with CMC so that no bubbles form and wait for it to settle.

2. Supply an electrical power to the heater at a value of 105.4 W using a digital power analyzer connected between the heater and the voltage variation device. The heater is working until the obstacle walls reach the hot temperature of (20 ^{o}C).

3. The constant cold temperature of the upper wall is fixed at (15 ^{o}C). The cold temperature is achieved by controlling the temperature of the inlet water to the cooling chamber. The value of the water flow rate (3 L/min) is measured by a flow meter.

4. (24) thermocouples are installed in different locations inside the enclosure, as shown in figure (3-10). The data logger with SD-RAM was turned on to read

and save temperature measurements during device operation time. The temperature reading is measured after being calibrated at all specified points in the container field.

5. It is found after 20 minutes of working time, the system reached a stable state, and the process is repeated three times until the readings are taken.
6. Repeat all the previous steps (1 to 5), with another value of aspect ratio (0.75).
7. Iterate all the previous steps (1 to 6), by using a hollow cylinder obstacle shape.
8. Recur all the preceding steps, change the value of the power supply to (220, 326.29, 415, and 435.456 W) to get the hot wall temperature of the obstacles are (25, 30, 35, and 40 ^{o}C), respectively.

The temperature measurements are presented in Appendix (A) for both shapes of obstacle and two values of aspect ratio (from the table (A-1) to (A-4)).

2. Test two

In this case, CMC of 1% concentration is used as a working fluid with an index power law (0.59) and an initial temperature 15 ^{o}C. All the steps (1 to 8) that are performed in test one are repeated.

Tables (A-5) to (A-8) in Appendix (A) are shown the temperature measurement. For both shapes of obstacle and two values of aspect ratio.

3. Test three

In this test, water is used as a working fluid which is a Newtonian fluid (n = 1). This test is done to compare its behavior results with CMC. The initial temperature of water is 15 ^{o}C. All steps (from 1 to 8) that are performed in one test are repeeated.

The temperature measurements are presented in Appendix A for both shapes of obstacle and two values of aspect ratio (see the tables (A-9) to (A-12)).

3.7 Experimental Analysis

1. Heat Transfer Coefficient

The heat transfer coefficient (h) inside the enclosure is obtained by cooling Newton's law:

$$h = \frac{q'}{(Th-Tf)} \qquad \text{..... (3.4)}$$

where:

q`: heat flux of electric heater is [46] :

$$q' = \frac{V \cdot I}{A} \qquad \text{..... (3.5)}$$

2. Nusselt number

It is the ratio of heat transfer rate by convection to heat transfer rate by conduction in a fluid [46] as :

$$\overline{Nu} = \frac{h \cdot L}{K} \qquad \text{..... (3.6)}$$

3. Prandtl number

In natural convection, the Prandtl number is a dimensionless number that describes the relative thickness of velocity and thermal boundary layers [27] :

$$\Pr = \frac{m(\alpha)^{(n-2)} L^{(2-2n)}}{\rho} \qquad \text{..... (3.7)}$$

4. Rayleigh Number

Rayleigh number (Ra) is the product of Grashof Number (Gr) and Prandtl numbers (Pr). The Grashof number is a dimensionless quantity that represents the ratio of buoyant force to viscous force within an enclosure [27]:

$$\mathrm{Gr} = \frac{g\beta(Th-Tc)L^{(4n-1)}}{\alpha^{(2n-2)}\left(\frac{m}{\rho}\right)^2} \qquad \text{..... (3.8)}$$

The Rayleigh Number expressed by Thohura et al., [27] as:

$$\mathrm{Ra} = Gr.\mathrm{Pr} = \frac{g\beta(Th-Tc)L^{(2n+1)}}{\left[\alpha^{n}\left(\frac{m}{\rho}\right)\right]} \qquad \ldots\ldots\ldots\ldots\ldots\ldots (3.9)$$

Tables (B-1) to (B-6) in Appendix (B) display the calculated values from the experimental analysis of all cases and all their variables.

3.8 Estimating Uncertainty

The discrepancy between the real and measured values is known as measurement error. However, it is difficult to determine which of these readings is the real quantity. As a result, while presenting experimental data, it is important to compute the uncertainty. In general, measurement uncertainty is defined as the number of mistakes or doubts caused by the measuring device, the measurement procedure, human error (operator skills), and operational conditions [47]. The standard uncertainty (S.u) may be computed for any collection of data by equation detailed by Bell [48] as:

$$\mathrm{S.u} = \frac{S.D}{\sqrt{N}} \qquad \ldots\ldots\ldots\ldots\ldots\ldots (3.10)$$

Where:

N: is the total number of measurement in each case.

S.D: is the standard deviation which is calculated as :

$$\mathrm{S.D} = \sqrt{\frac{\sum_{i=1}^{N}\left(xi-x_{\text{average}}\right)^{2}}{(N-1)}} \qquad \ldots\ldots\ldots\ldots\ldots\ldots (3.11)$$

Where:

x_{average} : is the average reading of temperature. The average experimental values of reading in each case were repeating (N) time.

The value of average readings is calculated as:

$$x_{\text{average}} = \frac{1}{N}\sum_{i=1}^{N} xi \quad \text{..... (3.12)}$$

Where:

xi: is represented the values for measurements data of temperature or any function measured in each case.

Table (3-26) shows a form of the standard temperature uncertainty results in the case of using CMC with a concentration of 1%, cuboid obstacle, AR fixed at (0.5), and hot temperature of walls (30 °C).

The other standard temperature uncertainty results are presented in Appendix (C).

Table (3-2) standard temperature uncertainty results

Point	S.D	Point	S.D	Point	S.D	Point	S.D
T1	0.346	**T7**	0.088	**T13**	0.185	**T19**	0.296
T2	0.115	**T8**	0.152	**T14**	0.075	**T20**	0.231
T3	0.14	**T9**	0.115	**T15**	0.121	**T21**	0.145
T4	0.176	**T10**	0.233	**T16**	0.2	**T22**	0.178
T5	0.145	**T11**	0.26	**T17**	0.15	**T23**	0.317
T6	0.147	**T12**	0.12	**T18**	0.21	**T24**	0.288

CHAPTER FOUR

THEORETICAL WORK

Theoretical Work

4.1 Introduction

Natural convection in a fluid-filled container refers to the movement of fluids produced by density changes with temperature or concentration in the presence of a gravitational field. It is important since this geometry is utilized in a variety of engineering and geophysical systems. Analytical solutions are feasible in some specific scenarios linked to engineering as well as natural boundary conditions placed on a particular system due to the nonlinear character of the governing equations. Natural convection in a shallow rectangular container explored by Lamsaad et al. [49] the container is filled with a non-Newtonian liquid heated from below. It cooled from the top by exposing it to a homogeneous heat flow, with adiabatic vertical sides. The behavior of Non-Newtonian fluid is fairly sensitive to temperature patterns, heat transfer, and fluid movement. They showed that when the power-law index is low (shear-thinning fluids), the flow system improves heat transfer through convection, but when it is high as (shear-thickening fluids), it has the opposite effect.

In the present work, natural convection in rectangular enclosures with hot obstacle-filled non-Newtonian fluids is studied numerically by using the Multiple Physics COMSOL 5.5 program. A 3-D numerical model is used to analyze the behavior of fluid flow within the enclosure, heat transfer, and temperature variations (varying the hot wall temperature). Different fluids concentrations, aspect ratio, and shapes of obstacles are studied in this work.

4.2 Geometry modeling

In COMSOL program modal builder, the rectangular enclosure geometry is set to be done in 3-D. In this study, the geometry is constructed to depict the case study model that is a rectangular enclosure with an obstacle. Cuboid obstacle shape with dimensions of (15×20×15) cm. While the cylindrical obstacle has a diameter of 20 cm and 15 cm height. Two heights of the enclosure 20 cm and 30 cm, are used to change the value of the aspect ratio in order to stady its effect on the heat transfer rate. The length and width of the enclosure are 30 cm and 40 cm respectively, which remain constant. The half symmetrical geometry in parallel to gravity direction is used to make the solution easier. Surface from sketches is created by using the geometry icon. Once the geometry is completed, the object will be imported into the mesh. Figure (4.1) shows the geometry modeling and the using design modeler for both shapes of obstacles.

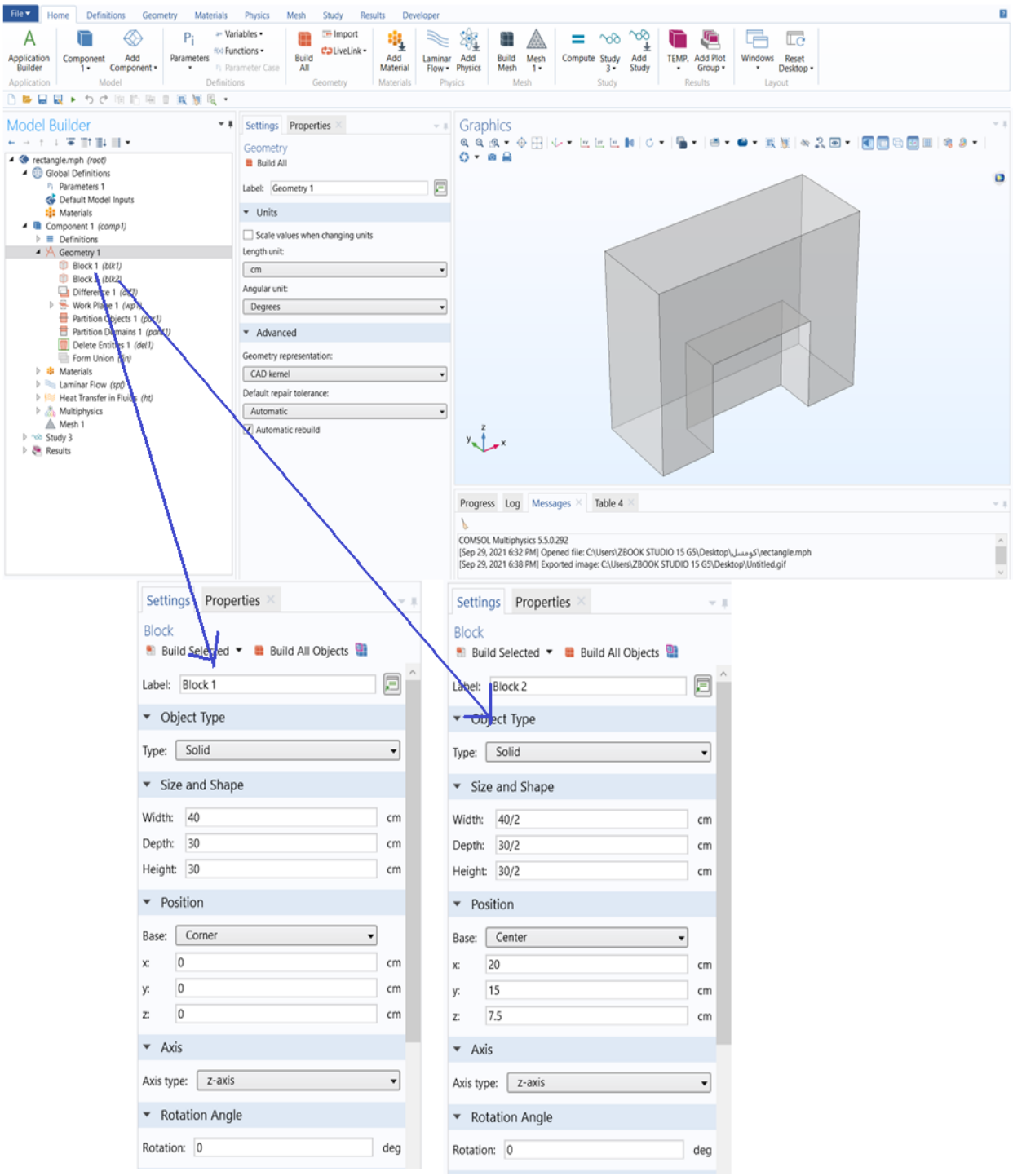

(a) the enclosure with cuboid obstacle.

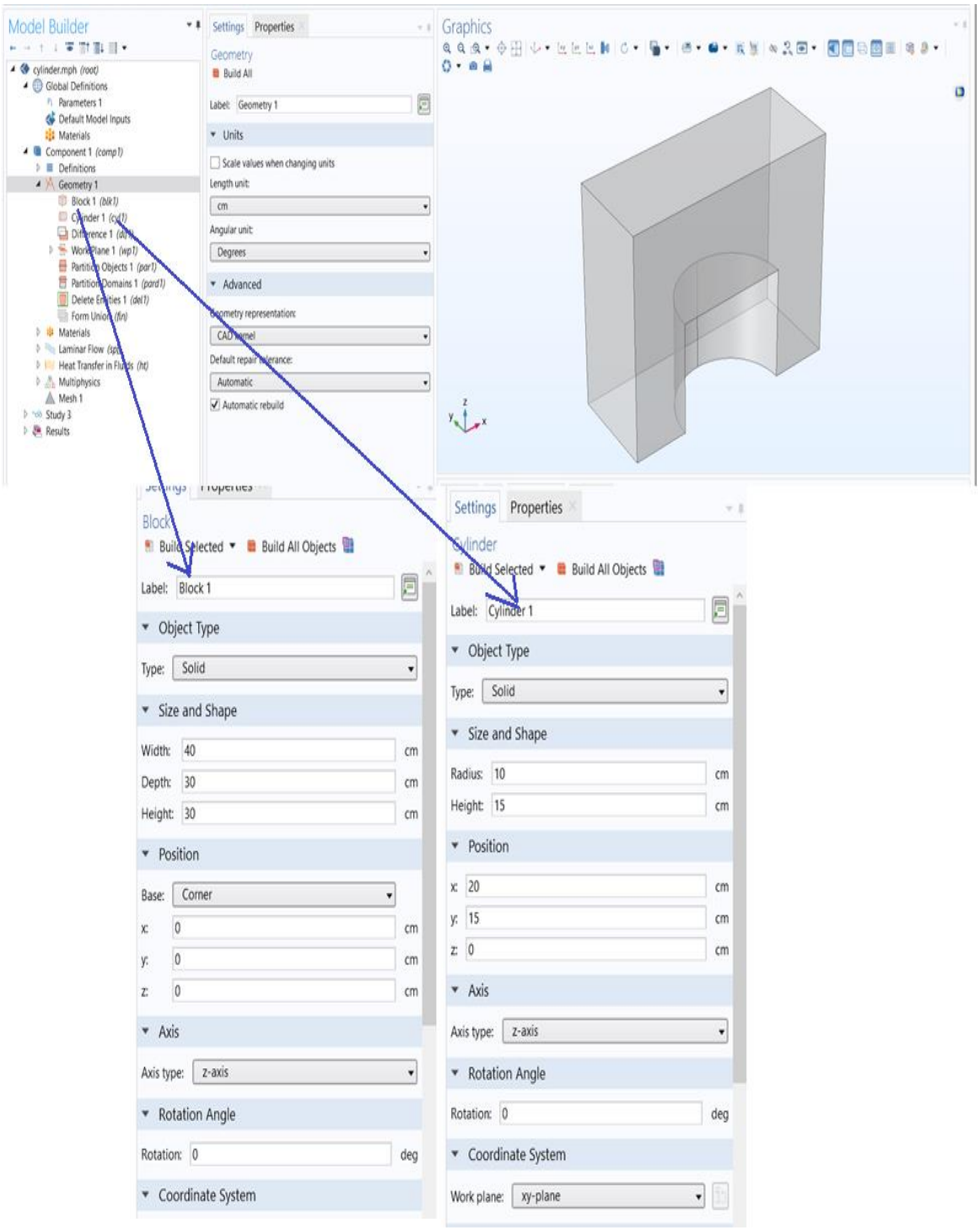

(b) the enclosure with cylindrical obstacle.

Figure (4- 1) geometry modeling using design modeler.

4.3 Governing Equations

The momentum and heat transport equations are used. The partial differential equations (PDEs) of the present system are complex, the finite element method converts these equations into an algebraic matrix depending on the boundary conditions and the mesh distribution. The algebraic equations of the momentum transport are solved first at the initial temperature condition. Then, the resultant velocity profile is introduced to the heat transfer equation in the convection term. The resultant temperature distribution is used to estimate the physical properties of momentum and heat transport. The momentum transport equation is solved again with a new temperature distribution and so on. The governing three-dimensional equations in the Cartesian coordinate system for the present study are described in this section by using the following assumptions and boundary conditions :-

1- The flow is considered as a steady state, three dimensional, incompressible, and laminar.
2- Radiation mode of the heat transfer is considered negligible.
3- Internal heat generation is neglected.
4- No slip in the walls of the enclosure.
5- The boundary conditions for the momentum transport are zero pressure at the top of the rectangular enclosure and the gravity for the whole enclosure. Th and Tc heat transfer boundary conditions are :

   Th is used at the hot surface (the five faces of the obstacle), Tc is used at the cold surface (the upper wall of the enclosure, and the other walls are isolated as shown in figure (4-2).

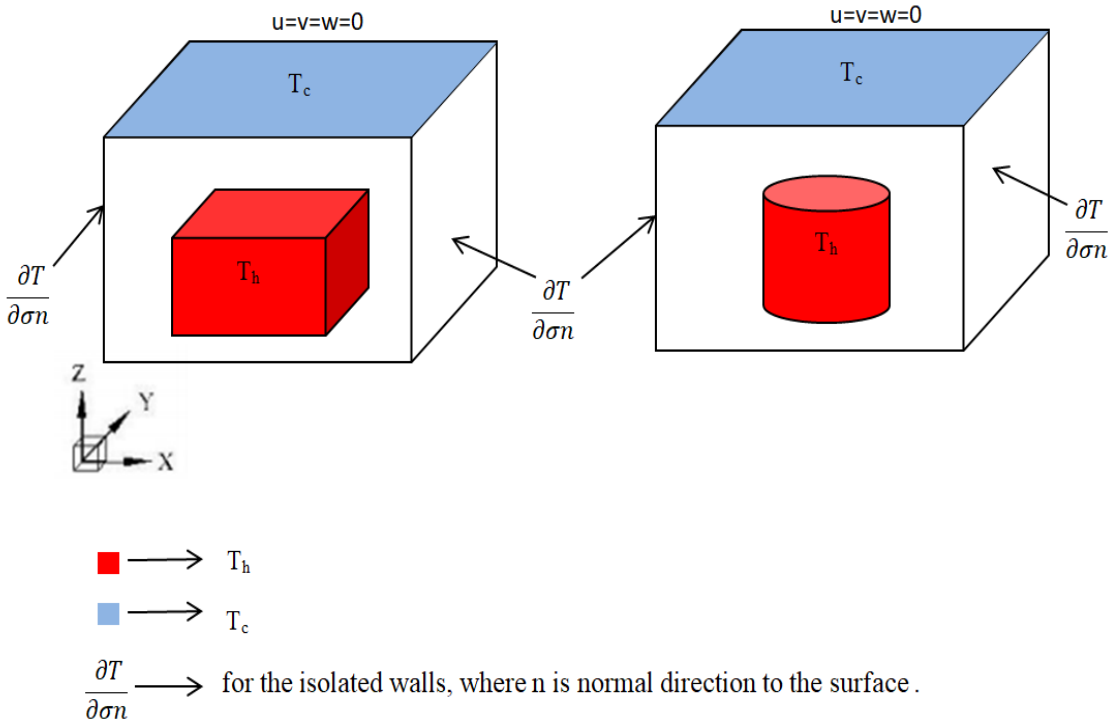

Figure (4- 2) physical domain and boundary conditions.

Therefore, the continuity, momentum and energy equations in the dimensional form are given by [50]:

- **Continuity equation**

$$\frac{\partial u}{\partial x} + \frac{\partial v}{\partial y} + \frac{\partial w}{\partial z} = 0 \qquad \text{.....(4.1)}$$

- **Momentum equations**

x-component of the momentum equation: -

$$u\frac{\partial u}{\partial x} + v\frac{\partial u}{\partial y} + w\frac{\partial u}{\partial z} = -\frac{1}{\rho}\frac{\partial p}{\partial x} + \frac{\mu}{\rho}\left(\frac{\partial^2 u}{\partial x^2} + \frac{\partial^2 u}{\partial y^2} + \frac{\partial^2 u}{\partial z^2}\right) \qquad \text{.....(4.2a)}$$

y-component of the momentum equation: -

$$u\,\frac{\partial v}{\partial x}+v\,\frac{\partial v}{\partial y}+w\,\frac{\partial v}{\partial z}=-\frac{1}{\rho}\frac{\partial p}{\partial y}+\frac{\mu}{\rho}\left(\frac{\partial^2 v}{\partial x^2}+\frac{\partial^2 v}{\partial y^2}+\frac{\partial^2 v}{\partial z^2}\right) \quad \text{……..……(4.2b)}$$

z-component of the momentum equation: -

$$u\,\frac{\partial w}{\partial x}+v\,\frac{\partial w}{\partial y}+w\,\frac{\partial w}{\partial z}=-\frac{1}{\rho}\frac{\partial p}{\partial z}+\frac{\mu}{\rho}\left(\frac{\partial^2 w}{\partial x^2}+\frac{\partial^2 w}{\partial y^2}+\frac{\partial^2 w}{\partial z^2}\right)+\rho\beta g(T-Tc)$$

…… (4.2c)

- **Energy equation**

$$u\,\frac{\partial T}{\partial x}+v\,\frac{\partial T}{\partial y}+w\,\frac{\partial T}{\partial z}=\frac{k}{\rho\, cp}\left(\frac{\partial^2 T}{\partial x^2}+\frac{\partial^2 T}{\partial y^2}+\frac{\partial^2 T}{\partial z^2}\right) \quad \text{…….…….....} \ (4.3)$$

The physical properties are taken from experimental tests of resultant fluid and solution. The physical properties (ρ, μ, k, cp) are a function of temperature.

4.3.1 Physical properties of non-Newtonian fluids

Viscosity is mainly affected by the use of non-Newtonian fluids. The nonlinear behavior between shear stress and shear rate is the hypothetical approach for non-Newtonian fluids. For the Ostwald-De Waele (power-law model), viscosity has been validated in the COMSOL Multiple Physics commercial package.Viscosity of a non-Newtonian fluid is calculated as [20]:

$$\mu = m\,(\dot{\gamma})^{n-1} \quad \text{……..... (4.4)}$$

And, the Shear rate is evaluated as:

$$\dot{\gamma} = \nabla u + (\nabla u)^{T} \quad \text{……..(4.5)}$$

When (n = 1) the fluid becomes Newtonian. The velocity tensors effects viscosity magnitude and become tensor component, when (n) is

greater or less than unity. Chhabra and Richardson [8] showed many fluids,such as polymer exhibit a shear-thinning property in the range of 0.1 ≤ n < 1 depending on the concentration and molecular weight of the polymer. Therefore, the power-law index of 0.59 and 0.72 are chosen in this work to analyze power-law fluids according to the CMC concentration in water, and the values for (n) are determined by the equation (4.4).

4.4 Meshing and the grid-independent test

Mesh is defined as the open spaces in a net or network. After the geometry is completed and stabilizing the boundary conditions, it is necessary to determine the correct meshing condition to obtain a more accurate display of the result. The choice of network type depends on several factors, such as system architecture and flow type. There are many types of mesh, such as extremely coarse, extra coarse, coarse, coarser, normal, and fine mesh. Figure (4-3) illustrated the setting of the mesh.

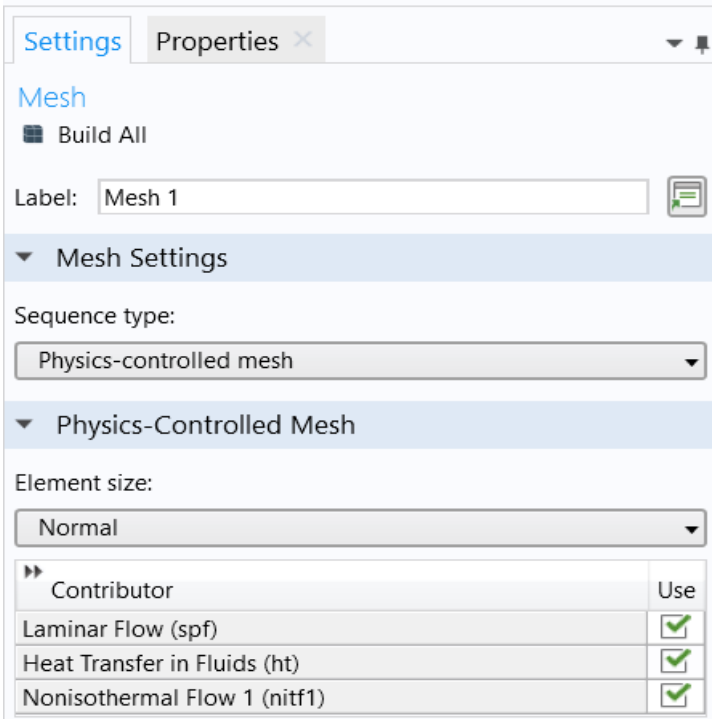

Figure (4- 3) mesh setting.

In this study, for cuboid obstacle at AR=0.5 the number of the elements are considered as 164160, where the number of the edge elements , the boundary element, and the vortex elements are 559, 12420 and 16, respectvely. While at AR=0.75 the number of the elements is considered as 196810, where the number of the edge elements and the boundary elements 635 and 14300, respectively. For cylindercal obstacle at AR= 0.5 the number of the element as 128034 where the number of edge elements, the boundary element and the vortex elements are 473, 10280, 14 respectively, while for AR= 0.75 the number of the element as 151050, where the number of edge elements and the boundary element 530 and 12112 respectively. Given that the discretization grid is triangular, unstructured, and non-uniform as shown in Figures (4.4) and (4.5). All the numbers of elements gave almost identical results for the Nusselt number as illustrated in table (4-1) for cuboid obstacle at AR = 0.5. Ultimately, a mesh number of 164160 is used in this work as it represents the best compromise in term of both accuracy and computational time.

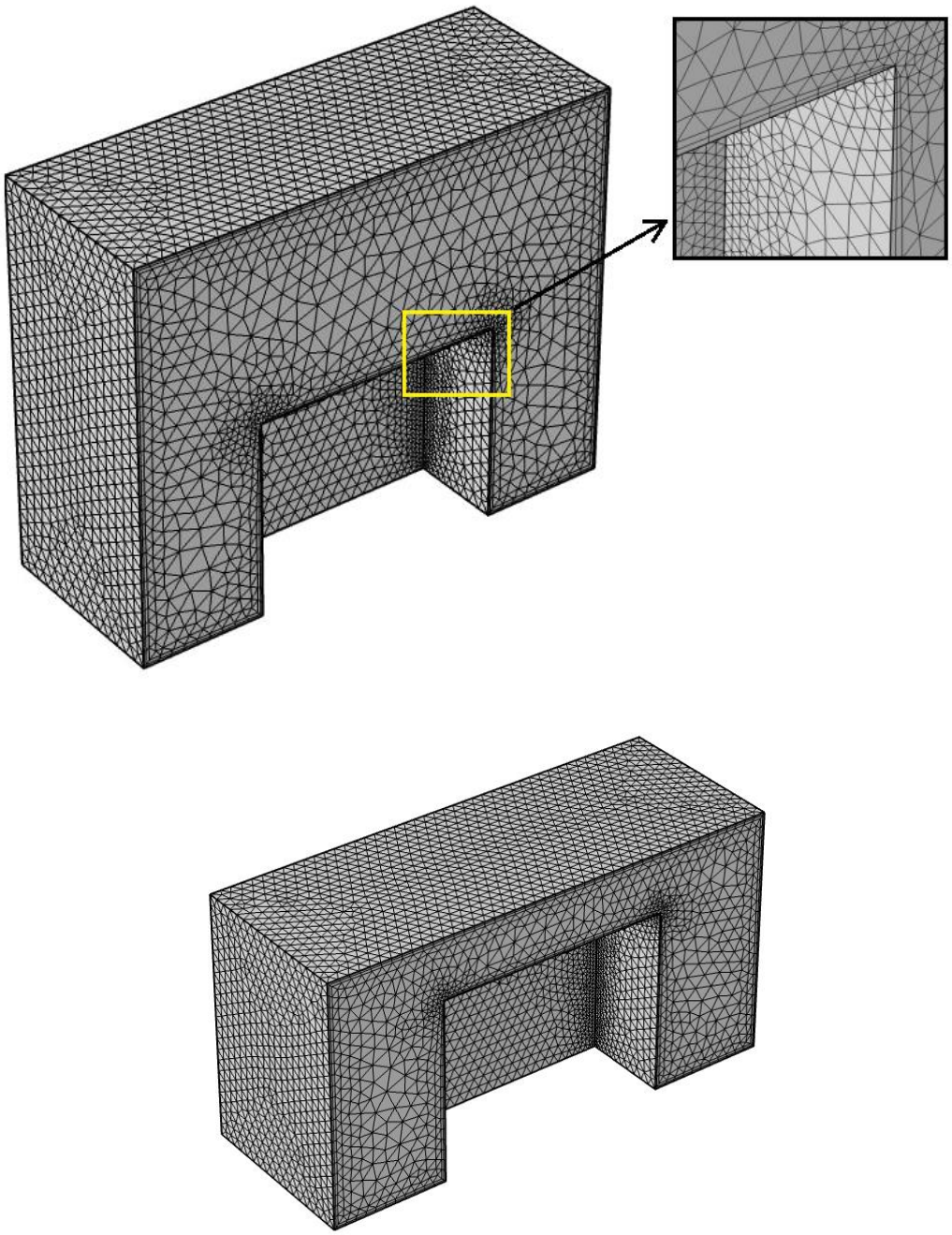

Figure (4- 4) geometry meshing of cuboid obstacle ,(a) AR=0.5, (b) AR=0.75.

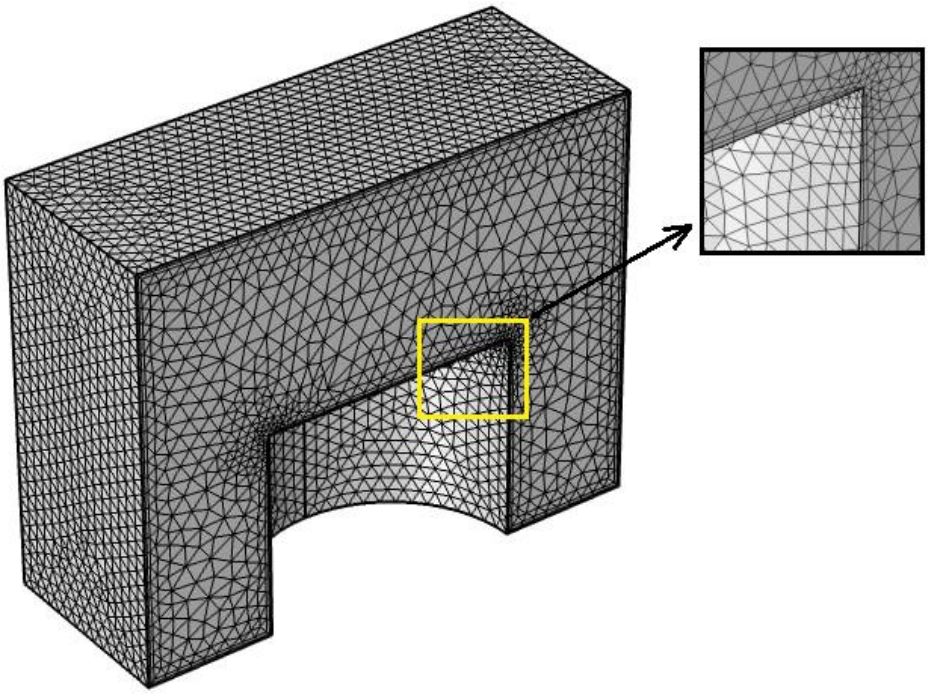

(a)

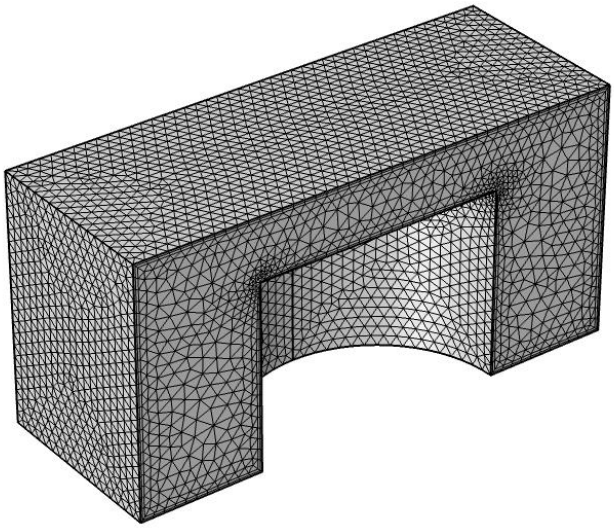

(b)

Figure (4- 5) geometry meshing of cylindrical obstacle(a) AR=0.5, (b) AR =0.75.

The relative error of the desired parameters is computed as [51]:

$$\text{Percentage } error = \frac{|A\ new - A\ old|}{A\ new} \times 100 \qquad \text{.....(4.6)}$$

Where (A) denotes any parameter, including the averge Nusselt number, coefficient of heat transfer, temperature, and parameter values obtained from the best grids. Table (4-1) displays a "fine" network that gives the

lowest error percentage, indicating that the network's independence is preserved but for a very long time and requires high specifications.

Table (4- 1) Type of element size and appearance of the Nusselt number.

Mesh size	Number of vortex element	Number of edge element	Number of boundary element	Number of element	$\overline{Nu}$	error%
Extra croase	16	236	2536	17163	27.7451	….
coarser	16	298	3932	34156	29.7376	6.7%
coarse	16	441	7994	85979	31.6694	6.09%
normal	16	559	12420	164160	32.6758	3.07%
fine	16	792	23974	398767	32.7445	0.209%

4.5 Results

The CFD post-processor is launched to verify the results calculated in form of graphical results of parameters such as temperature, Nusselt number, and Rayleigh number to show the behavior of different fluid flows. The results and data calculation can also be analyzed and imported to Excel for further analysis and verification.

To evaluate the heat transfer enhancement in the enclosure, the Nusselt number for natural convection of power-law fluids in a rectangular enclosure as [49]:

$$\overline{\mathrm{Nu}} = \frac{h \cdot L}{k} \qquad \ldots\ldots\ldots\ldots\ldots\ldots\ldots\ldots (4.7)$$

Where the average heat transfer coefficient can be obtained by using the integral averaged method as [52]:

$$\mathrm{h} = \frac{1}{\mathrm{v}} \int_0^{\mathrm{v}} \frac{\mathrm{q}}{\mathrm{T_h} - \mathrm{Tf}} \mathrm{dv} \qquad \ldots\ldots\ldots\ldots\ldots\ldots\ldots\ldots (4.8)$$

where T_h is the hot temperature and T_f is the appropriate fluid temperature.

4.6 Simulation step

To model the cavity computational fluid dynamic model, the following steps were performed.

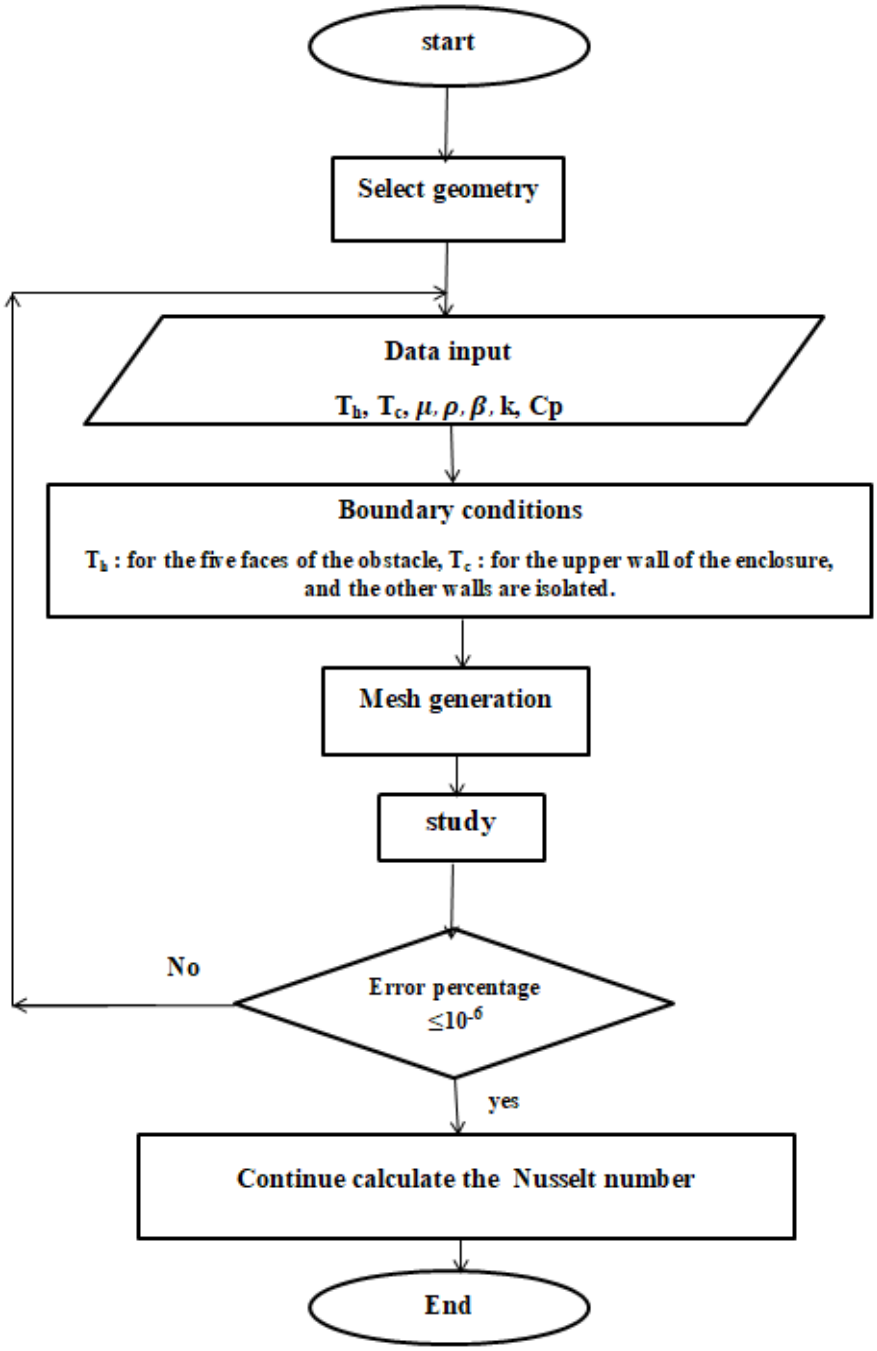

Figure (4- 6) flow chart of the study.

CHAPTER FIVE

RESULTS

AND

DISCUSSION

Results and Discussion

5.1 Experimental result

The experimental work describes the results of the temperature distribution of the liquid inside the enclosure for the three testes that are explained in the experimental approach. All figures in this chapter show the temperature inside the enclosure, according to the locations of the thermocouples that are shown in chapter three.

5.1.1 Temperature Distributions inside the enclosure

Temperature distributions across the enclosure are shown in figures (5-1) to (5-12). The figures are obtained by measuring the temperature inside the enclosure at different planes in three dimensions for a power value of 326.27 W. This power fixed the temperature of the hot walls at 30 ^{o}C for the three types of fluids used in the experimental work (water, CMC 0.5%, CMC 1%), for both aspect ratio, and shapes of obstacle.

Figures (5-1), (5-2), and (5-3) illustrate temperature distribution inside the enclosure with the z-axis at x and y certain point, for AR = 0.5 and a cuboid obstacle for three types of fluids. The maximum temperature is at or near the hot walls of the obstacle, while the temperature gradually decreases in the level of the z-axis upward to the top, to reach the cold wall at the top of the enclosure where the lowest temperature is at z = 30 cm. The temperature of all fluids has the same behavior, which is decreasing with clear differences in the path of heat transfer. Water shows a faster gain of temperature, while CMC 1% is lower. The reason is attributed to the heat transfer coefficient where water a higher value than 1% CMC. The temperature distribution is caused the spread of the hot fluid from the region near the obstacle to the upper region by convection vortices.

Figures (5-4), (5-5), and (5-6) represent temperature change inside the enclosure with z-axis at x and y specific point and the same obstacle shape, but various AR of 0.75 for the types of non-Newtonian fluids in addition to the water. The maximum temperature is measured by the thermocouple near the hot wall of the obstacle, while the temperature gradually decreases in the level of the z-axis upward to the top, to reach the surface of the cold wall where the lowest temperature is at z = 20 cm. The temperature distribution inside the enclosure has the same behavior as in the previous figures, and the reason is that the control of heat transfer is through the properties of the material and its effect on heat transfer. The higher values of the non-Newtonian materials properties, the lower value of the heat transfer coefficient.

Figures (5-7), (5-8), and (5-9) show the temperature distribution inside the enclosure with z-axis at certain x and y at AR = 0.5 with a cylindrical obstacle. The maximum temperature is at or near the hot obstacle wall and the temperature gradually decreases upward z-direction until it reach the lowest temperature at z =30 cm. All fluids have the same behavior, where their temperture decreases with the clear differences in the path of heat transfer. Water is being the faster in terms of temperature gain, while CMC 1% is due to the dependence on the physical properties of the material, the most important of which is the density and heat transfer coefficient , which is low for non-Newtonian fluids CMC1% and CMC 0.5% compared to Newtonian fluid (water). This temperature distribution is induced by moving the cold fluid from the upper to lower zone and the transfer of heat from the hot wall by a difference in temperature.

Figures (5-10), (5-11), and (5-12) demonstrate the temperature distribution inside the enclosure in the z-direction with x and y as fixed points with the same cylindrical obstacle shape but at AR = 0.75. The

maximum temperature for water, CMC 0.5% and CMC 1% respectively, represents the wall temperature of the hot obstacle, while the temperature gradually decreases in z-direction, to reach the same temperature of the cold surface of the enclosure at z = 20 cm. Also in these figures, the working fluids behave the same, where the highest temperatures are for water and the lowest is for CMC 1%, this is because of the high heat transfer coefficient of water at the expense of the CMC coefficient in both concentrations.

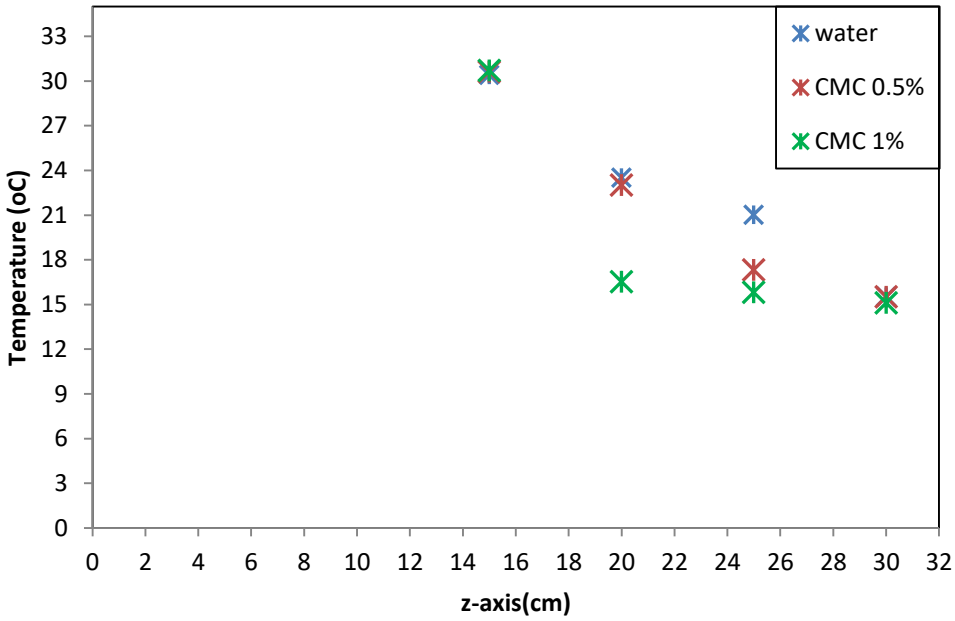

Figure (5- 1) temperature distribution with z-axis at x = 20 cm, y = 15cm for cuboid obstacle shape and AR = 0.5.

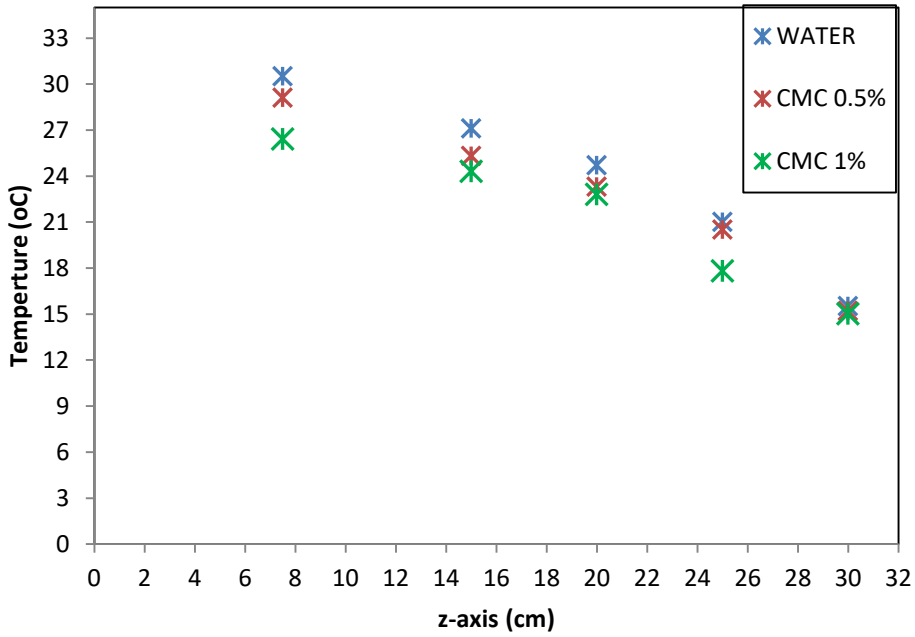

Figure (5- 2) temperature distribution with z-axis at x = 20 cm ,y = 3.5 cm for cuboid obstacle shape and AR =0.5.

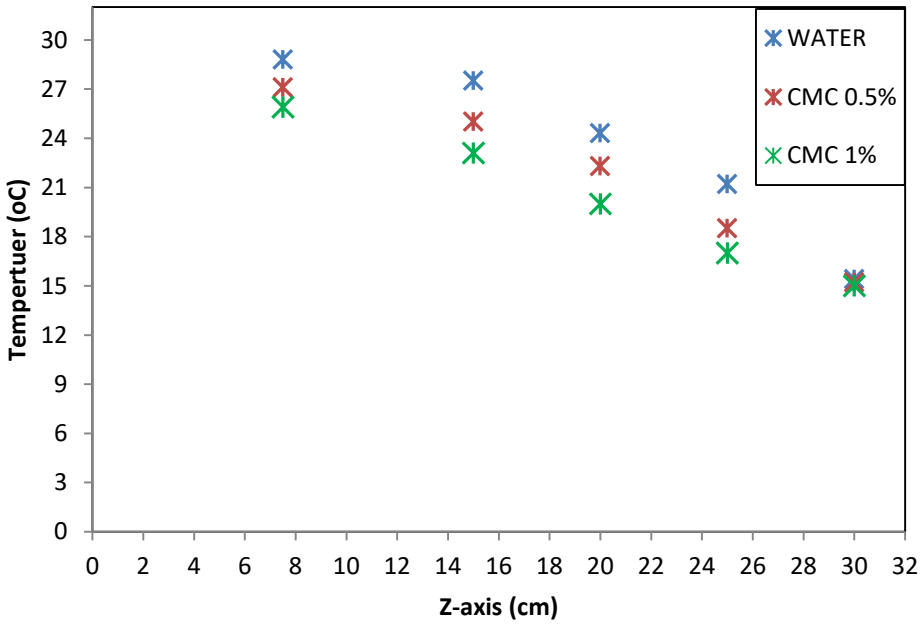

Figure (5- 3) temperature distribution with z-axis at x = 5 cm ,y = 15 cm for cuboid obstacle shape and AR =0.5.

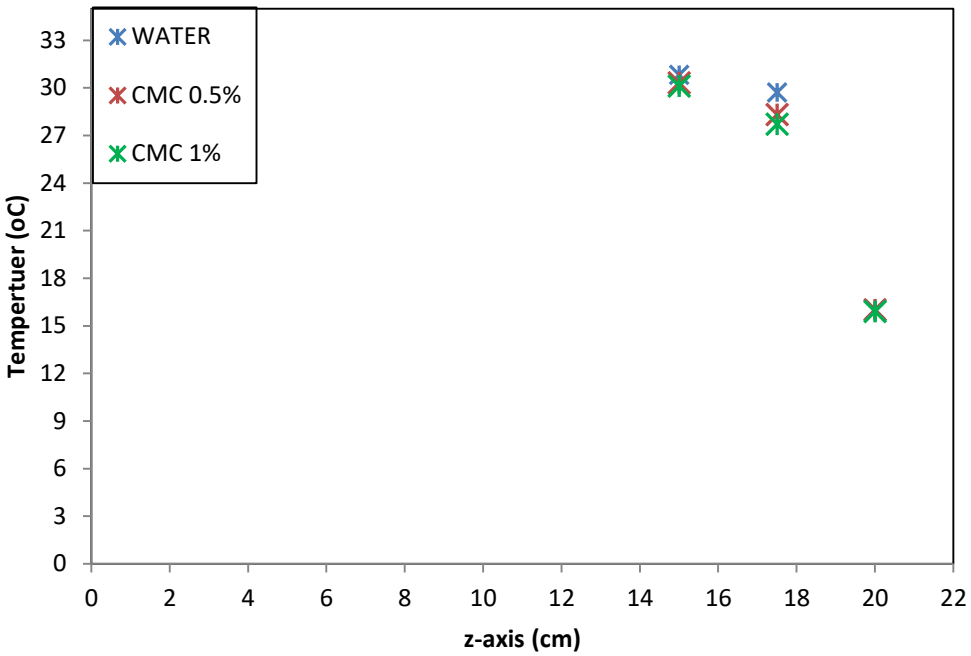

Figure (5- 4) temperature distribution with z-axis at x =20 cm ,y = 15 cm for cuboid obstacle shape and AR =0.75.

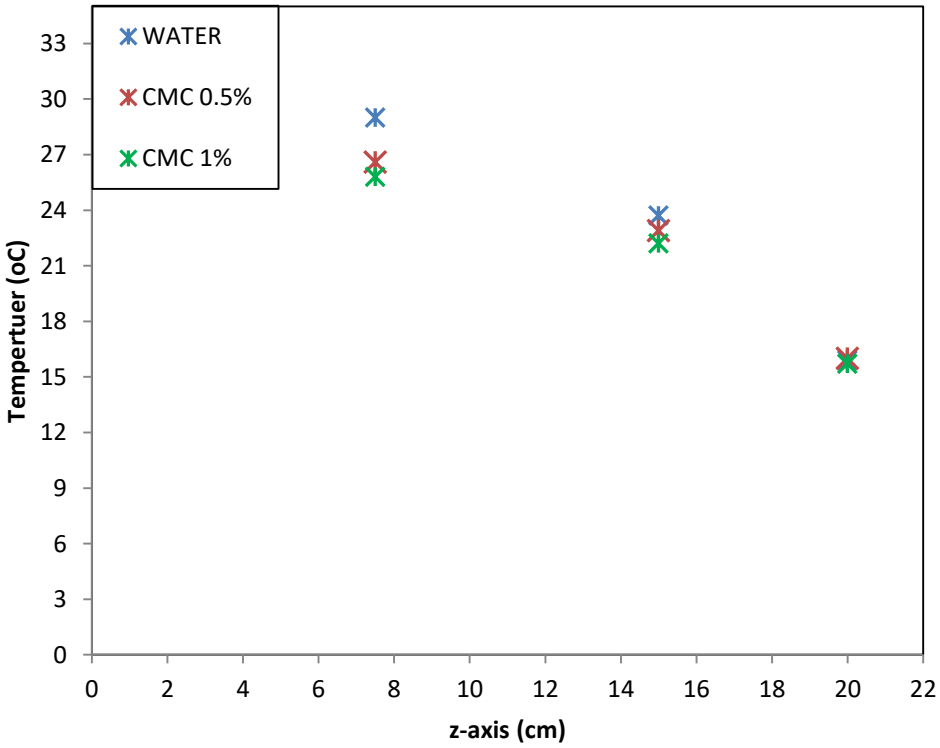

Figure (5- 5) temperature distribution with z-axis at x =20 cm ,y = 3.5 cm for cuboid obstacle shape and AR = 0.75.

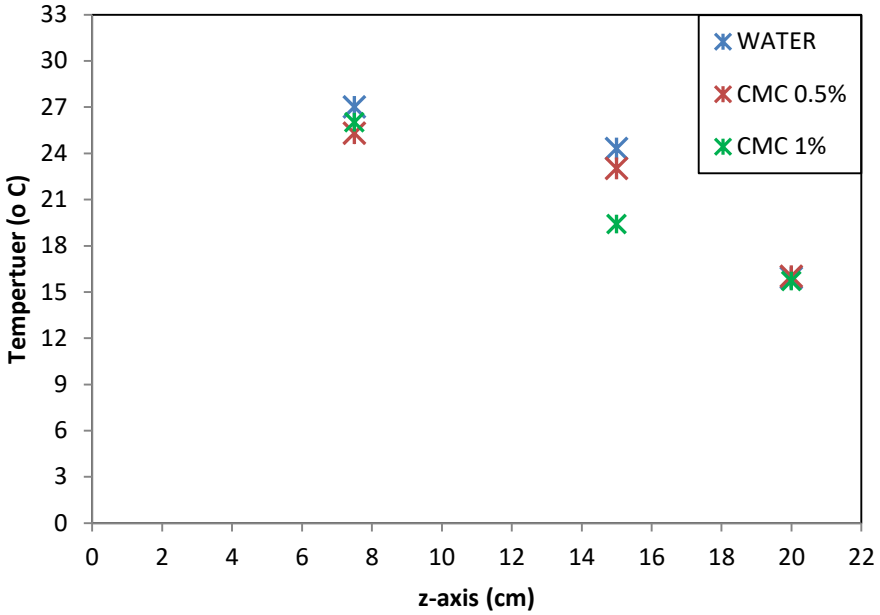

Figure (5- 6) temperature distribution with z-axis at x = 5 cm ,y =15 cm for cuboid obstacle shape and AR = 0.75.

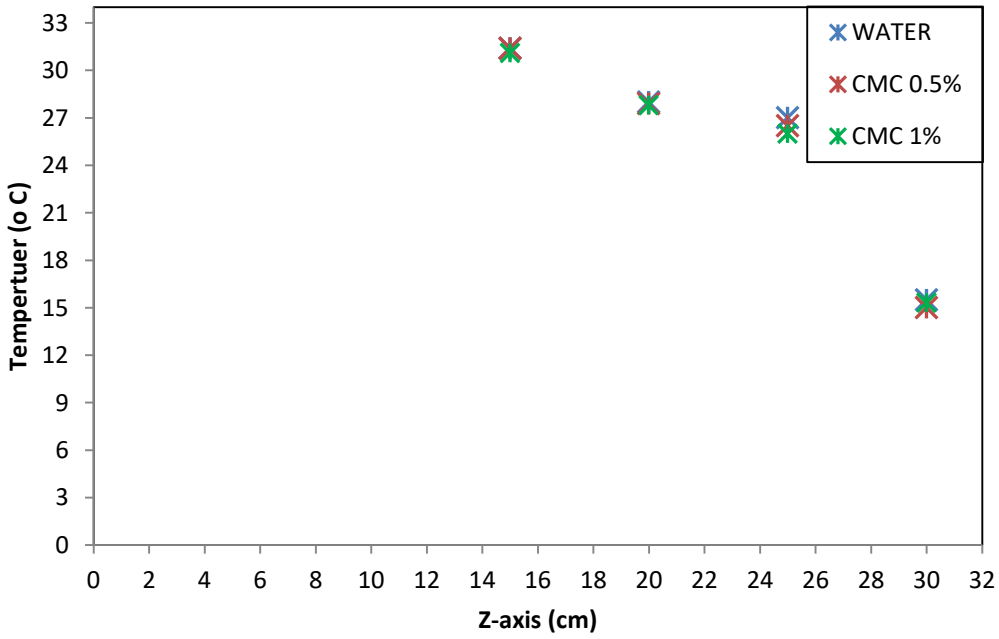

Figure (5- 7) temperature distribution with z- axis at x = 20 cm, y = 15 cm for cylindrical obstacle shape and AR = 0.5.

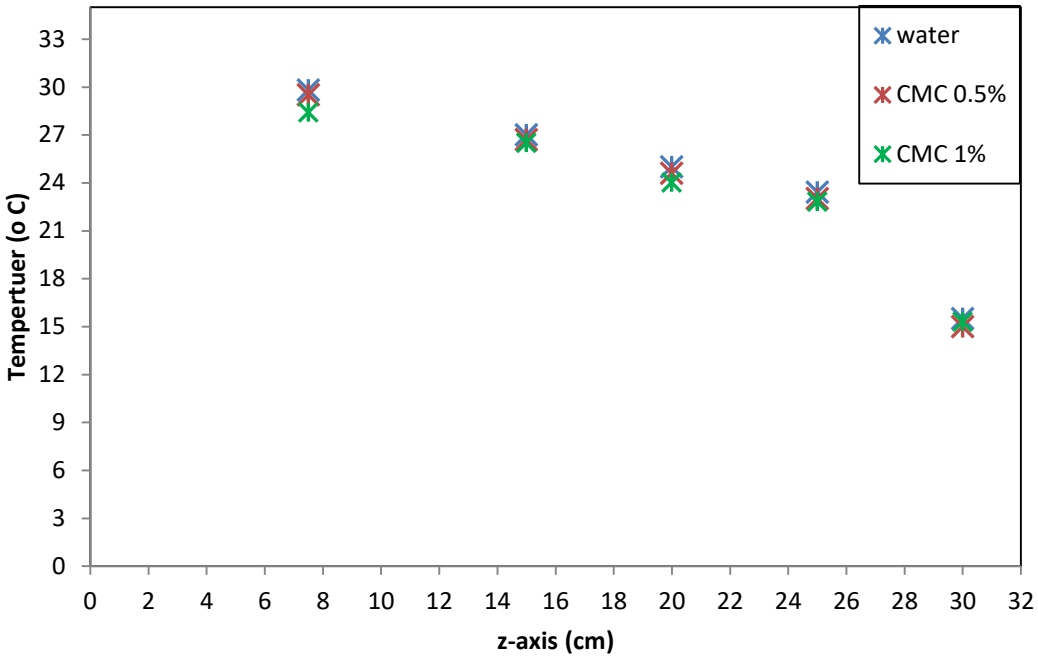

Figure (5- 8) temperature distribution with z-axis at x = 20 cm ,y = 3.5 cm for cylindrical obstacle shape and AR = 0.5.

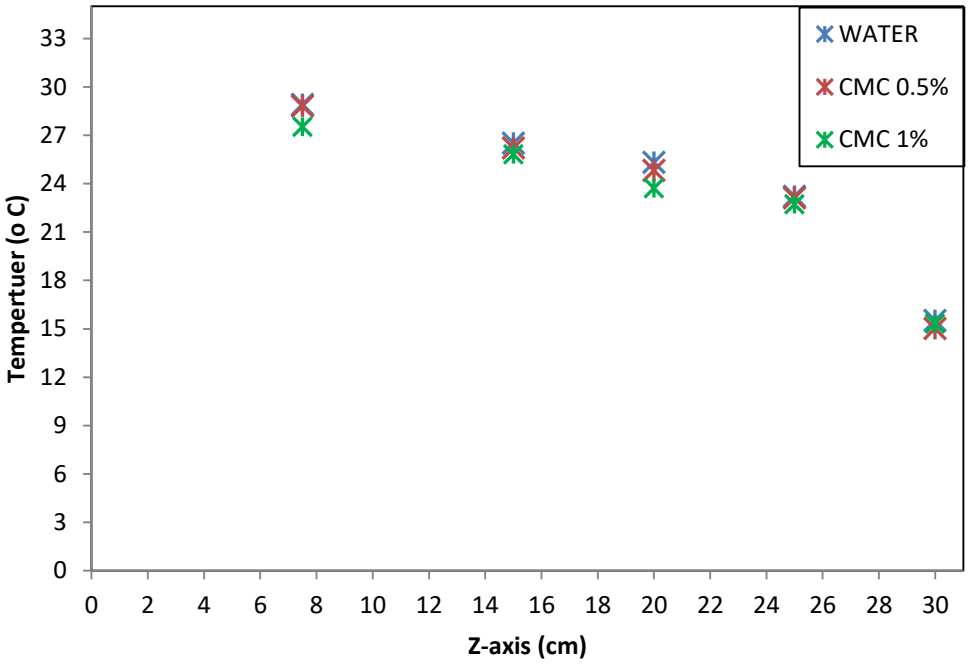

Figure (5- 9) temperature distribution with z-axis at x = 5 cm ,y =15 cm for cylindrical obstacle shape and AR = 0.5.

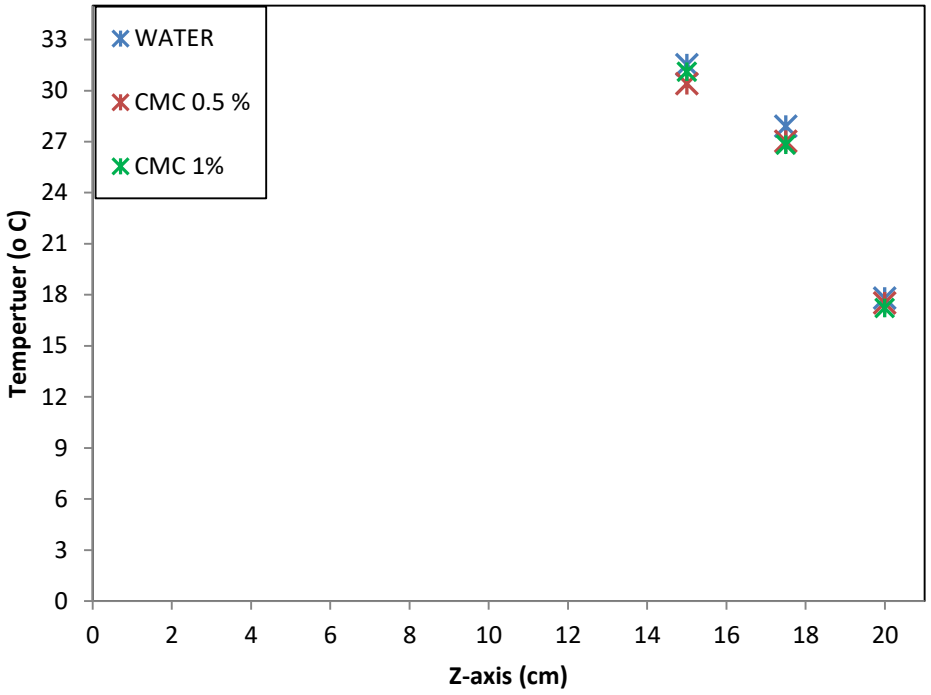

Figure (5- 10) temperature distribution with z-axis at x =20 cm, y=15 cm for cylindrical obstacle shape and AR = 0.75.

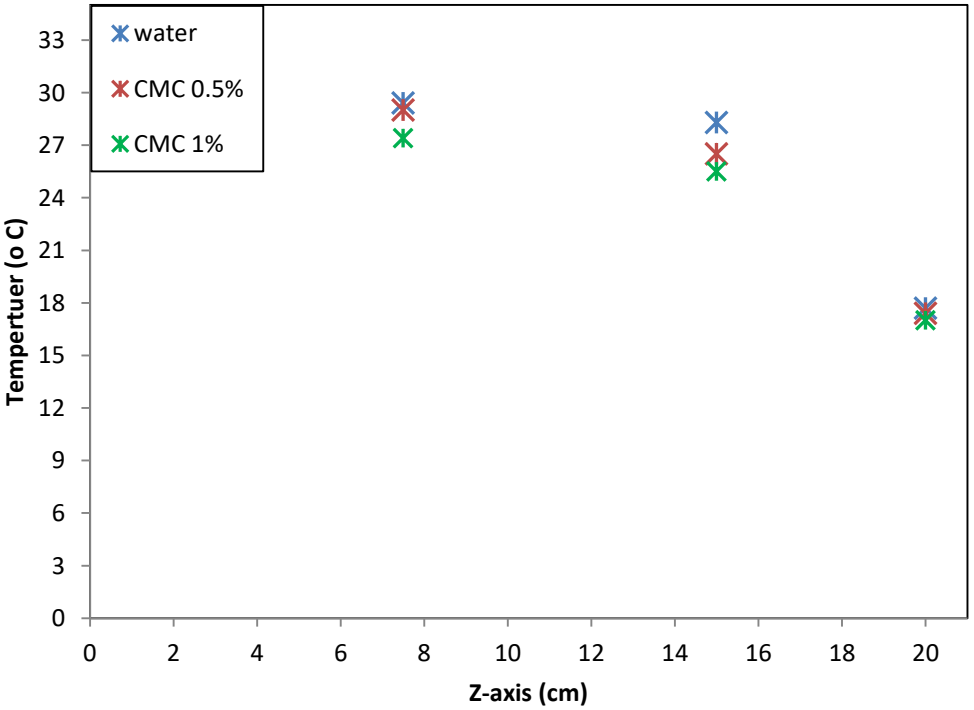

Figure (5- 11) temperature distribution with z-axis at x =20 cm, y ***= 3.5 cm for cylindrical obstacle shape and AR = 0.75.***

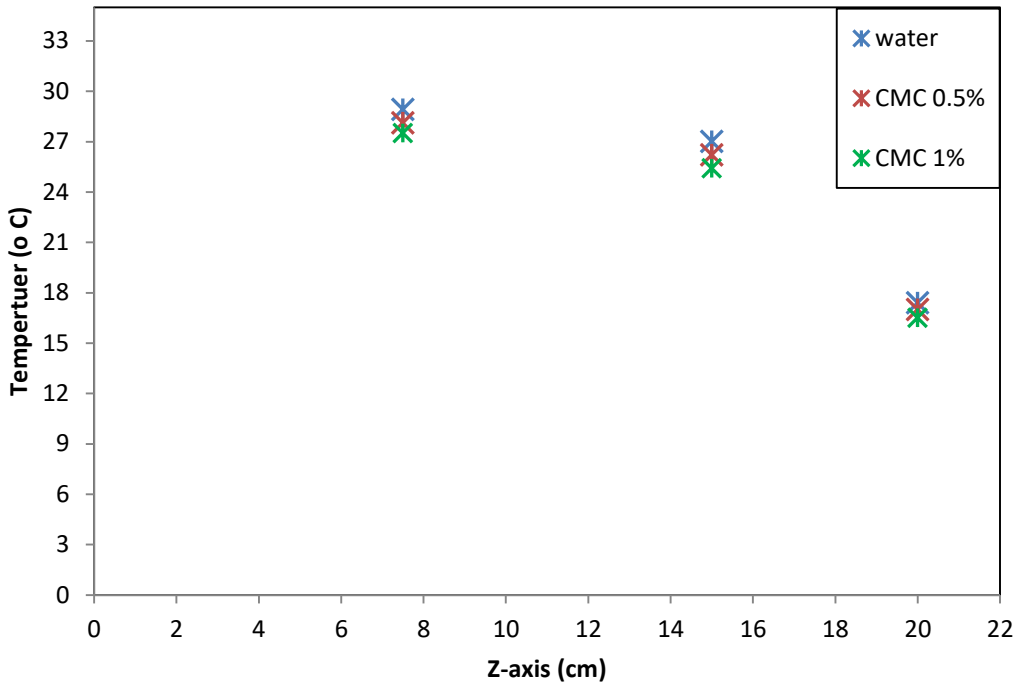

Figure (5- 12) temperature distribution with z-axis at x = 5 cm ,y =15 cm for cylindrical obstacle shape and AR = 0.75.

5.1.2 The effect of Ra number, n index, AR, and shape of obstacle on the calculated natural convection factors

The natural heat flow within the fluid layer is controlled by the aspect ratio AR, the power-law index n, and the Rayleigh number Ra. In this study, the values of the power-law index differ according to the concentration of CMC two concentrations are used, where n = 0.59 and 0.72 for a concentration of 1 % and 0.5 % respectively. In addition to water that is considered as a Newtonian fluid with n =1.

Rayleigh number does not change with the change in the shape of the obstacle. Ilyas et al.[53] indicated that the Rayleigh number is dependent on three factors; (a) the change in the thermophysical properties of the working fluid (b) the change in the temperature difference between hot and cold walls and (c) the aspect ratio of the enclosure.

Figure (5-13)and (5-14) demonstrate the variation of the temperature difference with the Rayleigh number for the three types of fluids at AR=0.5 and AR=0.75, respectively. In both cases Rayleigh number increases with increasing the temperature due to the increase in the thermal gradient. In addition, temperature changes the physical properties of the fluid such as viscosity, density, and thermal conductivity which effect Rayleigh number. The viscosity decreases with the increase of temperature, this will increase the movement of the molecules within the fluid and as a result, the forces of attraction between the molecules will be relatively reduced. For all Rayleigh numbers, convection is weakened by an increase in the power-law index, thereby increasing the heat source temperature. It is noted that in figure (5-13) the largest Rayleigh number was $9.76\mathbf{x}10^{8}$ when AR = 0.5, but in figure (5-14) the value was $4.36 \mathbf{x} 10^{7}$with the same properties, the reason is that the increase of Ra with the increase of enclosure size. The increase in volume enhances the velocity of the fluid as well as the Rayleigh number due to its depending on the distance between the hot and cold surface of the enclosure.

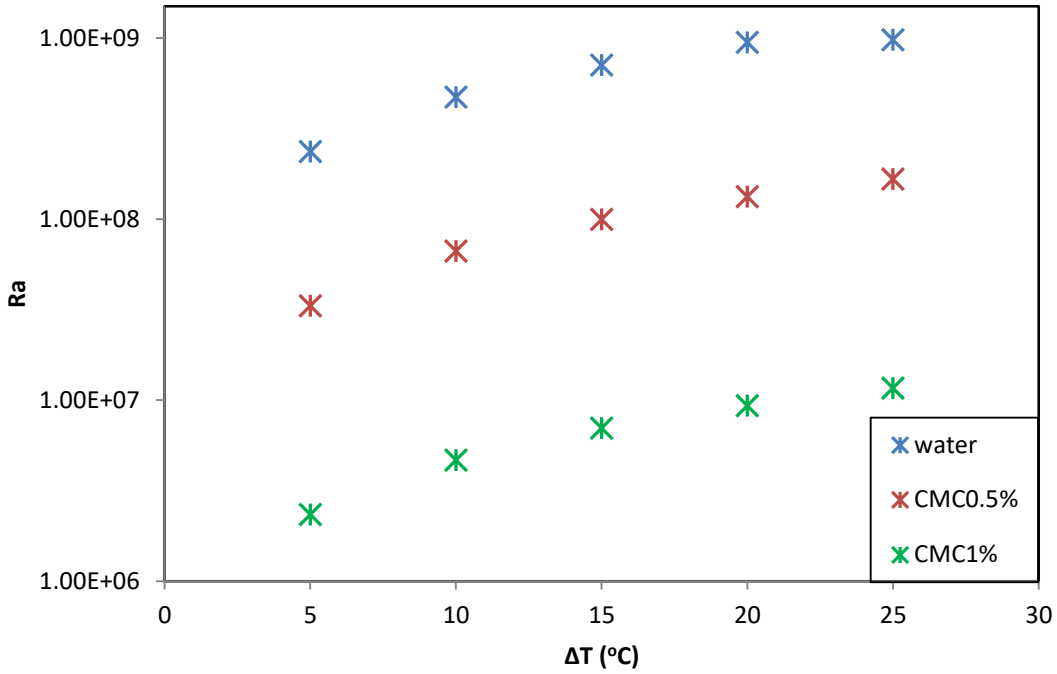

Figure (5- 13) variation of the Rayleigh number with different temperatures at AR=0.5.

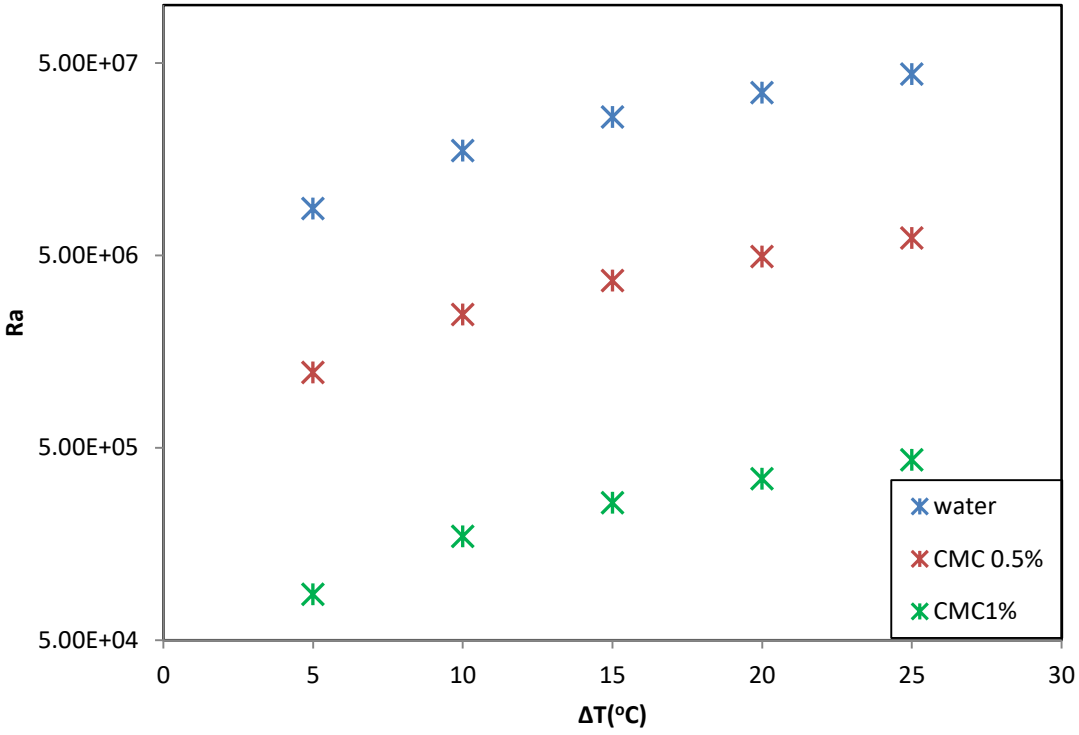

Figure (5- 14) variation of the Rayleigh number with different temperatures at AR=0.75.

Figures (5-15) to (5-18) show the variation of the Rayleigh number of the base fluids with Nusselt number for different initial conditions. Nusselt number represents the heat transfer by convection to the heat transfer by the conduction. Nusselt number increases with an increase in Rayleigh number for both shear-thinning (n < 1) and Newtonian (n = 1) fluids regardless of the initial and boundary condition and this is consistent with the result of Kim et al.[9] and Kefayati [54]. Increasing the Rayleigh number leads to an increase in the buoyancy forces, it becomes increasingly dominant over viscous resistance, which in turn increases the temperature difference and thus increases the flow, which increases the heat transfer from the source of heat to cold walls. The value of the Rayleigh number is excess due to enhanced convection that carries heat energy with increased momentum. The relationship between the Nusselt and Rayleigh numbers is irregular due to the difference in the value of the aspect ratio and the shape of the obstacle. The highest value of the Nusselt number is 77.92 for 1% CMC at AR = 0.5, with cylindrical obstacle, while the lowest value is 34.47 for water at a temperature difference of $\Delta T = 25$ ^{o}C.

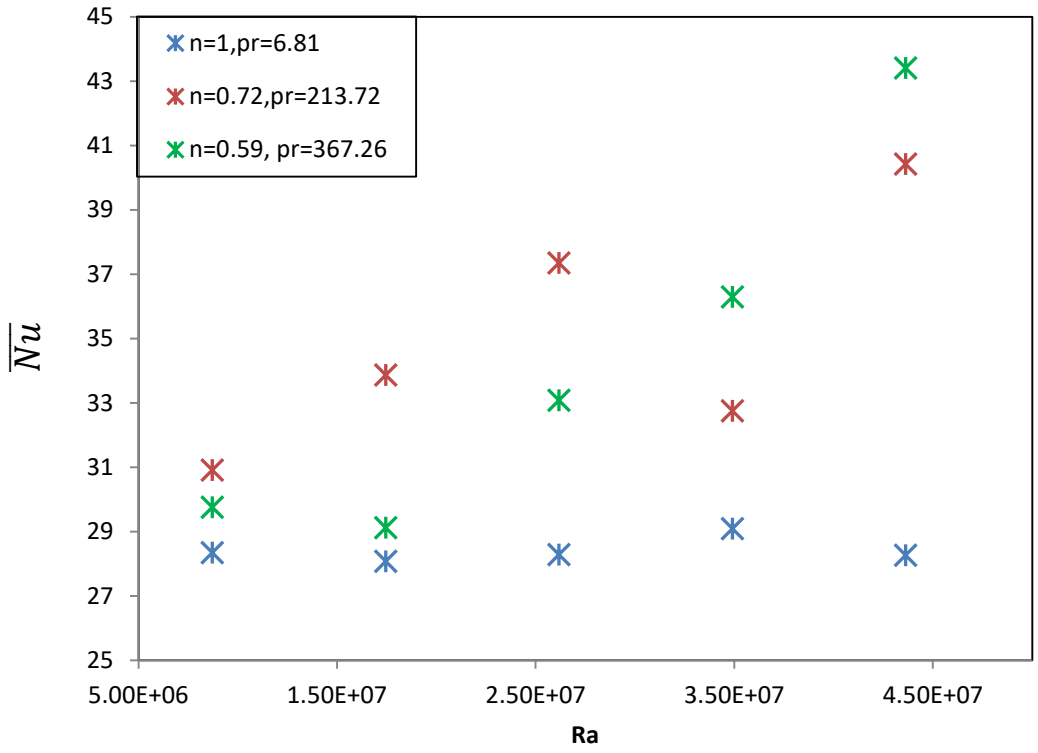

Figure (5- 15) variation of Rayleigh number with Nusselt number for a cuboid obstacle at AR =0.5.

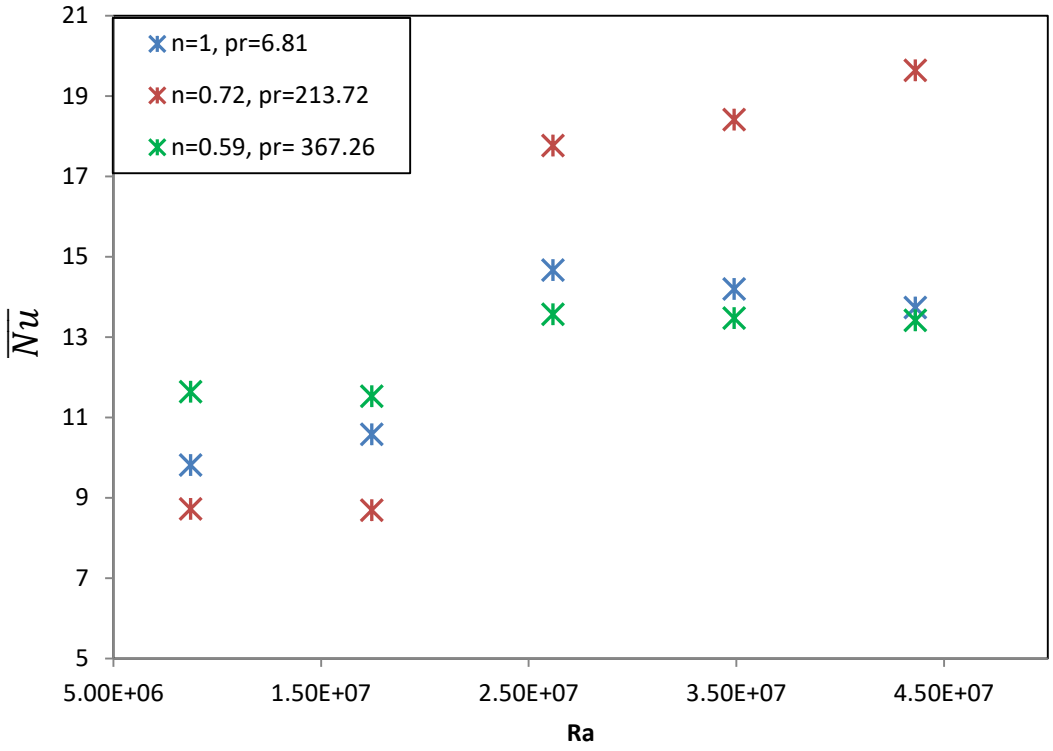

Figure (5- 16) variation of Rayleigh number with Nusselt number for a cuboid obstacle at AR =0.75.

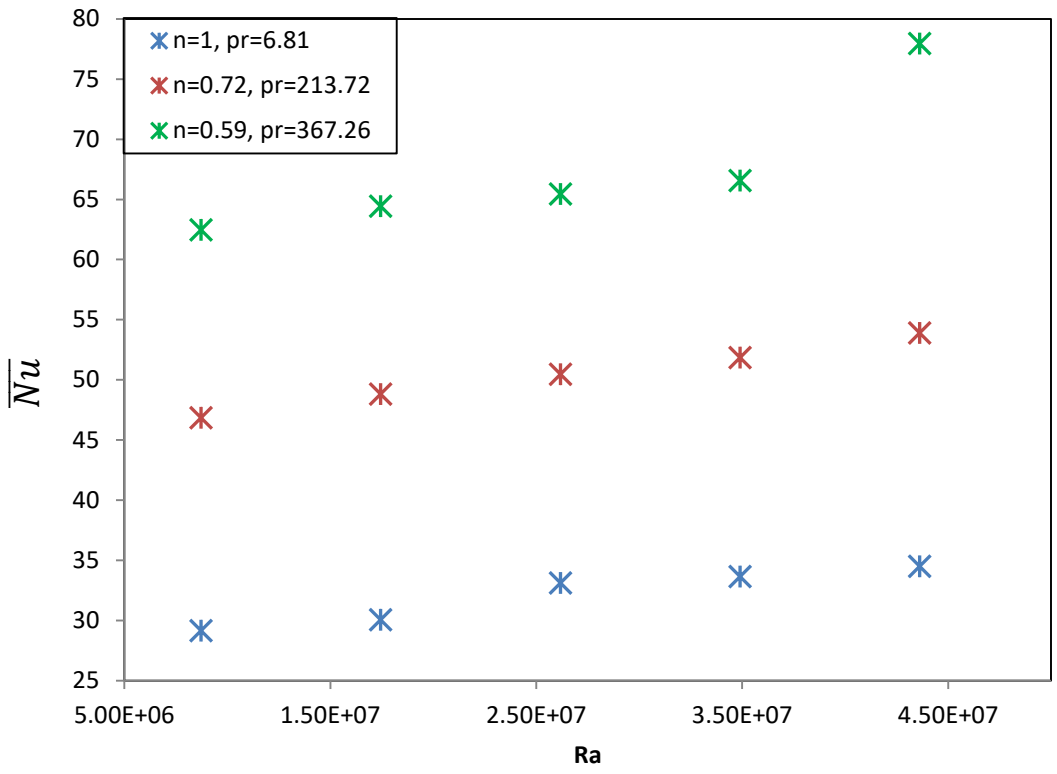

Figure (5- 17) variation of Rayleigh number with Nusselt number for a cylindrical obstacle at AR =0.5.

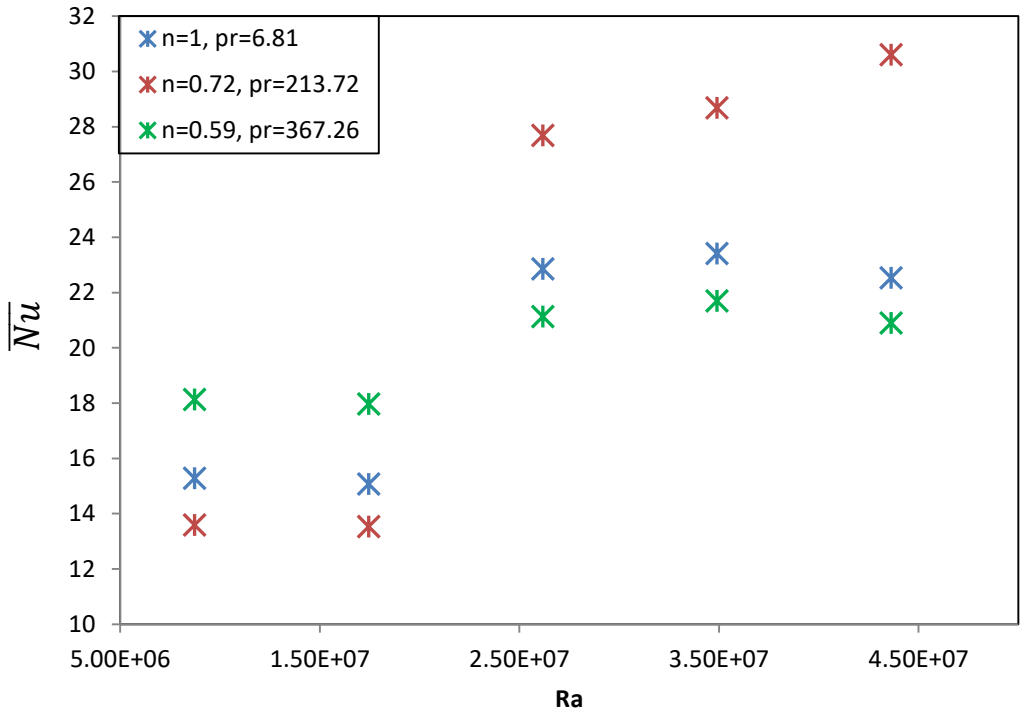

Figure (5- 18) variation of Rayleigh number with Nusselt number for a cylindrical obstacle at AR =0.75.

Figures (5-19) to (5-22) illustrate the effect of the non-Newtonian behavior represented by the power-law index with Nusselt number. It was noted that Nusselt number reduces with the increase of the power-law index for both obstacle shapes as shown in figures (5-19) and (5-20) at aspect ratio (0.5). It was exposed that at AR = 0.75 for both obstacle shapes there is an increase and decrease with the excess value of the power-law index. This is happened due to the behavior of the non-Newtonian fluids, as well as the narrow distance between the cold and hot walls as indicated in figures (5-21) and (5-22). The maximum value of the Nusselt number was 77.92 at AR = 0.5, index power law n =0.59, and Ra =9.76×10^{8}, with a cylindrical obstacle shape. While for a cuboid obstacle it was 43.4 at the same conditions. Yigit et al.[20] indicated that the increasing of the power-law index leads to a reduction in the Nusselt number. The decrease of a power-law index as a result of an increase of the concentration of non-Newtonian fluid (shear-thinning fluid (n < 1)) and the increase of the viscosity, which lead to a slower bulk movement of the fluid and consequently the velocity decreases. This results in an accumulation of heat in the enclosure and an increase in the temperature of the working fluid. This explains why CMC 1% has the highest value in all the indicated figures for both obstacle shapes.

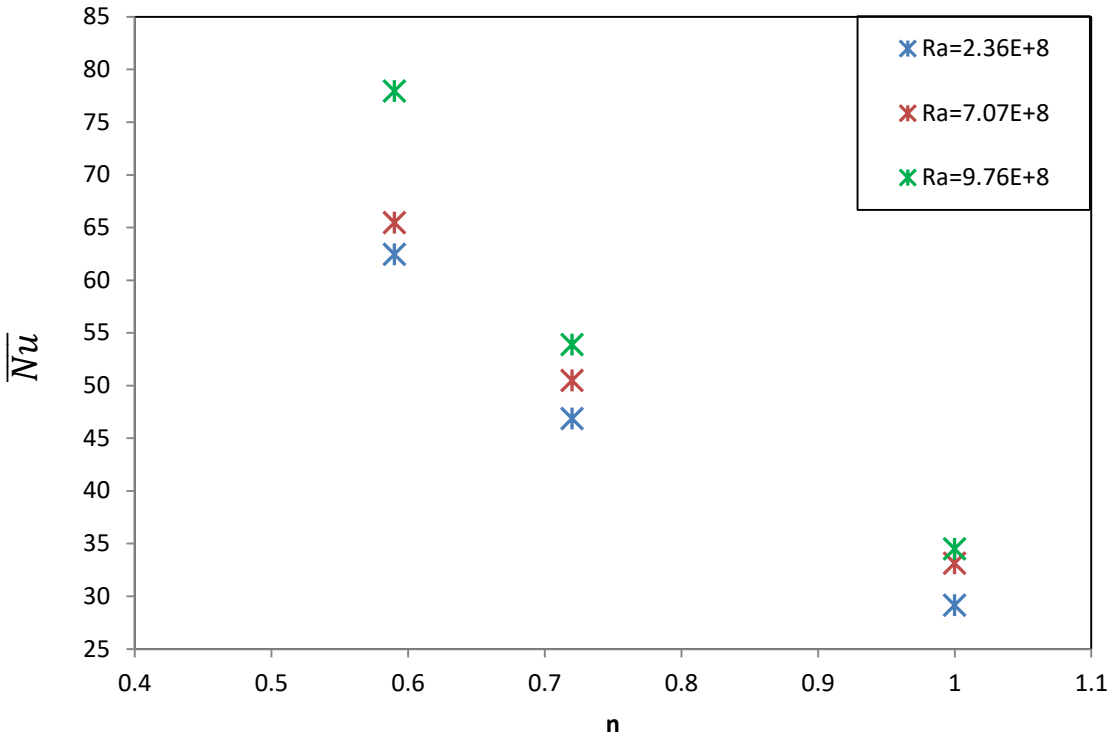

Figure (5- 19) Nusselt number variation with the power-law index for the enclosure with a cylindrical and AR = 0.5.

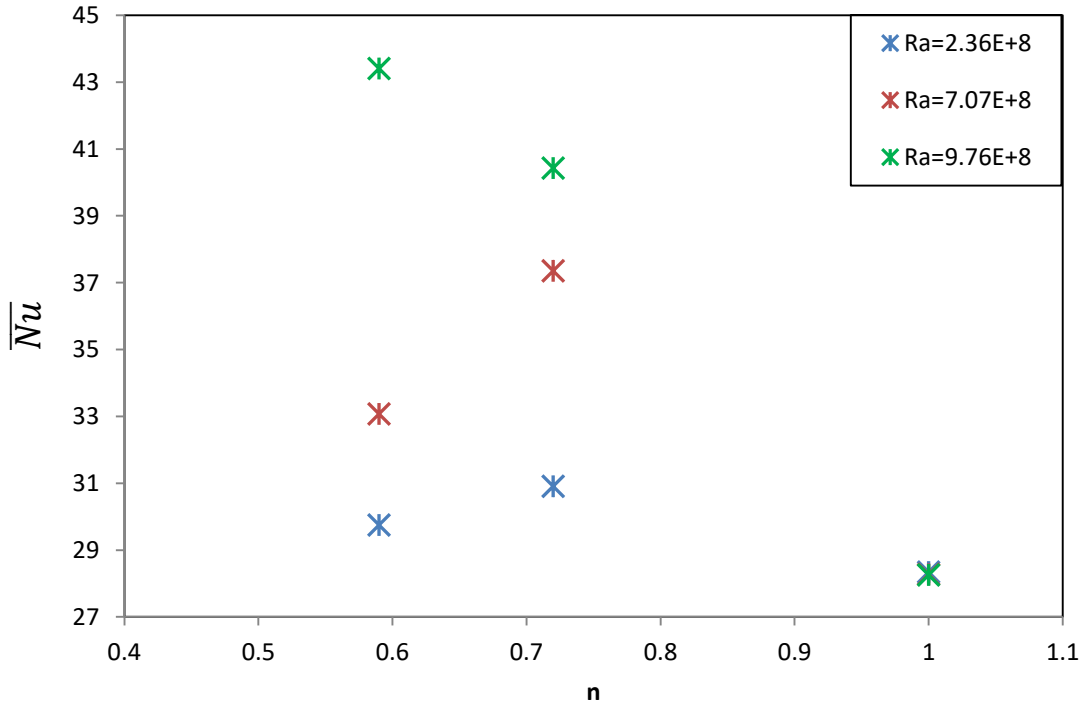

Figure (5- 20) Nusselt number variation with the power-law index for the enclosure with a cuboid and AR = 0.5.

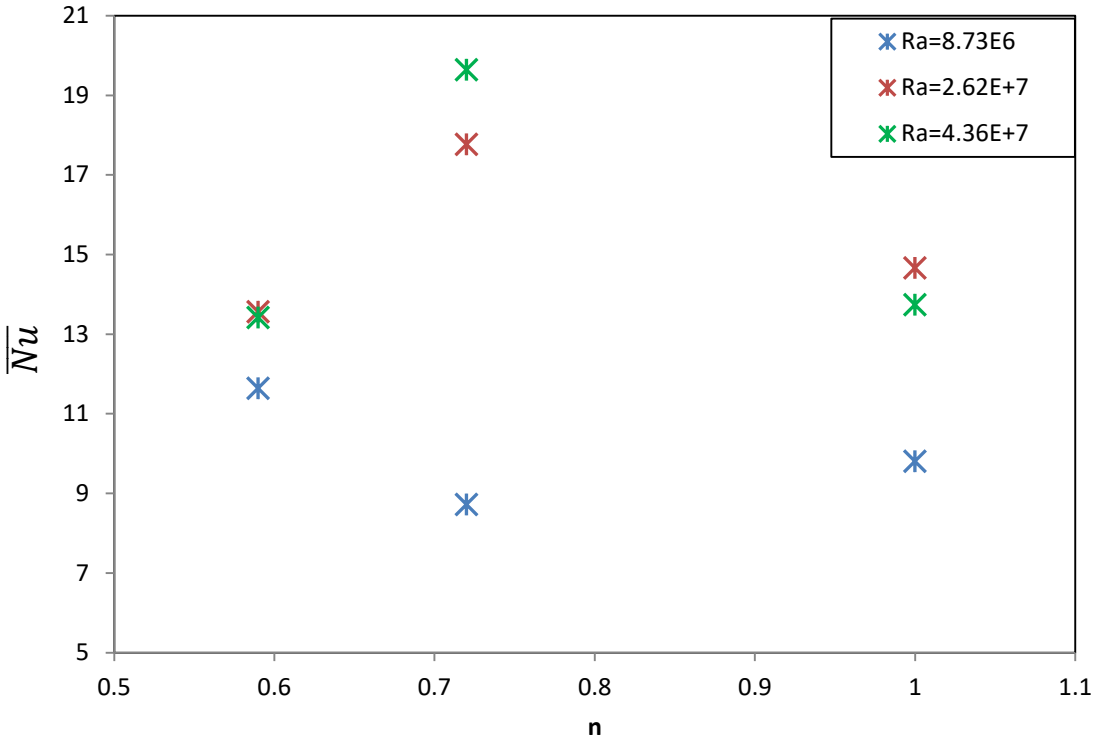

Figure (5- 21) Nusselt number variation with the power-law index for the enclosure with a cuboid and AR = 0.75.

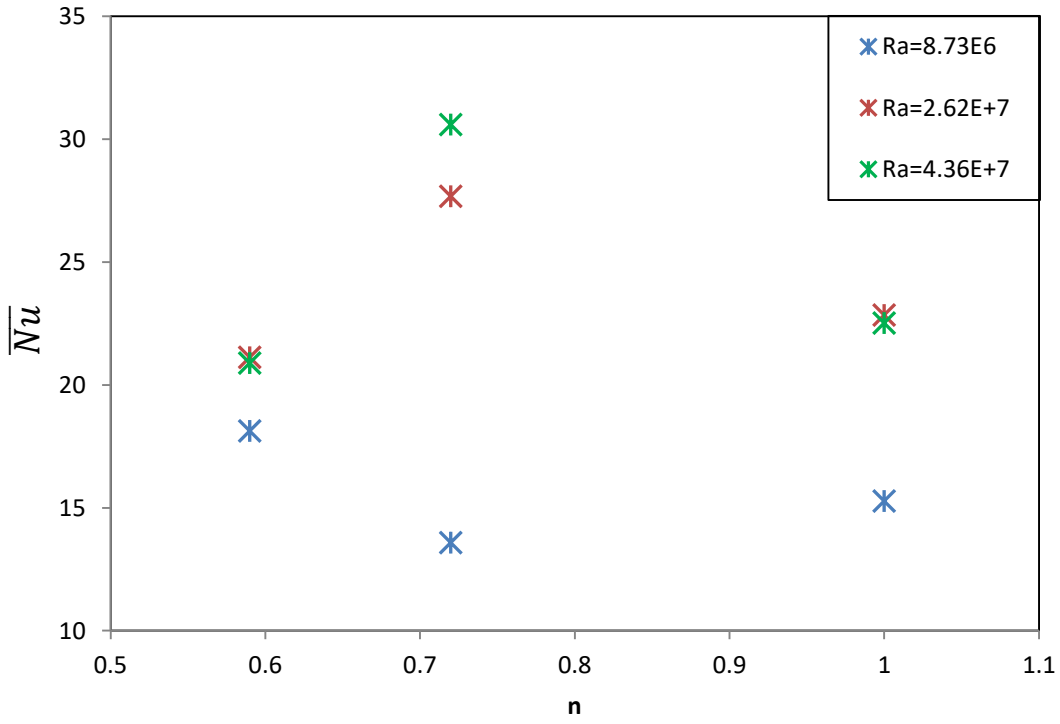

Figure (5- 22) Nusselt number variation with the power-law index for the enclosure with a cylindrical and AR = 0.75.

Figures (5-23) to (5-28) show the relationship between the values of average Nusselt number and Rayleigh number for each shape of obstacle with two values of aspect ratio 0.5 and 0.75 for water, CMC 0.5%, and CMC 1%. It was observed that a higher value of the Rayleigh number leads to a maximal value of the average Nusselt number for all types of working fluids used in the experimental work and for both shapes of obstacle and aspect ratio. It was found that the values of the Nusselt number in the case of using the cylindrical obstacle were greater than the values of the Nusselt number in the cuboid obstacle under the same condition. The reason for this behavior is that the bouncy force increases with increasing temperature in addition to the surface area and which has relatively very large curvatures of the cylindrical obstacle was greater than a cuboid obstacle.

While at 0.75 aspect ratio, the percentage increase in the heat transfer is estimated as 35 %, 35.6%, and 38.8 % in the cylindrical obstacle shape for working fluids, water, CMC 0.5%, and CMC 1%, respectively under the same conditions. It was noted that when the aspect ratio of the enclosure is reduced, this leads to an increase in the heat transfer or an increase in the Nusselt number as mentioned by Yigit et al., [20]. As the AR increased (the volume increased),the movement of fluid density is affected in the heat transfer will decrease.

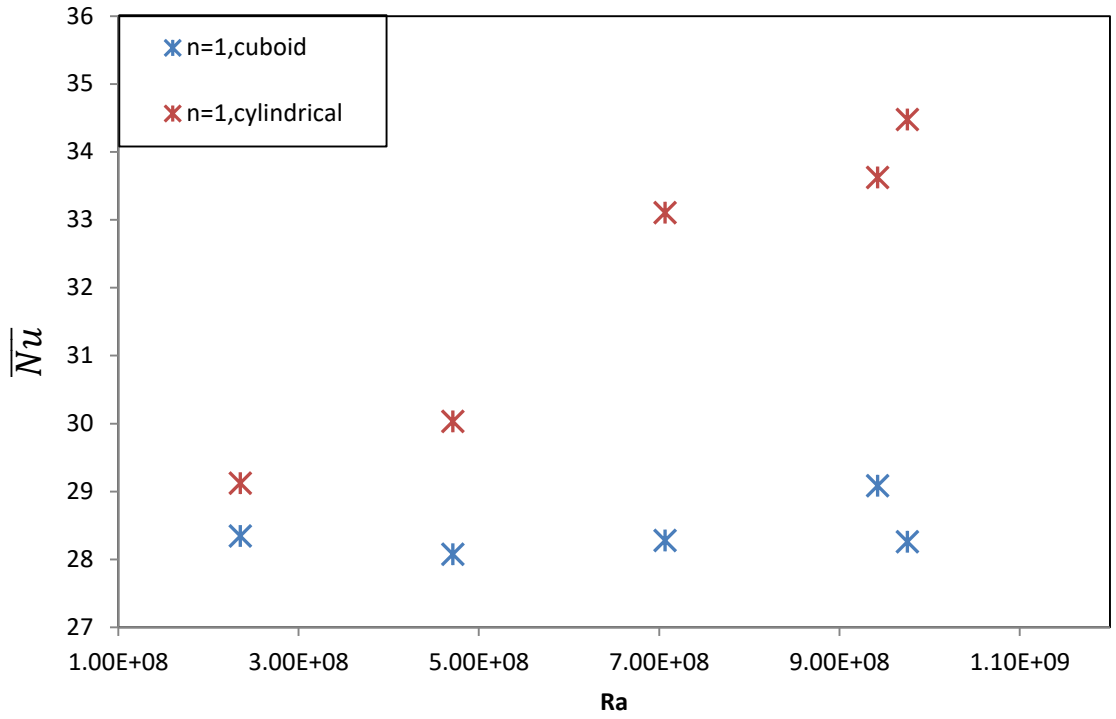

Figure (5- 23) effect of the shape of obstacle on Nusselt number for water and AR =0.5.

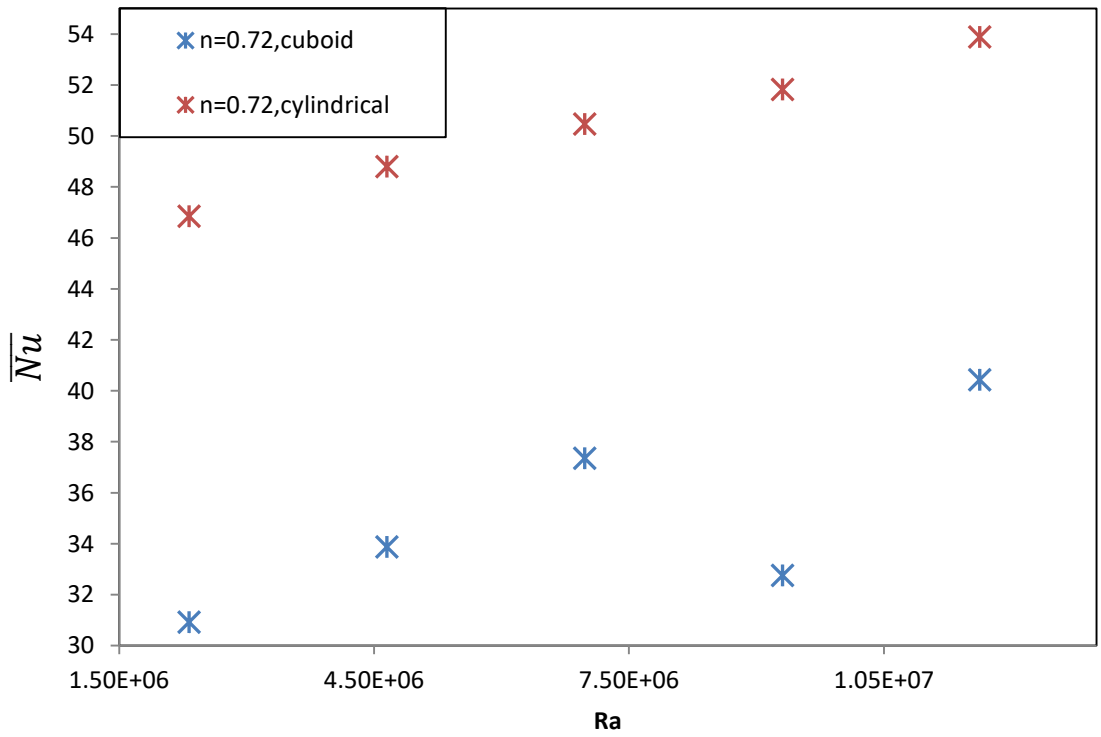

Figure (5- 24) effect of the shape of obstacle on Nusselt number for CMC 0.5% and AR=0.5.

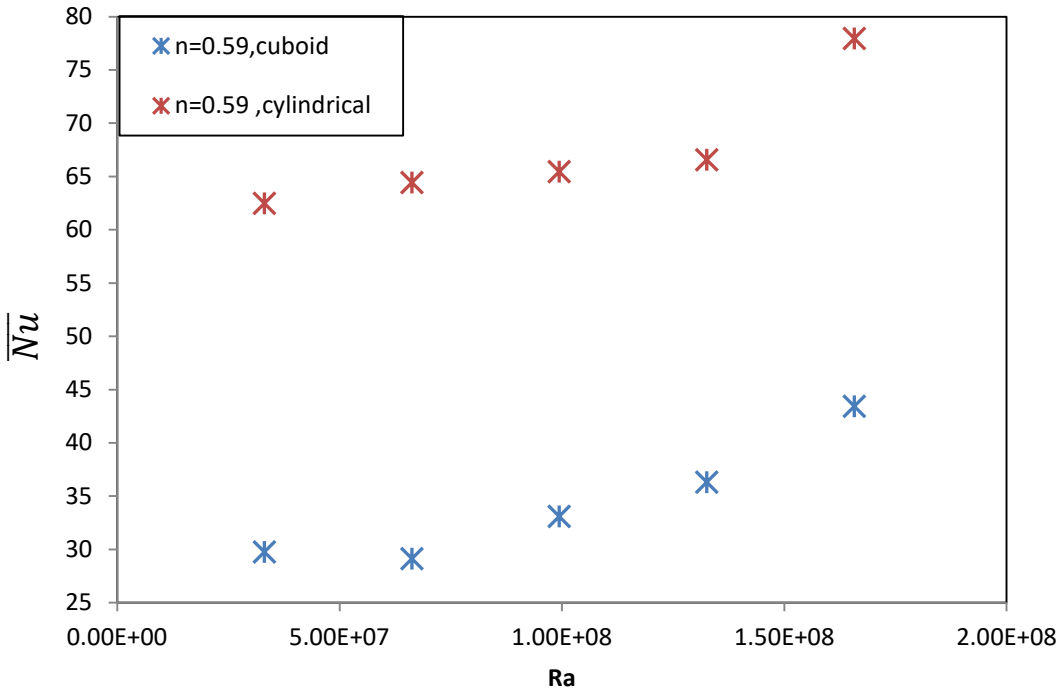

Figure (5- 25) effect of the shape of obstacle on Nusselt number for CMC 1% and AR=0.5.

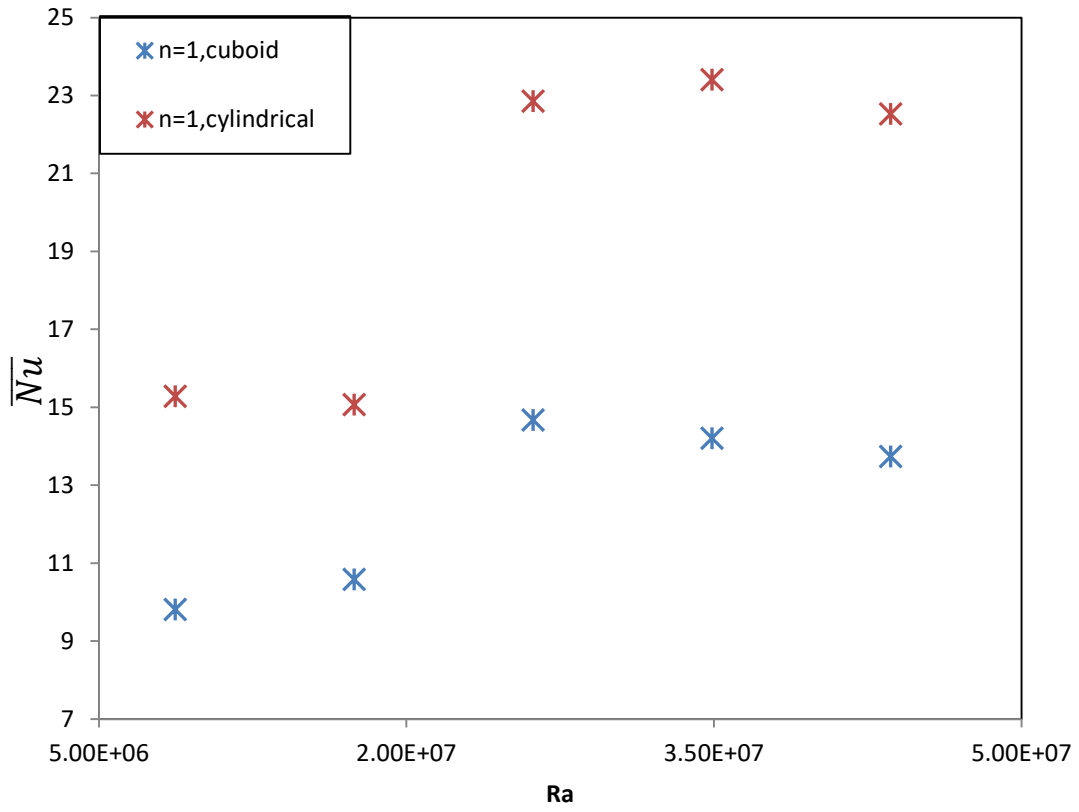

Figure (5- 26) effect of the shape of obstacle on Nusselt number for water and AR=0.75.

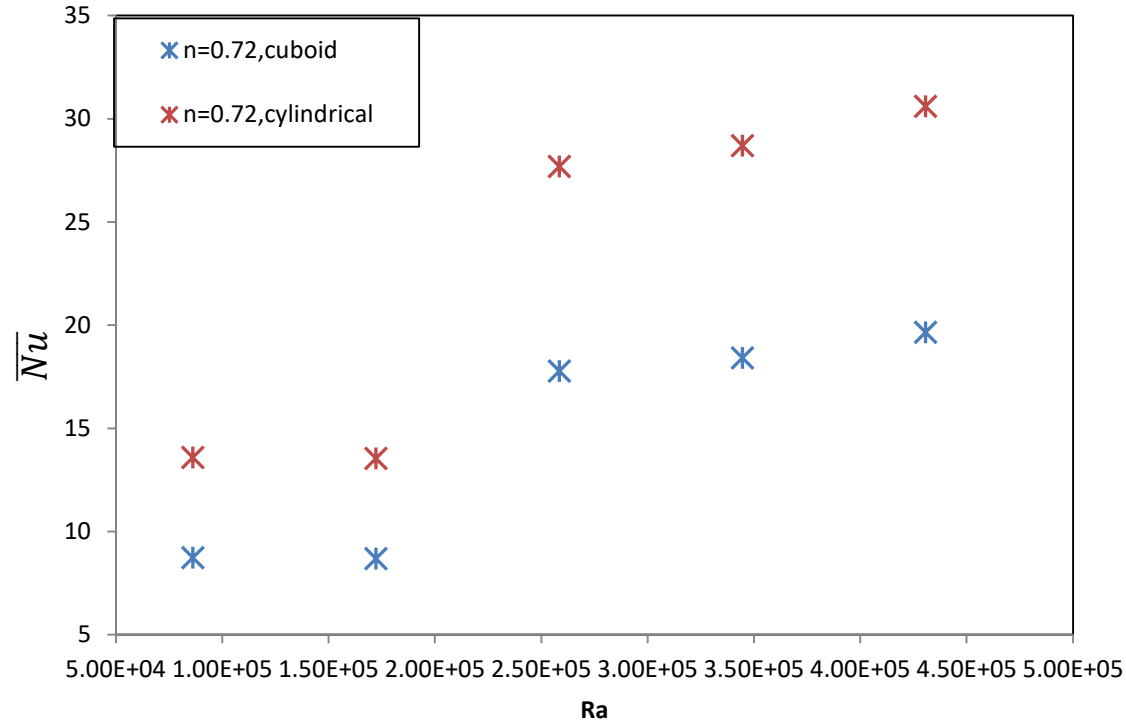

Figure (5- 27) effect of the shape of obstacle on Nusselt number for CMC 0.5% and AR=0.75

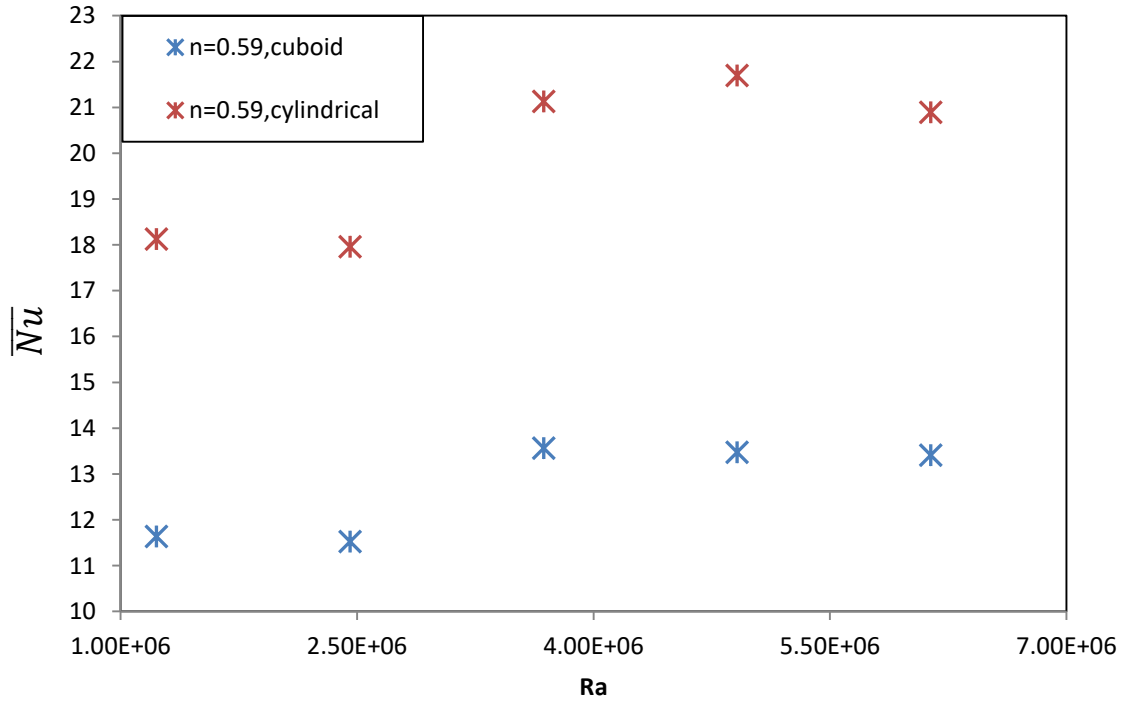

Figure (5- 28) effect of the shape of obstacle Nusselt number for CMC 1% and AR=0.75.

5.2 Theoretical result

Theoretical calculations have been carried out to solve the governing equations by the finite element approach are utilized by using COMSOL programming to find the temperature distribution as well as the mean Nusselt number.

The present simulation is validated with the results of the works performed by Kefayati [54] who studied "simulation of non-Newtonian molten polymer on natural convection inside the cavity", for all streamlines, isotherm contours, and average Nusselt number. The comparisons are presented in figures (5-29). It can be concluded that there are close agreements between the previous and current results for the same boundary conditions, where the error rate is about 1.9 %.

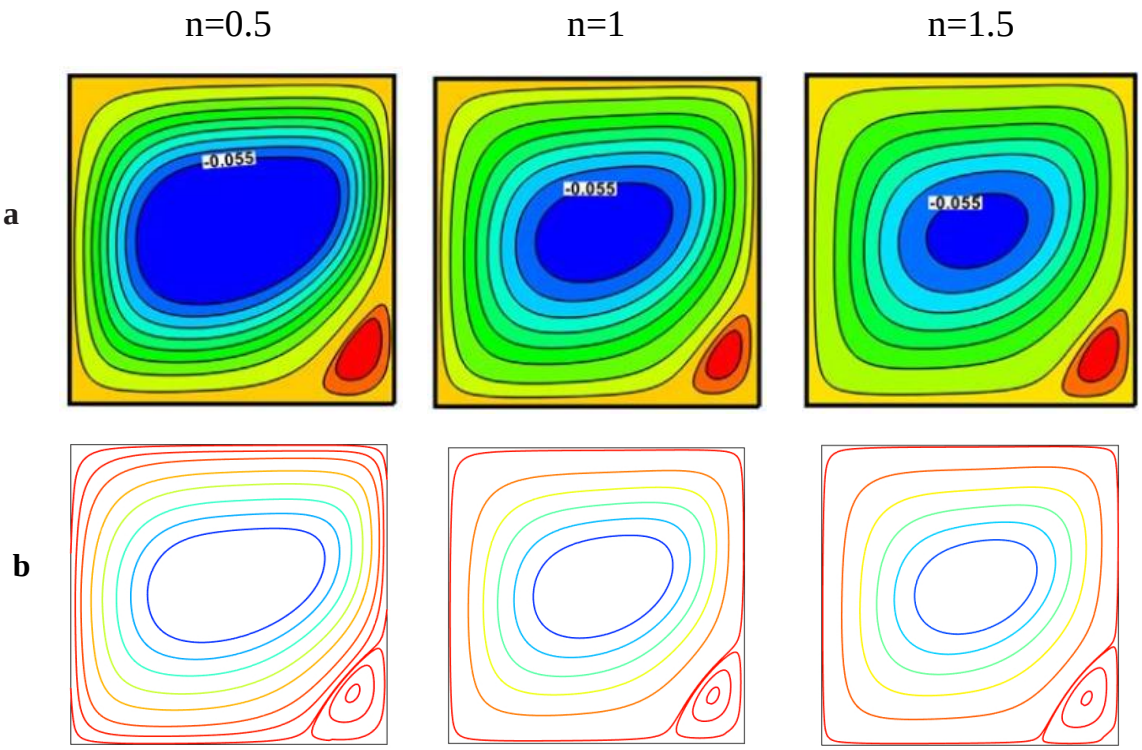

Figure (5-29 a) Comparison of the streamlines for various power-law indexes & $Ra=10^4$.

a:kefayati **b: present work**

a

b

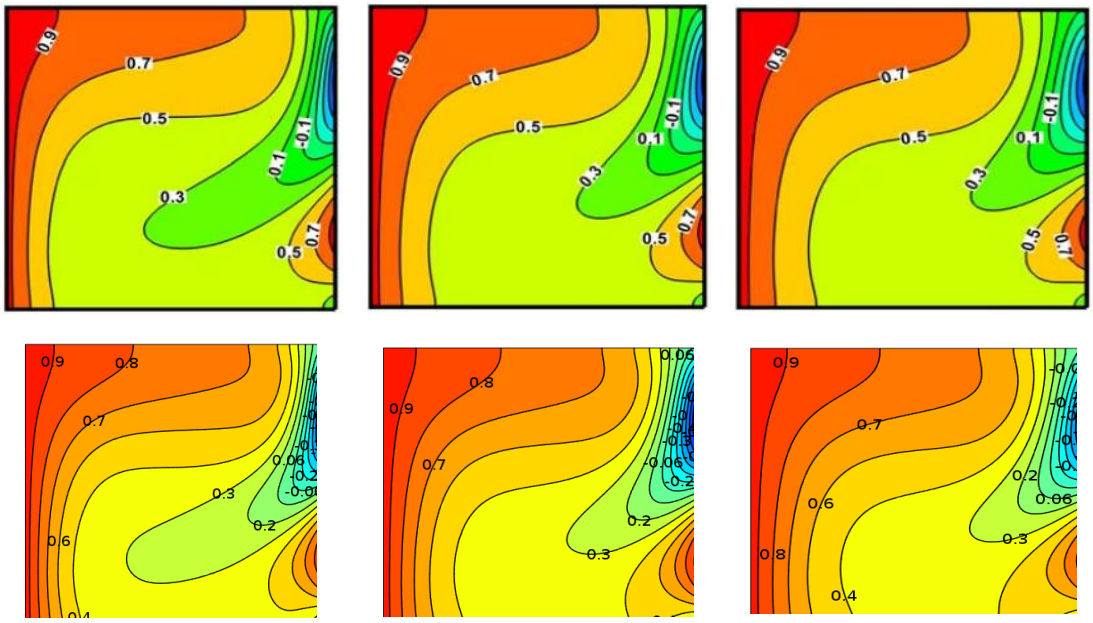

Figure (5-29 b) Comparison of the isotherms for various power-law indexes & Ra=10^4.

a:kefayati **b: present work**

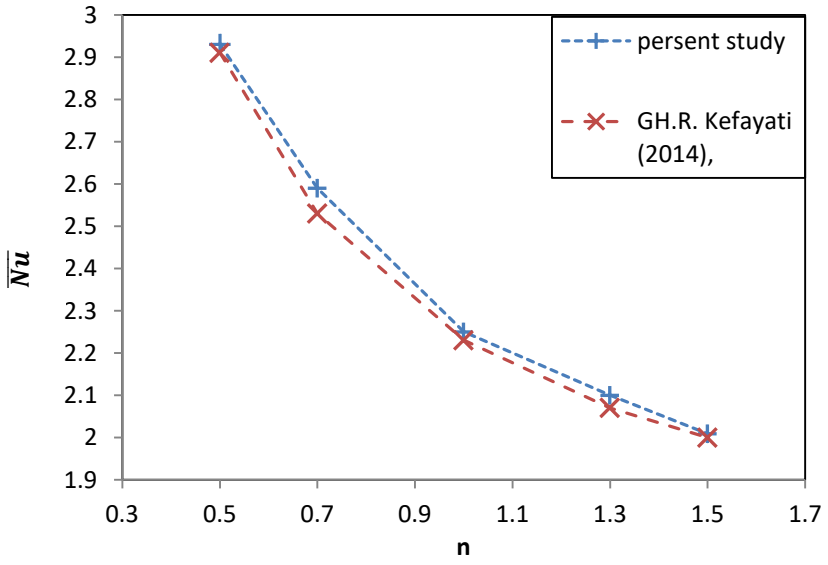

Figure (5- 29 c) Comparison of the average Nusselt number for various power-law indexes and Ra=10^4.

5.2.1 Temperature distribution

Since the obstacle is heated so the heat is transferred from the obstacle into the fluid. Hot fluid around the obstacle exhibits buoyancy forces and starts to rise against gravity and the temperature distribution depends upon the heat transfer physics configuration and momentum transport results in convection terms. The differences are more visible, especially at the top of the obstacle. Figures (5-30) to (5-33) appear the temperature distribution for various CMC content (n value as Non-Newtonian fluid indication) and shapes of obstacle. The increasing of the hot temperature T_h or Ra (by increasing temperature difference) increases the temperature range inside the enclosure. The increasing of power-law index lowers the heat transfer tendency, the results show the hot fluid particles migrate upward against the effect of gravity. The higher Ra means a higher volume of migrated fluid by gravity forces or density difference. As the Rayleigh number rises, so does the intensity of the rotating buoyancy force. The improvement biggest in convection intensity occurred at n = 0.59 because the shear-thinning fluids have a lower apparent viscosity than Newtonian fluids. The effect of CMC concentration appears directly upon the physical properties including, viscosity, density, and thermal conductivity. The correction factor of non-Newtonian fluid acts as braking forces to Newtonian behavior. In other words, the decreasing of temperature promotes the increasing of viscosity for Newtonian fluid whereas the shear stress which is powered to n reduces the action of viscosity. For various obstacle shapes and AR, the decreasing of n dissipates the temperature, where a wider area has a low gradient tendency. The higher temperature shows sharp behavior toward the index power-law value.

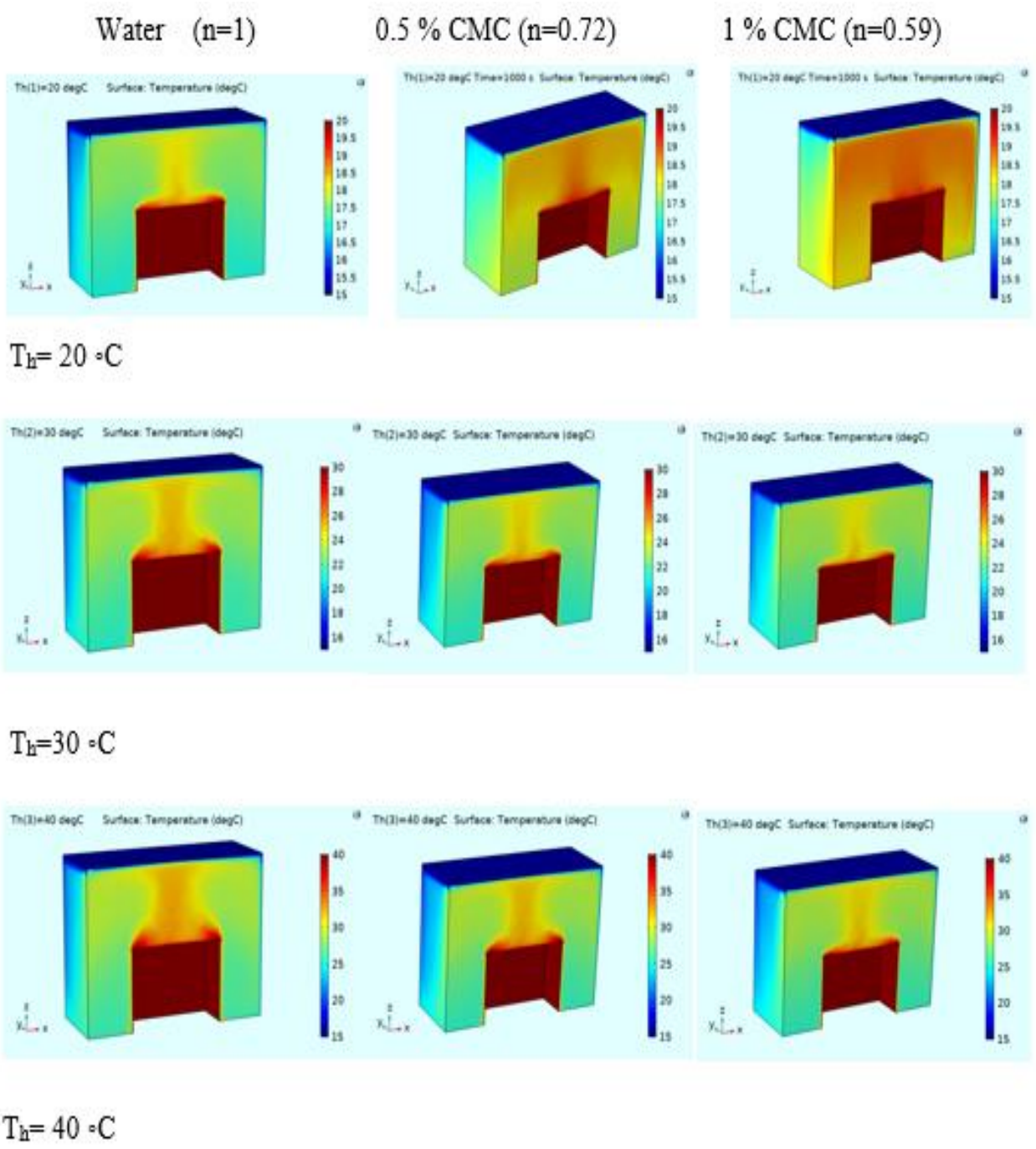

Figure (5- 30) temperature distribution of water, 0.5 % CMC and 1 % CMC inside a cuboid obstacle of AR=0.5 for various Ra and Th.

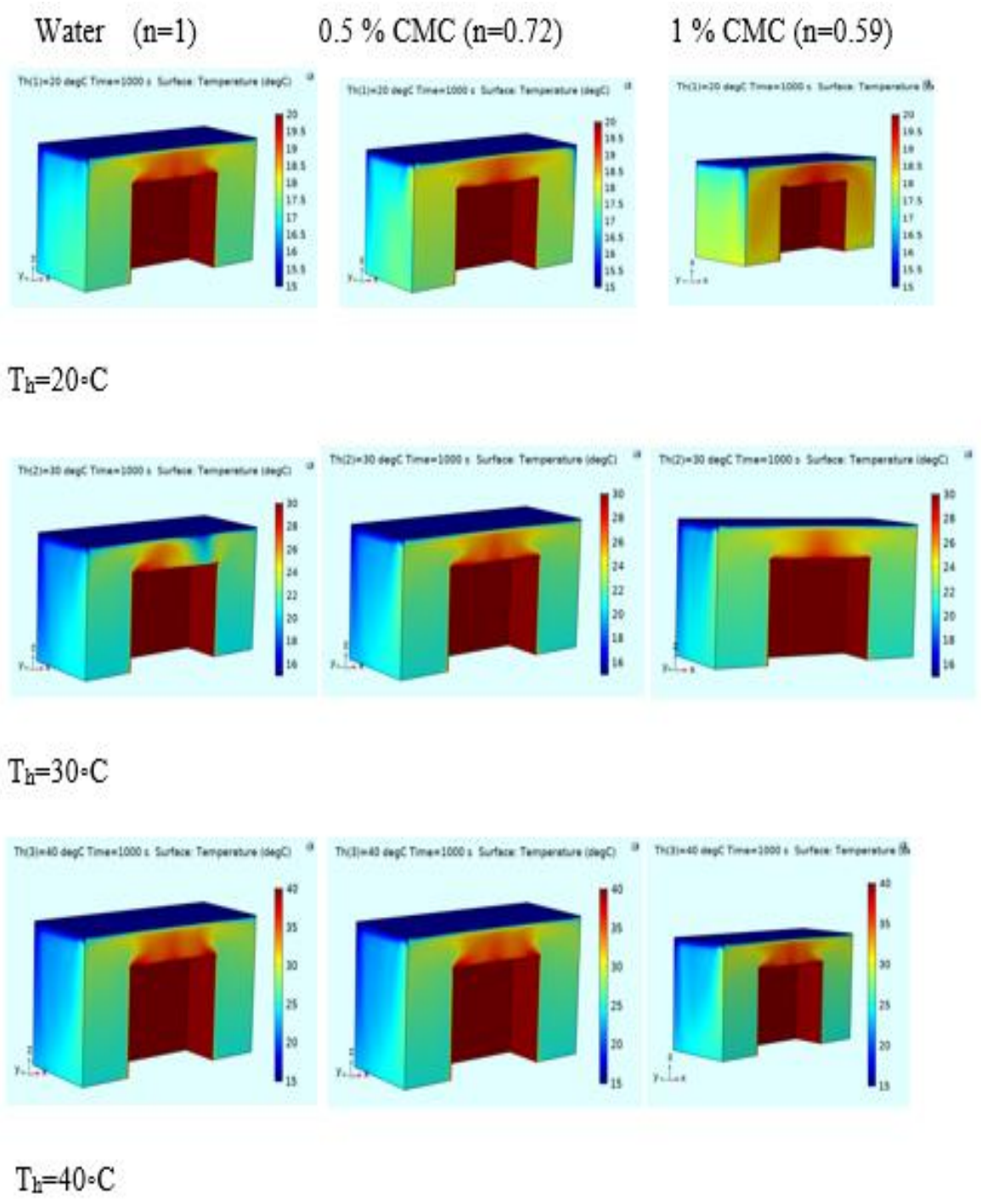

Figure (5- 31) temperature distribution of water, 0.5 % CMC and 1 % CMC inside a cuboid obstacle of AR=0.75 for various Th.

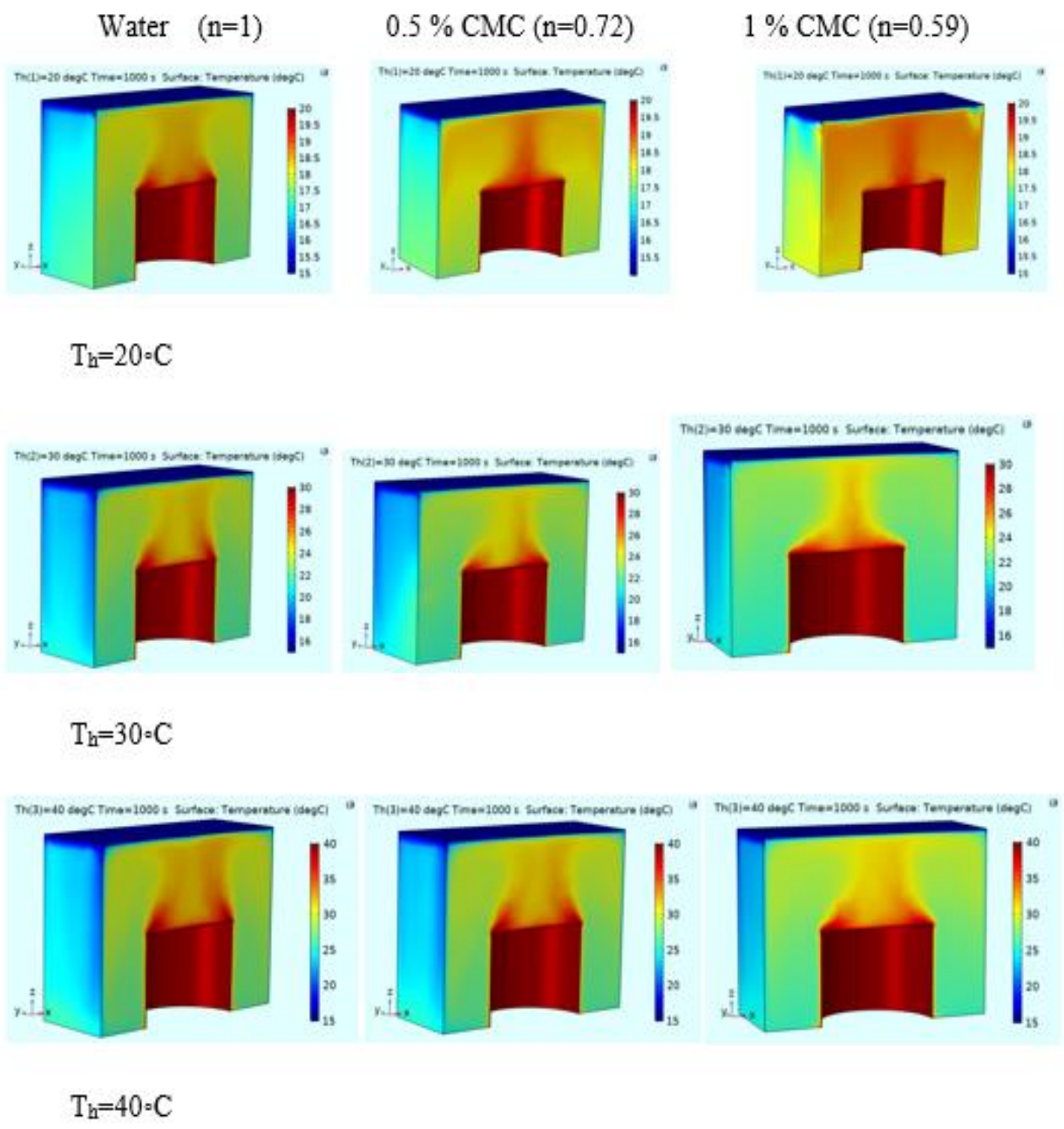

Figure (5- 32) temperature distribution of water, 0.5 % CMC and 1 % CMC inside cylinder obstacle of AR=0. 5 for various Th.

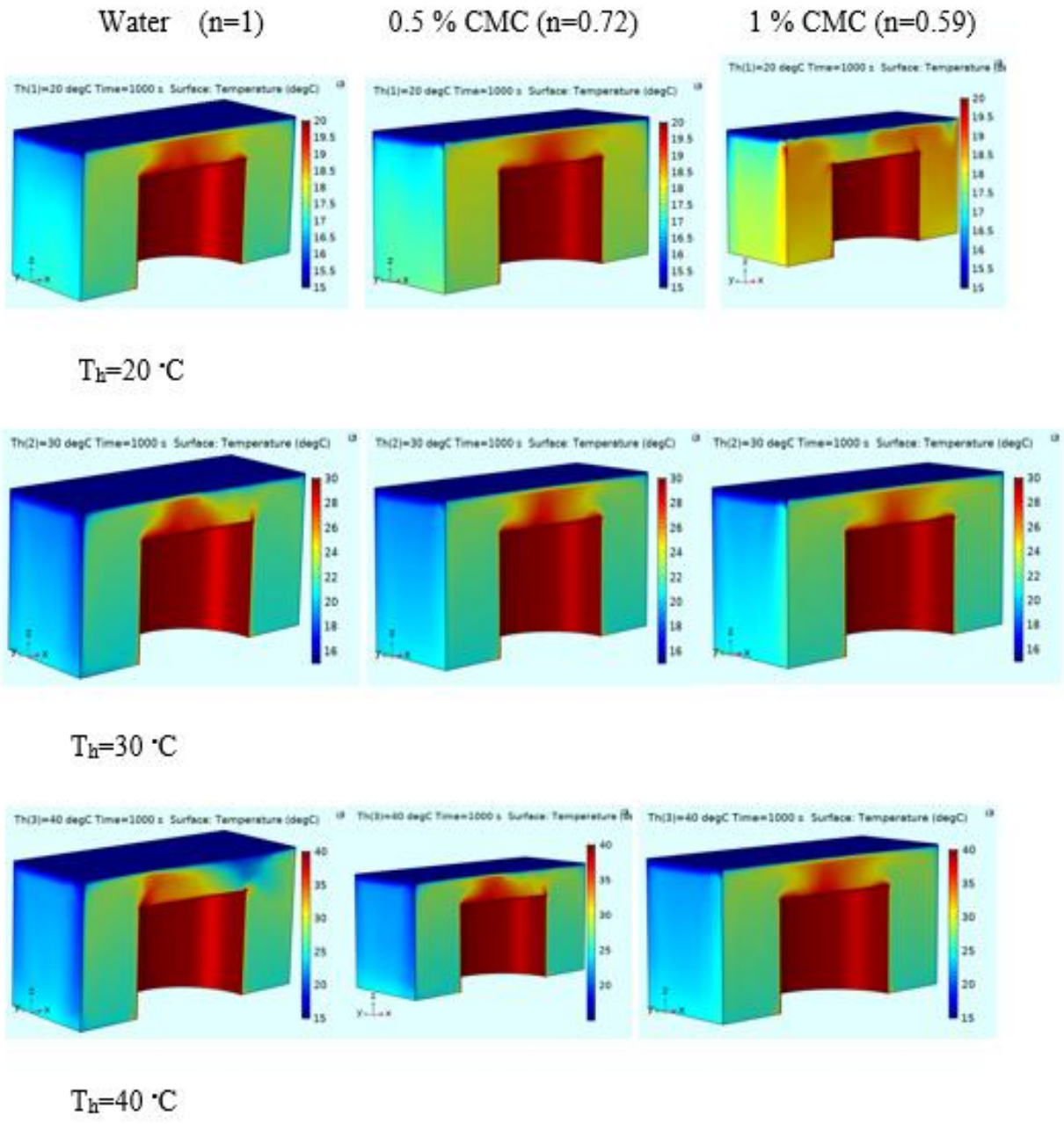

Figure (5- 33) temperature distribution of water, 0.5 % CMC and 1 % CMC inside cylinder obstacle of AR=0. 75 for various Th.

Figure (5-34) indicates the effect of AR of cuboid obstacles on temperature distribution. The heat transfer distribution when AR=0.75 is not regular natural convection compared with AR=0.5, in space between the enclosure and obstacle because of the boundary layers' interactions and the conductive heat transfer tendency. The increasing temperature

difference rises the natural convection action and reduces the conductive heat transfer.

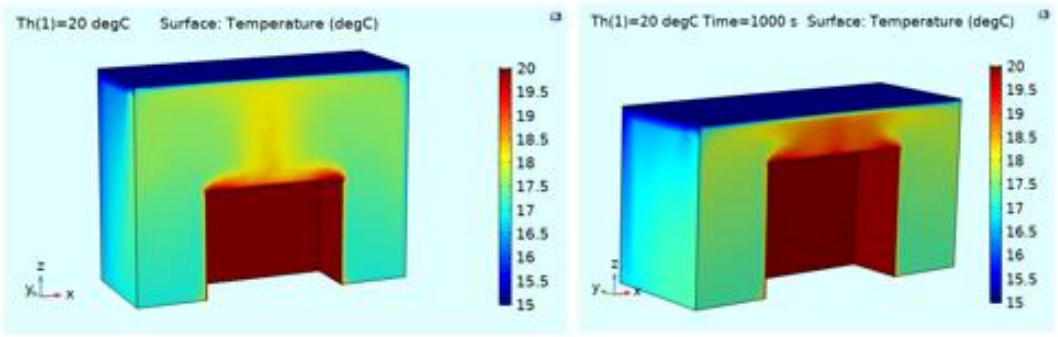

T_h= 20 ◦C

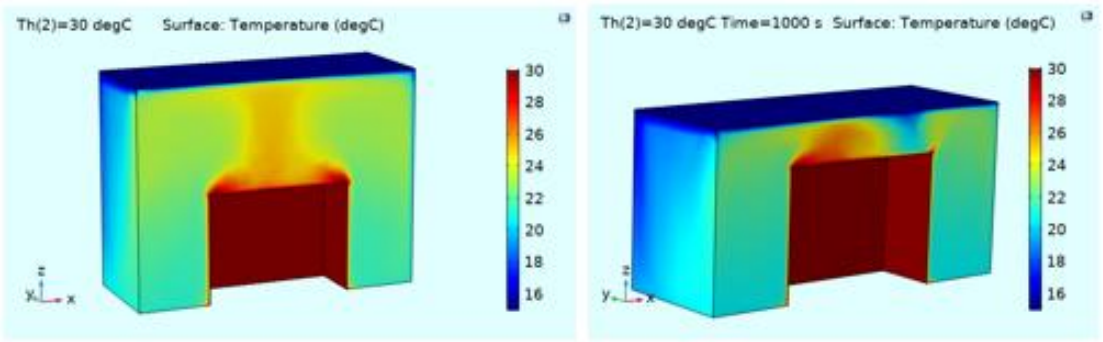

T_h=30 ◦C

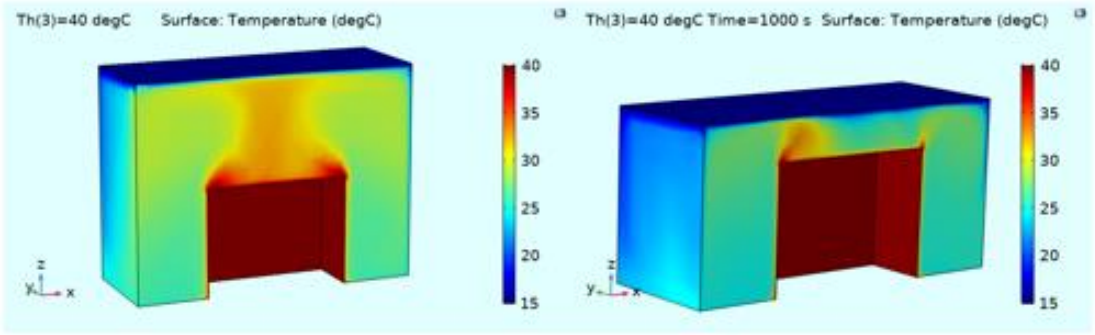

T_h= 40 ◦C

Figure (5- 34) temperature distribution water inside a cuboid obstacle of AR=0.5 and 0.75 for various Th.

Figures (5-35) and (5-36) show the effect of obstacle shape on temperature distribution for various aspect ratios and hot temperatures. The curvature area of hot particles migration upwards appears for a cylindrical

obstacle in general cases. At AR=0.5 the migration rate seemed to be equal with the maximum behavior of heat transfer natural convection in rectangle case. The cuboid hot surface area in a perpendicular direction to gravity action is higher than the cylinder case. For AR=0.75, the conductive heat transfer mechanisms are seemed to be the major control mechanism within the system because of the short distance between the two surfaces of the enclosure.

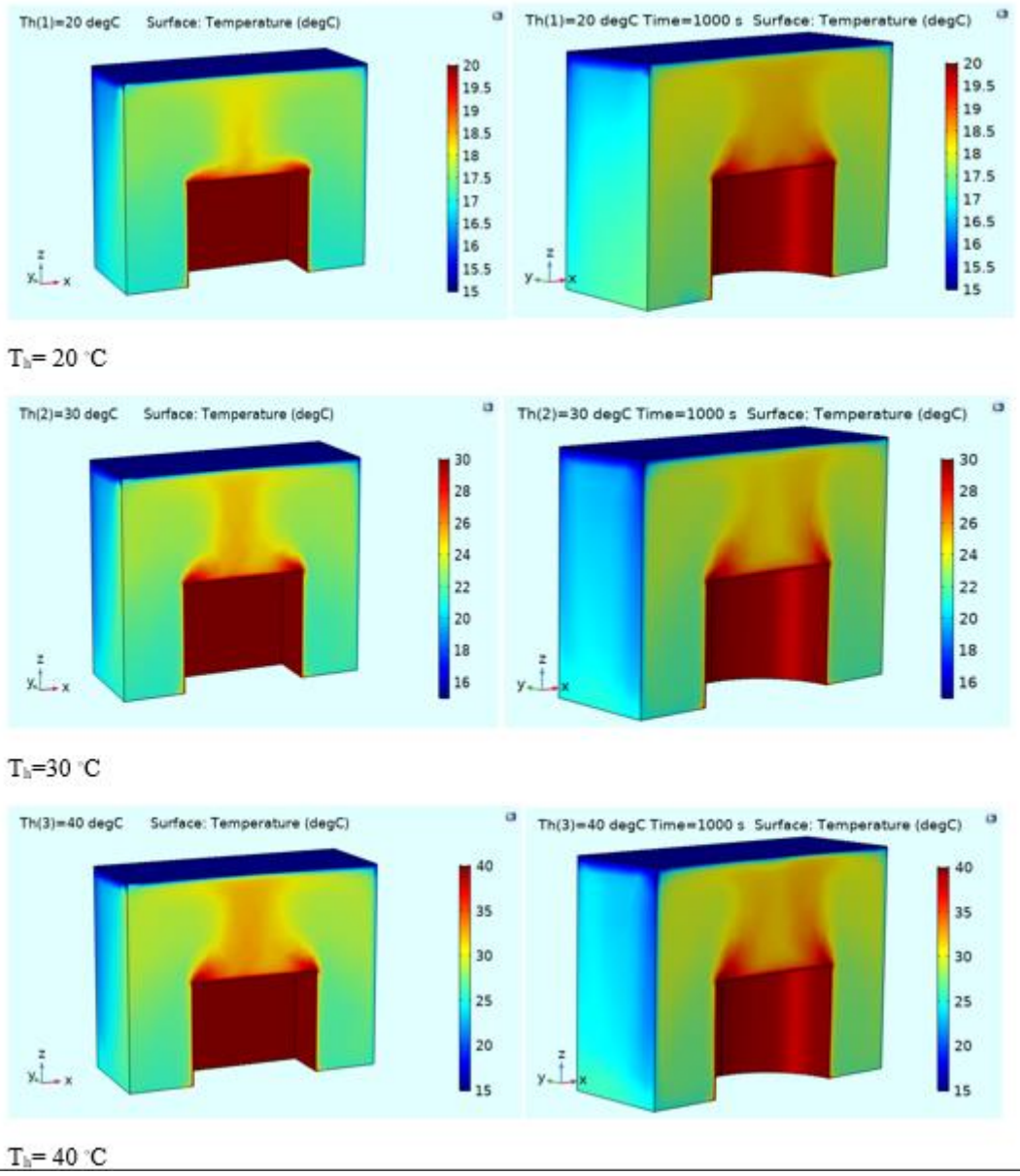

Figure (5- 35) temperature distribution water inside a cuboid and cylindrical obstacle of AR=0.5 for various Th.

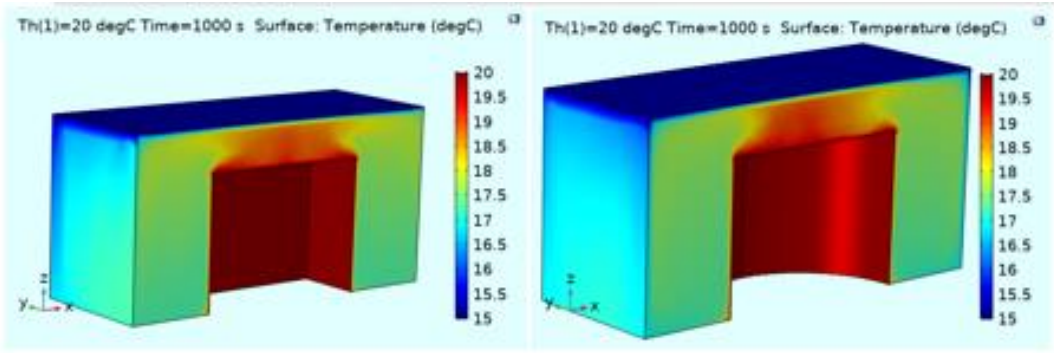

T_h= 20 °C

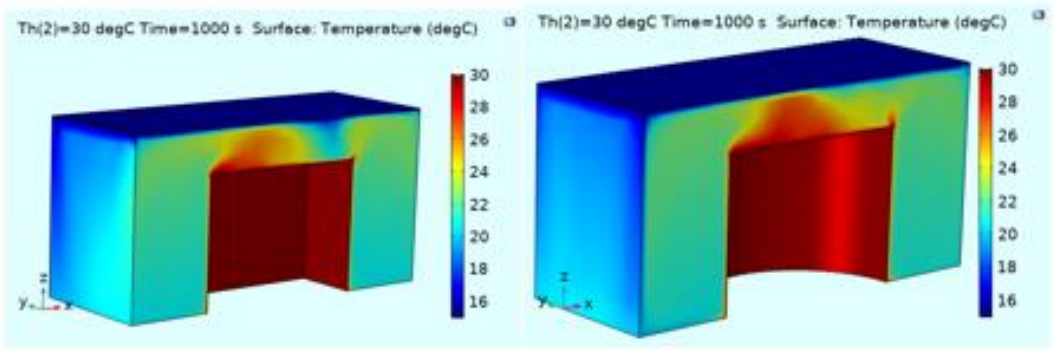

T_h=30 °C

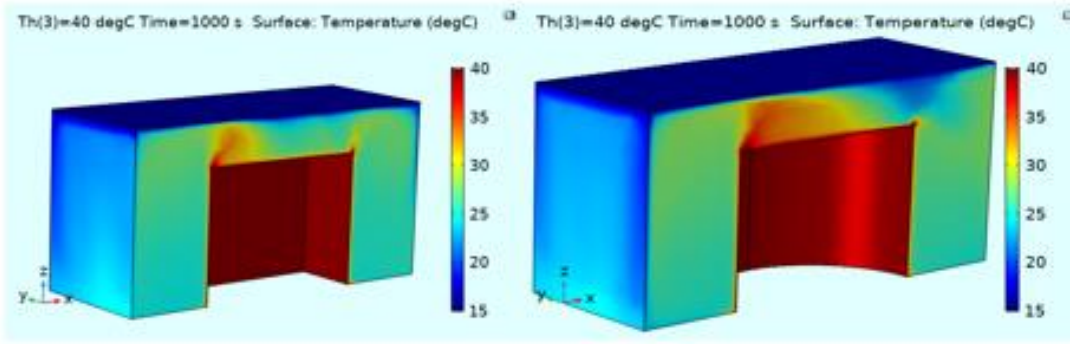

T_h= 40 °C

Figure (5- 36) temperature distribution water inside a cuboid and cylindrical obstacle of AR=0.75 for various Th.

5.2.2 Heat transfer coefficient

The heat transfer coefficient is determined by applying equation (4.5) for the whole enclosure. Figures (5-37) to (5-40) show the Nu with Ra plots for various AR, CMC %, and obstacle shapes. The non-direct proportional between the Ra and Nu is shown for CMC content and

AR=0.75. while the water case explains the linear behavior of Ra on Nu. The non-Newtonian fluids have dependent on temperature, so the nonlinear behavior is converted into polynomial behavior. For the AR effect, the thermal boundary layers of two surfaces will be interacted by increasing AR in addition to decreasing the gravity momentum region by decreasing the distance. The cylinder shape has non-uniform temperature distribution, so the hot fluid particles will be slightly minimum values and have non-regular polynomial Nu with Ra trends. The heat transfer coefficient decreases by increasing n (increasing CMC %) but the general case of Nu is reverse to heat transfer coefficient because the deducing in heat transfer coefficient ratio is less than thermal conductivity reduction.

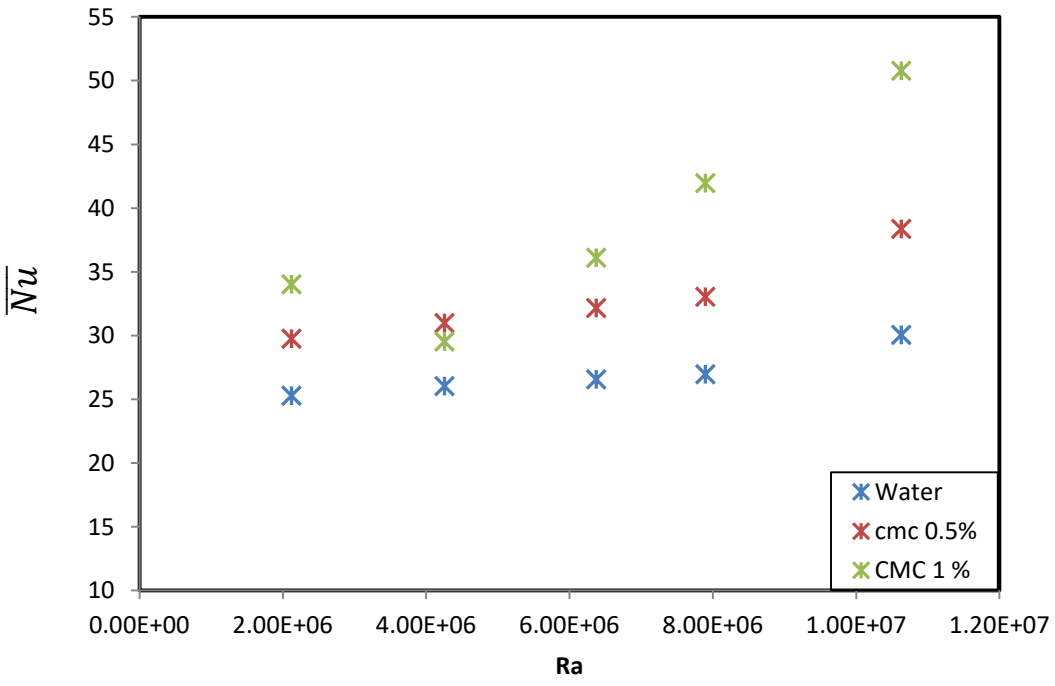

Figure (5- 37) $\overline{Nu}$ and Ra plots for various CMC % for a cuboid obstacle, AR=0.5.

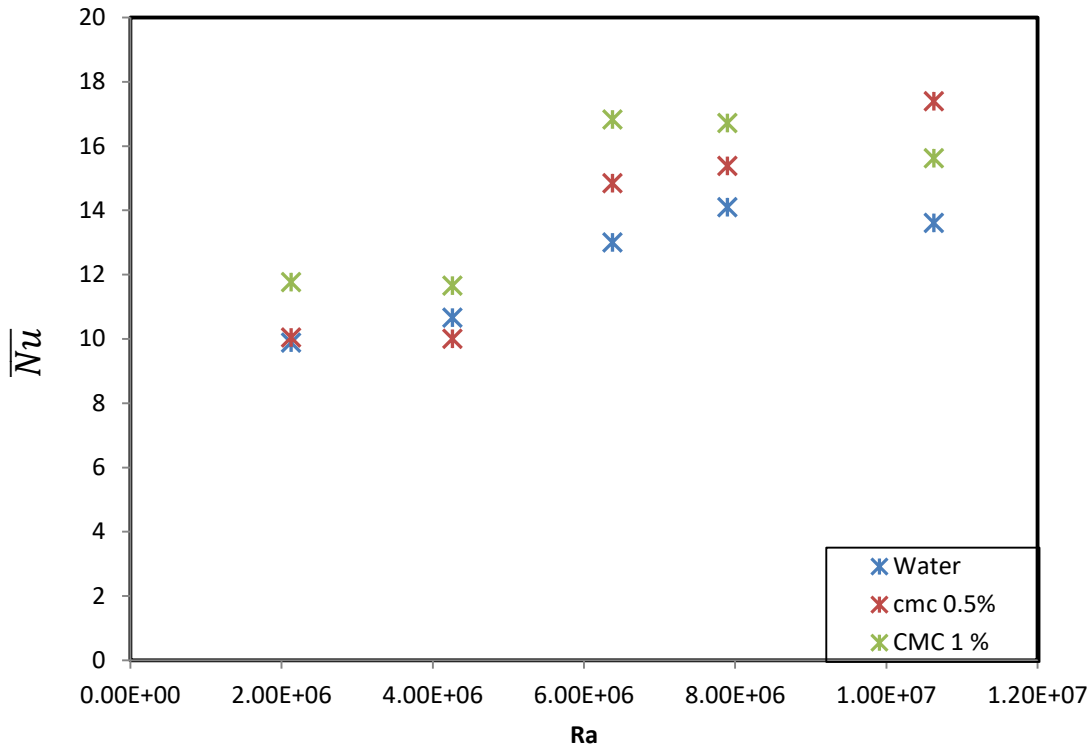

Figure (5- 38) $\overline{Nu}$ and Ra plots for various CMC % for a cuboid obstacle , AR=0.75

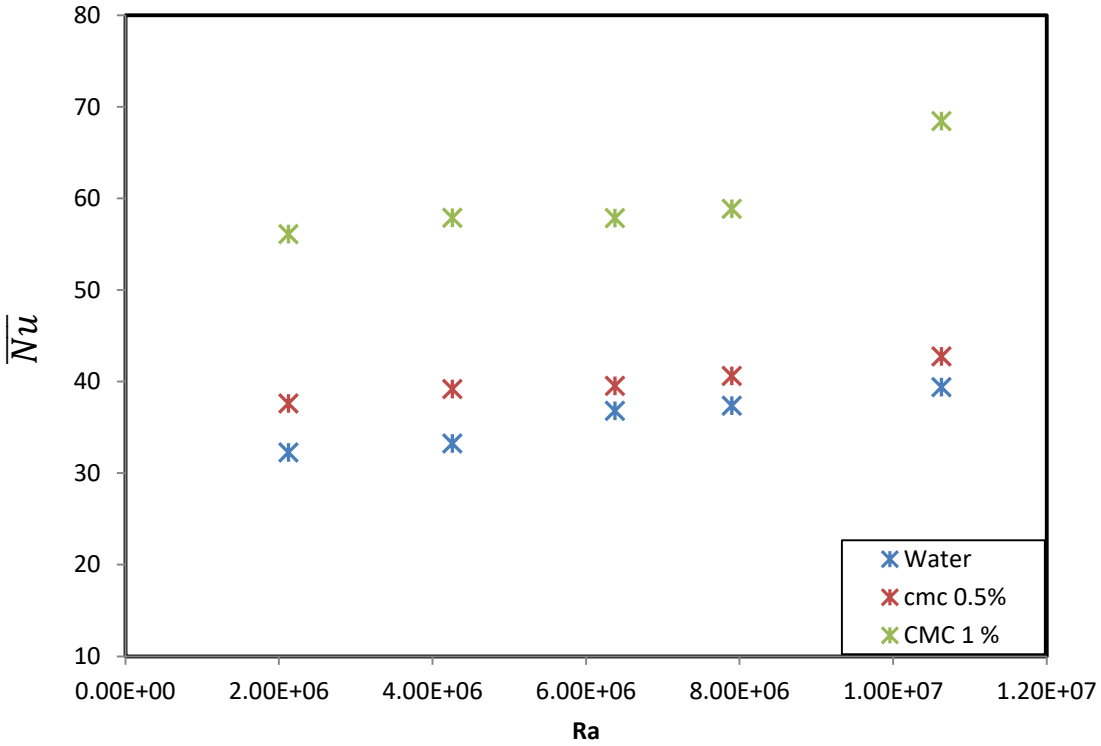

Figure (5- 39) $\overline{Nu}$ and Ra plots for various CMC % for a cylindrical obstacle, AR=0. 5.

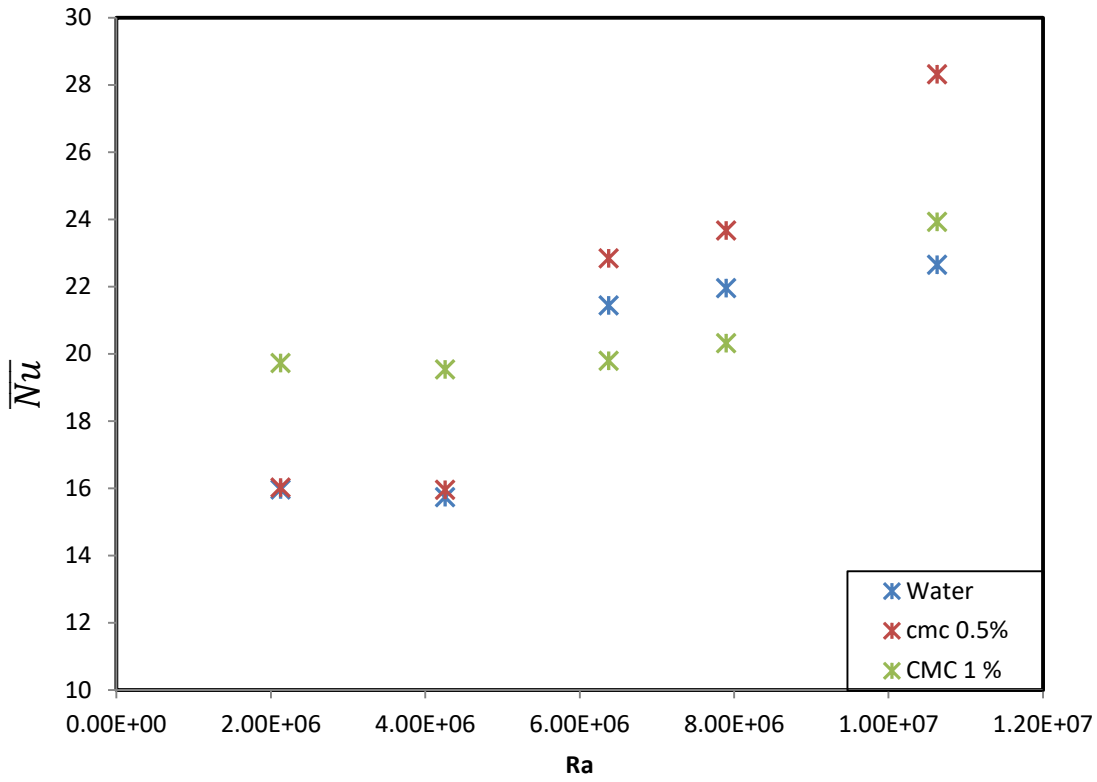

Figure (5- 40) $\overline{Nu}$ and Ra plots for various CMC % for cylindrical obstacle, AR=0.75.

5.3 Comparison of experimental and theoretical results

To verify the simulation (CFD) model, the three tests of experimental results were compared with theoretical results under the same organizational and technological conditions. The wall temperature of the obstacle and the fluid inside the enclosure was measured experimentally for different flow rates using CMC1%, CMC 0.5%, and water, and by comparison with the theoretical results, a good match was obtained where the error rate ranged 8.9% for all the three tests in terms of using the three fluids, using Configurable obstacle, and both values for aspect ratio.

Figures (5-41) to (5-44) illustrate the comparisons between the experimental and theoretical results of the Nusselt number and the temperature difference between the hot and cold walls (ΔT).

These figures show that the Nusselt number increases with the increase of the temperature difference. The increase of the difference leads to an increase in the Rayleigh number that associated with the buoyancy forces and thus the increase in the Nuslet number. A similarity in the behavior and a clear convergence were observed. The maximum deviation between the theoretical and the experimental average Nusselt numbers is observed at AR=0.75 with a cylinderical obstacle shape and 0.5% CMC which is a 21%. While a lower value is 0.7% which shown at AR = 0.5 in water at different obstacle shapes. The difference between the experimental and numerical results are due to the experimental uncertainty, the numerical simulation hypotheses, some experimental errors, the accuracy of the instruments, and the laboratory conditions.

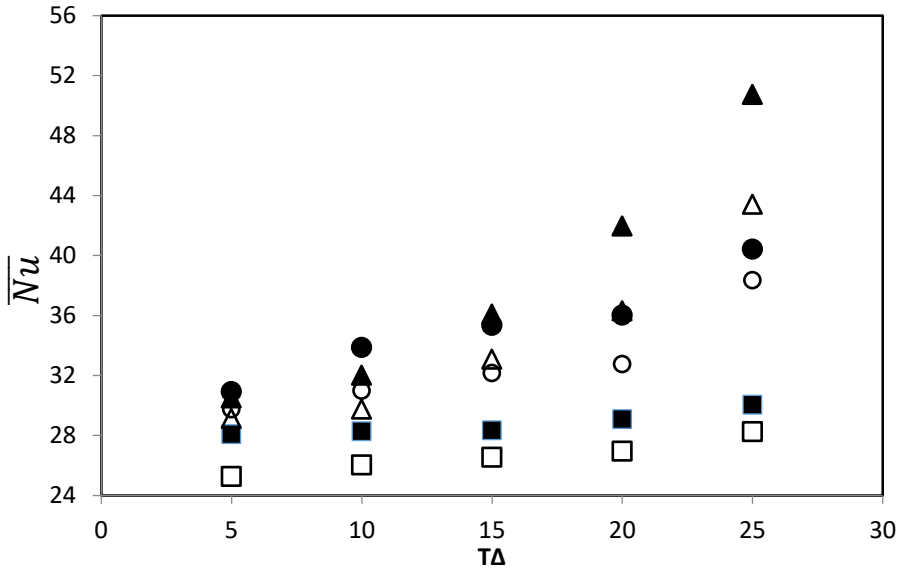

Figure (5- 41) $\overline{Nu}$ and ΔT plots for various CMC % for a cuboid obstacle at AR=0.5 for water (squares), 0.5% CMC (circles), and 1% CMC (tiangles). The experimental and numerical works appear with filled black and open black symbols respectively.

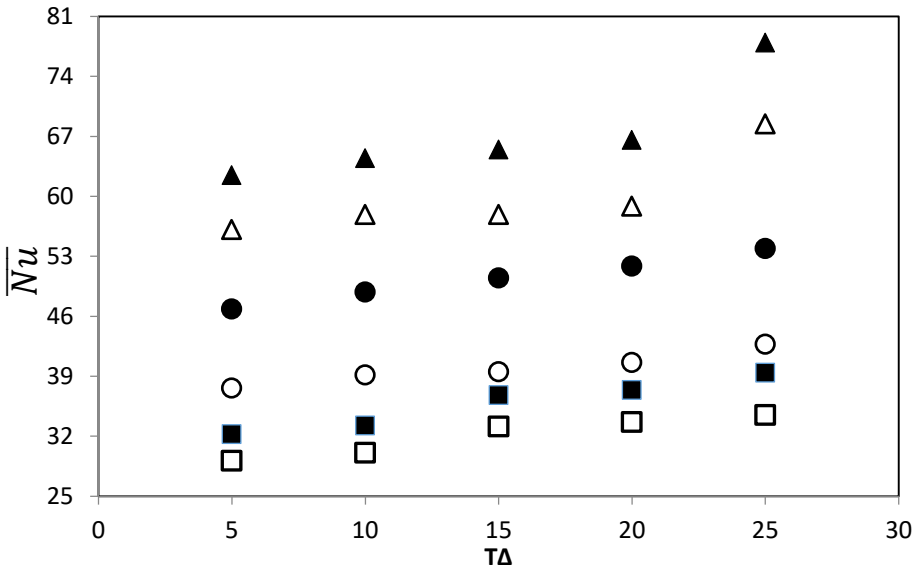

Figure (5- 42) $\overline{Nu}$ and ΔT plots for various CMC % for a cylindercal obstacle at AR=0.5 for water (squares), 0.5% CMC (circles), and 1% CMC (tiangles). The experimental and numerical works appear with filled black and open black symbols respectively.

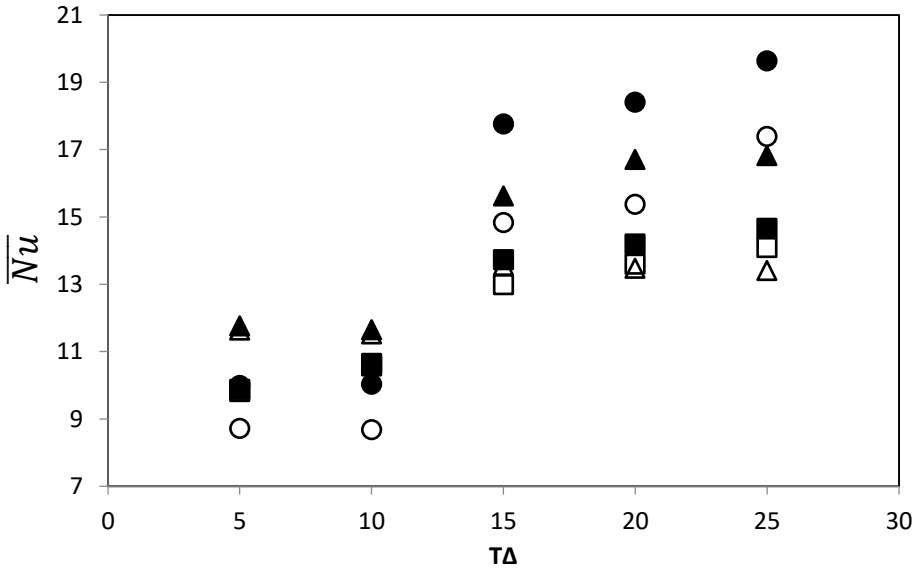

Figure (5- 43) $\overline{Nu}$ and ΔT plots for various CMC % for a cuboid obstacle at AR=0.75 for water (squares), 0.5% CMC (circles), and 1% CMC (tiangles). The experimental and numerical works appear with filled black and open black symbols respectively.

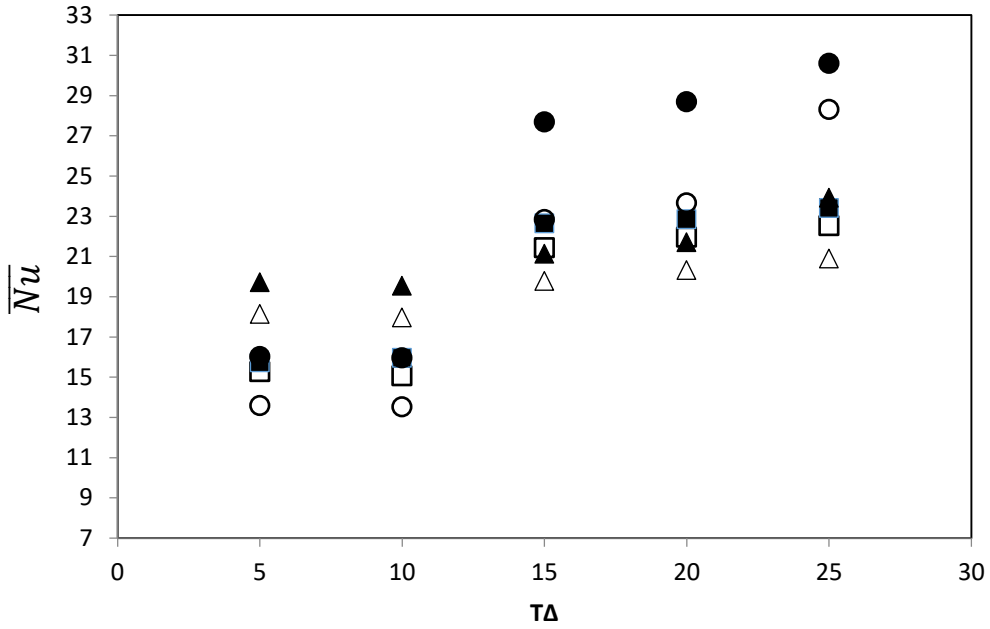

Figure (5- 44) $\overline{Nu}$ and ΔT plots for various CMC % for a cylindercal obstacle at AR=0.75 for water (squares), 0.5% CMC (circles), and 1% CMC (tiangles). The experimental and numerical works appear with filled black and open black symbols respectively.

CHAPTER SIX

CONCLUSIONS

AND

RECOMMENDATION

Conclusions and Recommendation

6.1 Conclusions

In this study, power-law fluid at steady-state and laminar natural convection in the rectangular enclosure containing hot obstacle has been investigated experimentally and theoretically. The most important conclusions in this study can be summarized as follows:

1. The experimental work showed the effect of the change in the temperature difference between cold and hot enclosure walls, the concentrations of CMC, the aspect ratio, and the shape of the obstacle on the heat transfer inside the enclosure.
2. Increasing the temperature difference between the cold and hot walls lead to the motion of vortices enhanced in the enclosure medium increases.
3. The temperature gradient in all cases increases with the increase of the temperature difference between the cold and hot walls increase.
4. Nusselt number increases with the increase of the concentration of the non-Newtonian (CMC), which leads to a decrease in the value of power law index (n).
5. Nusselt number increases with increasing Ra due to a strengthening of the thermal advection irrespective of boundary condition.
6. Nusselt number shows a decrease with an increase in AR for the same set of Ra values for shear thinning fluid and Newtonian fluid.
7. The experimental work agreed well with the theoretical work with an average deviation rate of about 8.9 %.

6.2 Recommendation for future work

The current study addressed some of the major issues related to the natural convection of non-Newtonian fluids in the enclosure, however, further efforts should be directed to further improvement in the basic understanding of this topic. These efforts are :

1. Investigation of turbulent convection for non-Newtonian fluids in enclosures.
2. Studying the effect of adding the Nanofluids to the non-Newtonian fluids.
3. Examine the same problem as the present work for more complex forms of the enclosure.
4. studying the effect of the magnetic field on the natural convection in a three-dimensional cavity
5. Using another fluid that works like carboxy polymethylene (Carbopol-series) or Bingham model to study its effect on enhancing heat transfer.
6. Study of forced and mixed convection (turbulent and laminar) in the 3-D cavity for the same studied cases.

REFERENCES

References

[1] T. L. Bergman, A. S. Lavine, F. P. Incropera, and D. P. Dewitt“Fundamentals of Heat and Mass Transfer. Book, 7th Edition.” p. 1048, 2011.

[2] S. Yigit, “A numerical investigation on laminar natural convection of non-Newtonian fluids in enclosed spaces,” Thesis, 2018.

[3] W. P. Graebel, Advanced Fluid Mechanics, Book, vol. 53. 2013.

[4] Ali A. Rashaida “Flow of a Non-Newtonian Bingham Plastic Fluid Over a Rotating Disk,” Thesis, no. August, 2005.

[5] F. White, “Viscous Fluid Flow” Book, 3rd Edition McGraw Hill_ p. 656, 2005.

[6] A. Sharma, V. V. Tyagi, C. R. Chen, and D. Buddhi, “Review on thermal energy storage with phase change materials and applications,” Renew. Sustain. Energy Rev., vol. 13, no. 2, pp. 318–345, 2009, doi: 10.1016/j.rser.2007.10.005.

[7] X. Han, Y. Wang, and L. Zhu, “The performance and long-term stability of silicon concentrator solar cells immersed in dielectric liquids,” Energy Convers. Manag., vol. 66, pp. 189–198, 2013, doi: 10.1016/j.enconman.2012.10.009.

[8] R. P. Chhabra and J. F. Richardson, “Non-Newtonian Flow in the Process Industries British Library Cataloguing in Publication Data,” p. 6, 1999.

[9] G. Bin Kim, J. M. Hyun, and H. S. Kwak, “Transient buoyant convection of a power-law non-Newtonian fluid in an enclosure,” Int.

J. Heat Mass Transf., vol. 46, no. 19, pp. 3605–3617, 2003, doi: 10.1016/S0017-9310(03)00149-2.

[10] M. Lamsaadi, M. Naïmi, and M. Hasnaoui, "Natural convection heat transfer in shallow horizontal rectangular enclosures uniformly heated from the side and filled with non-Newtonian power law fluids," Energy Convers. Manag., vol. 47, no. 15–16, pp. 2535–2551, 2006, doi: 10.1016/j.enconman.2005.10.028.

[11] M. Lamsaadi, M. Naimi, M. Hasnaoui, and M. Mamou, "1 Natural convection in a vertical rectangular cavity filled with a non-newtonian power law fluid and subjected to a horizontal temperature gradient," Numer. Heat Transf. Part A Appl., vol. 49, no. 10, pp. 969–990, 2006, doi: 10.1080/10407780500324988.

[12] M. Lamsaadi, M. Naïmi, M. Hasnaoui, and M. Mamou, "Natural convection in a tilted rectangular slot containing non-newtonian power-law fluids and subject to a longitudinal thermal gradient," Numer. Heat Transf. Part A Appl., vol. 50, no. 6, pp. 561–583, 2006, doi: 10.1080/10407780600599513.

[13] A. Muhadi, "Laminar Natural Convection of Newtonian and Non – Newtonian Fluids Inside Triangular Enclosure," vol. 3, no. 1, 2007.

[14] O. Turan, N. Chakraborty, and R. J. Poole, "Laminar natural convection of Bingham fluids in a square enclosure with differentially heated side walls," J. Nonnewton. Fluid Mech., vol. 165, no. 15–16, pp. 901–913, 2010, doi: 10.1016/j.jnnfm.2010.04.013.

[15] O. Turan, A. Sachdeva, N. Chakraborty, and R. J. Poole, "Laminar natural convection of power-law fluids in a square enclosure

with differentially heated side walls subjected to constant temperatures," J. Nonnewton. Fluid Mech., vol. 166, no. 17–18, pp. 1049–1063, 2011, doi: 10.1016/j.jnnfm.2011.06.003.

[16] O. Turan, A. Sachdeva, R. J. Poole, and N. Chakraborty, "Laminar natural convection of power-law fluids in a square enclosure with differentially heated sidewalls subjected to constant wall heat flux," J. Heat Transfer, vol. 134, no. 12, pp. 1–15, 2012, doi: 10.1115/1.4007123.

[17] P. Ternik and R. Rudolf, "Laminar natural convection of non-Newtonian nanofluids in a square enclosure with differentially heated side walls," Int. J. Simul. Model., vol. 12, no. 1, pp. 5–16, 2013, doi: 10.2507/IJSIMM12(1)1.215.

[18] A. Sojoudi, S. C. Saha, Y. T. Gu, and M. A. Hossain, "Steady natural convection of non-newtonian power-law fluid in a trapezoidal enclosure," Adv. Mech. Eng., vol. 2013, 2013, doi: 10.1155/2013/653108.

[19] P. Ternik, R. Rudolf, and Z. Žunič, "Heat-transfer characteristics of a non-newtonian Au nanofluid in a cubical enclosure with differentially heated side walls," Mater. Tehnol., vol. 49, no. 1, pp. 87–93, 2015.

[20] S. Yigit, R. J. Poole, and N. Chakraborty, "Effects of aspect ratio on laminar Rayleigh-Bénard convection of power-law fluids in rectangular enclosures: A numerical investigation," Int. J. Heat Mass Transf., vol. 91, pp. 1292–1307, 2015, doi: 10.1016/j.ijheatmasstransfer.2015.08.032.

[21] A. Raisi, "Natural convection of non-Newtonian fluids in a square cavity with a localized heat source," Stroj. Vestnik/Journal

Mech. Eng., vol. 62, no. 10, pp. 553–564, 2016, doi: 10.5545/sv-jme.2015.3218.

[22] K. M. Gangawane and B. Manikandan, “Laminar natural convection characteristics in an enclosure with heated hexagonal block for non-Newtonian power law fluids,” Chinese J. Chem. Eng., vol. 25, no. 5, pp. 555–571, 2017, doi: 10.1016/j.cjche.2016.08.028.

[23] A. I. Alsabery, A. J. Chamkha, H. Saleh, and I. Hashim, “Transient natural convective heat transfer in a trapezoidal cavity filled with non-Newtonian nanofluid with sinusoidal boundary conditions on both sidewalls,” Powder Technol., vol. 308, pp. 214–234, 2017, doi: 10.1016/j.powtec.2016.12.025.

[24] E. Khalili, A. Saboonchi, and M. Saghafian, “Experimental study of nanoparticles distribution in natural convection of Al2O3-water nanofluid in a square cavity,” Int. J. Therm. Sci., vol. 112, pp. 82–91, 2017, doi: 10.1016/j.ijthermalsci.2016.09.031.

[25] H. Abou-Ziyan, A. Kalender, M. Shedid, and H. Abdel-Hameed, “Experimental investigation of free convection from short horizontal cylinder to Newtonian and power-law liquids of large Prandtl numbers,” Exp. Therm. Fluid Sci., vol. 86, pp. 102–116, 2017, doi: 10.1016/j.expthermflusci.2017.04.004.

[26] Z. M. Hasan, H. Awad, K. Saad, A. H. Ali, and H. G. Hameed, “Numerical Investigation of Free Convection Heat Transfer with non-Newtonian Fluid in Different Enclosures Geometries,” pp. 736–744, 2018.

[27] S. Thohura, M. M. Molla, and M. M. A. Sarker, “Natural convection of non-Newtonian shear-thinning fluid flow inside a

skewed cavity," AIP Conf. Proc., vol. 2121, no. July, 2019, doi: 10.1063/1.5115859.

[28] I. Pishkar, B. Ghasemi, A. Raisi, and S. M. Aminossadati, "Numerical study of unsteady natural convection heat transfer of Newtonian and non-Newtonian fluids in a square enclosure under oscillating heat flux," J. Therm. Anal. Calorim., vol. 138, no. 2, pp. 1697–1710, 2019, doi: 10.1007/s10973-019-08253-1.

[29] Z. H. Khan, W. A. Khan, and M. Hamid, "Non-Newtonian fluid flow around a Y-shaped fin embedded in a square cavity," J. Therm. Anal. Calorim., 2020, doi: 10.1007/s10973-019-09201-9.

[30] Z. Li, A. Shahsavar, K. Niazi, A. A. A. A. Al-Rashed, and P. Talebizadehsardari, "The effects of vertical and horizontal sources on heat transfer and entropy generation in an inclined triangular enclosure filled with non-Newtonian fluid and subjected to magnetic field," Powder Technol., vol. 364, pp. 924–942, 2020, doi: 10.1016/j.powtec.2019.10.076.

[31] S. Pandey, Y. G. Park, and M. Y. Ha, "Flow and heat transfer characteristics of non-Newtonian fluid in a square enclosure containing an internal cylinder," J. Mech. Sci. Technol., vol. 34, no. 7, pp. 3079–3094, 2020, doi: 10.1007/s12206-020-0639-9.

[32] S. Pandey, Y. G. Park, and M. Y. Ha, "Unsteady analysis of natural convection in a square enclosure filled with non-Newtonian fluid containing an internal cylinder," Numer. Heat Transf. Part B Fundam., vol. 77, no. 1, pp. 1–21, 2020, doi: 10.1080/10407790.2019.1685838.

[33] R. Zhang, S. Aghakhani, A. Hajatzadeh Pordanjani, S. M. Vahedi, A. Shahsavar, and M. Afrand, "Investigation of the entropy

generation during natural convection of Newtonian and non-Newtonian fluids inside the L-shaped cavity subjected to magnetic field: application of lattice Boltzmann method," Eur. Phys. J. Plus, vol. 135, no. 2, 2020, doi: 10.1140/epjp/s13360-020-00169-2.

[34] M. I. Khan, M. Nazeer, N. Shehzad, A. Saleem, and F. Ahmad, "Scrutiny of entropy optimized tangent hyperbolic fluid (non-Newtonian) through perturbation and numerical methods between heated plates," Adv. Mech. Eng., vol. 12, no. 12, pp. 1–12, 2020, doi: 10.1177/1687814020970772.

[35] F. H. Ali, H. K. Hamzah, K. Egab, M. Arıcı, and A. Shahsavar, "Non-Newtonian nanofluid natural convection in a U-shaped cavity under magnetic field," Int. J. Mech. Sci., vol. 186, p. 105887, 2020, doi: 10.1016/j.ijmecsci.2020.105887.

[36] S. O. Giwa, M. Sharifpur, and J. P. Meyer, "Experimental study of thermo-convection performance of hybrid nanofluids of Al2O3-MWCNT/water in a differentially heated square cavity," Int. J. Heat Mass Transf., vol. 148, no. xxxx, p. 119072, 2020, doi: 10.1016/j.ijheatmasstransfer.2019.119072.

[37] M. A. Hassan, M. Pathak, M. K. Khan, and N. H. Khan, "Natural convection of viscoplastic fluids in an enclosure with partially heated bottom wall," Int. J. Therm. Sci., vol. 158, no. March 2017, 2020, doi: 10.1016/j.ijthermalsci.2020.106527.

[38] S. Rostami, R. Ellahi, H. F. Oztop, and A. S. Goldanlou, "A study on the effect of magnetic field and the sinusoidal boundary condition on free convective heat transfer of non-Newtonian power-law fluid in a square enclosure with two constant-temperature obstacles using lattice Boltzmann method," J. Therm. Anal. Calorim.,

no. 0123456789, 2020, doi: 10.1007/s10973-020-10202-2.

[39] P. Ye, D. Li, Z. Yu, and H. Zhang, “Effects of a centered conducting body on natural convection of a non-newtonian fluid in a square enclosure with time-periodic temperature distribution,” Can. J. Phys., vol. 99, no. 2, pp. 55–69, 2021, doi: 10.1139/cjp-2019-0504.

[40] M. Shahabadi, S. A. M. Mehryan, M. Ghalambaz, and M. Ismael, “Controlling the natural convection of a non-Newtonian fluid using a flexible fin,” Appl. Math. Model., vol. 92, pp. 669–686, 2021, doi: 10.1016/j.apm.2020.11.029.

[41] M. R. Khadangi Mahrood, S. G. Etemad, and R. Bagheri, “Free convection heat transfer of non Newtonian nanofluids under constant heat flux condition,” *Int. Commun. Heat Mass Transf.*, vol. 38, no. 10, pp. 1449–1454, 2011, doi: 10.1016/j.icheatmasstransfer.2011.08.012.

[42] Maiti and Bidinger, “Heat transfer enhancement using hybrid nanoparticles in ethylene glycol through a horizontal heated tube,” *J. Chem. Inf. Model.*, vol. 53, no. 9, pp. 1689–1699, 1981.

[43] A. R. Rahmati, O. A. Akbari, A. Marzban, D. Toghraie, R. Karimi, and F. Pourfattah, “Simultaneous investigations the effects of non-Newtonian nanofluid flow in different volume fractions of solid nanoparticles with slip and no-slip boundary conditions,” *Therm. Sci. Eng. Prog.*, vol. 5, pp. 263–277, 2018, doi: 10.1016/j.tsep.2017.12.006.

[44] S. Ghanbari and K. Javaherdeh, “Investigation of applying nanoporous graphene non-Newtonian nanofluid on rheological properties and thermal performance in a turbulent annular flow with perforated baffles,” *J. Therm. Anal. Calorim.*, vol. 139, no. 1, pp. 629–647, 2020, doi: 10.1007/s10973-019-08389-0.

[45] I. D. Garbadeen, M. Sharifpur, J. M. Slabber, and J. P. Meyer, “Experimental study on natural convection of MWCNT-water nanofluids in a square enclosure,” *Int. Commun. Heat Mass Transf.*, vol. 88, pp. 1–8, 2017, doi: 10.1016/j.icheatmasstransfer.2017.07.019.

[46] M. Torki and N. Etesami, “Experimental investigation of natural convection heat transfer of SiO2/water nanofluid inside inclined enclosure,” *J. Therm. Anal. Calorim.*, vol. 139, no. 2, pp. 1565–1574, 2020, doi: 10.1007/s10973-019-08445-9.

[47] Administrration ,N.A.a.s. “Measurement Uncertainty Analysis principles and Methods ”Book ,July 2010, NASA- HDBK, washington,Dc.p.275.

[48] Bell, S., Abeginners guide to uncetainty of Measurement, 2001, National physical laboratory Teddington, Middlesex, U.K.

[49] M. Lamsaadi, M. Naïmi, and M. Hasnaoui, “Natural convection of non-Newtonian power law fluids in a shallow horizontal rectangular cavity uniformly heated from below,” Heat Mass Transf. und Stoffuebertragung, vol. 41, no. 3, pp. 239–249, 2005, doi: 10.1007/s00231-004-0530-8.

[50] Hussein , A. ," Entropy generation due to the transient mixed convection in a three- dimensional right-angle triangular cavity", International Journal of Mechanical Sciences ,Vol. 146–147, 2018 , pp. 141–151.

[51] Muhammad, N. M. A., Sidik, N. A. C., Saat, A., & Abdullahi, B. Effect of Nanofluids on Heat Transfer and Pressure Drop Characteristics of Diverging-Converging Minichannel heat sink. CFD Letters, 11, 105-120.

[52] L. Khezzar, D. Siginer, and I. Vinogradov, “Natural convection of power law fluids in inclined cavities,” Int. J. Therm. Sci., vol. 53, pp. 8–17, 2012, doi: 10.1016/j.ijthermalsci.2011.10.020.

[53] S. U. Ilyas, R. Pendyala, and M. Narahari, “An experimental study on the natural convection heat transfer in rectangular enclosure using functionalized alumina-thermal oil-based nanofluids,” Appl. Therm. Eng., vol. 127, pp. 765–775, 2017, doi: 10.1016/j.applthermaleng.2017.08.088.

[54] G. R. Kefayati, “Simulation of non-Newtonian molten polymer on natural convection in a sinusoidal heated cavity using FDLBM,” J. Mol. Liq., vol. 195, pp. 165–174, 2014, doi: 10.1016/j.molliq.2014.02.031.

APPENDIX

Appendix (A): table of temperature measurement

Table (A-1) Temperature measurement for case one : Cuboid obstacle, AR = 0.5

T(x, y, z)	Q=105.413 W T (^{o}C)	Q=220 W T (^{o}C)	Q=326.271 W T (^{o}C)	Q= 415.103 W T (^{o}C)	Q=435.423 W T (^{o}C)
T1	20.3	25.1	30.5	35.2	40.5
T2	19.2	24	23	31.1	35
T3	17	18.5	19.3	21.2	27.5
T4	19.9	25	30	35	40
T5	20	25.2	29.8	35.1	39.9
T6	20	25	30	34.9	39.3
T7	20	24.8	29.9	35	40
T8	19.2	23.9	29.1	33.9	37.5
T9	17.4	23	26	31.1	35.2
T10	16.9	21.7	23.3	25	28
T11	16.1	17.5	21.2	22	25
T12	18.9	22.1	25.4	32	32.5
T13	17.7	21	23.5	29.3	30.3
T14	17	19.3	22.2	24.1	26.8
T15	15	15.1	15.3	15.2	15.5
T16	19	23.3	27.1	31.6	36.3
T17	18	22.8	26	28.5	33.7
T18	17.5	22	22.3	25	27.5
T19	16.5	17.3	18.5	20.1	23
T20	18.2	21.9	26.4	25.7	34.8
T21	17.7	21.1	23.3	23.9	29.8
T22	17	20.8	21.1	22.2	27.4
T 23	13.9	13.1	13	12.5	12
T 24	16	16.8	17.5	17	17.8

Table (A-2) Temperature measurement for case one : Cuboid obstacle, AR = 0.75

T(x, y, z)	Q=105.413 W T (^{o}C)	Q=220 W T (^{o}C)	Q=326.271 W T (^{o}C)	Q= 415.103 W T (^{o}C)	Q=435.423 W T (^{o}C)
T 1	20.2	25.1	30.3	35.5	40.3
T2	18.3	22.6	28.3	30	32
T 3	15.1	16	16.2	16.7	18
T4	20.2	25	30	35	39.7
T5	20	25.1	29.2	35	39.7
T6	19.8	24.9	29.9	34.8	40
T7	20	24.8	30	35	40
T 8	19	21.3	26.6	31.8	36
T 9	17.9	19.1	24	27.5	30.2
T10	15.1	15.8	16.3	16.5	16.8
T12	18	23.2	26	28.4	32
T13	16.7	19.2	20.4	20.7	21.1
T14	15.2	15.3	15.4	15.8	16
T15	15	15	15.3	15.4	15.5
T16	18	21	28	30.3	36.5
T17	17	19.2	22	23.6	34.4
T18	15.1	15.4	15.6	16	16.3
T20	18.8	20.8	28	33.1	38
T21	17.2	18.1	20.6	27.1	28
T22	15	15.2	15.3	15.9	16
T23	13	13	12	11	10.3
T 24	16	16.3	16.5	16.7	17.3

Table (A-3) Temperature measurement for case one : cylindrical obstacle, AR = 0.5

T(x, y, z)	Q=105.413 W T (^{o}C)	Q=220 W T (^{o}C)	Q=326.271 W T (^{o}C)	Q= 415.103 W T (^{o}C)	Q=435.423 W T (^{o}C)
T1	20.1	25.1	31.4	35.3	41.5
T2	19.4	24.1	27.9	30.3	37.9
T3	18.9	19.3	26.5	29.1	32.4
T4	20	25	29.8	35	40
T5	19.7	24.9	30	34.9	40.1
T6	20.3	25	30.2	35	40
T7	20	24.8	30	34.8	40.1
T8	19.5	23.9	29.5	31.2	37
T9	19.1	23	26.7	28.3	36.5
T10	18.3	21.7	24.6	26.1	30.5
T11	15.7	17.5	23	24.7	25.9
T12	19.1	20.1	20.9	21	22.4
T13	19	20.3	20.5	20.7	21.7
T14	16.9	19.3	19.4	20	20.8
T15	15	15	15.2	15.1	15.3
T16	19.7	23.3	28.8	32.2	37.6
T17	19.6	22.8	26.2	29.1	36
T18	18.7	22	24.8	26.5	30
T19	17.5	17.3	23.1	20.6	26
T20	18.1	21.9	22	22.7	23.7
T21	17.4	21.1	21.5	21.8	22.2
T22	16.5	18.8	19.9	20	20.5
T 23	13.6	13.1	12.7	12.3	11.8
T 24	16	16.8	17.1	17.3	17.6

Table (A-4) Temperature measurement for case one : cylindrical obstacle, AR = 0.75

T(x, y, z)	Q=105.413 W T (^{o}C)	Q=220 W T (^{o}C)	Q=326.271 W T (^{o}C)	Q= 415.103 W T (^{o}C)	Q=435.423 W T (^{o}C)
T 1	20.1	25.4	30.4	35.5	41.6
T2	19.3	23.3	27	30	35.9
T 3	18.2	21	21.5	21.9	22.3
T4	20.5	25.1	30.8	35	40
T5	20.3	24.9	30	35	40.5
T6	19.7	24.9	30.2	35	40
T7	20	25	30	34.8	40.1
T 8	19.5	23.9	29	31.8	37.9
T 9	19.2	21.2	26.5	27.5	33.8
T10	17.4	18	18.4	18.5	19.9
T12	19.1	20.8	24.9	28.4	31.4
T13	18.7	18.9	19.5	20.7	24.7
T14	16	16.2	16.5	16.8	17
T15	15	15	15	15.4	15.3
T16	19.7	22.8	28.1	31.3	37.6
T17	19.5	21.7	26.2	27.6	35
T18	16.3	17	17.3	17	17.5
T20	18.1	19.1	21.9	23.7	33.1
T21	17	18.7	20.8	22.2	27.1
T22	16.2	16.7	16.9	16.9	17
T23	13.6	13	12.7	11	12
T 24	15.8	16.6	17.6	16.7	17.9

Table (A-5) Temperature measurement for case (2) : cuboid obstacle, AR = 0.5

T(x, y, z)	Q=105.413 W T (^{o}C)	Q=220 W T (^{o}C)	Q=326.271 W T (^{o}C)	Q= 415.103 W T (^{o}C)	Q=435.423 W T (^{o}C)
T1	20.5	25.4	30.7	35.2	40.7
T2	17	22.1	23.5	31.1	31.6
T3	16.9	19	20.8	21.2	26
T4	20.1	25.1	29.9	35	40.2
T5	19.5	24.9	30	35.1	39.7
T6	20.5	24.9	29.5	34.9	40
T7	20	25	30.1	35	40
T8	17.4	23.9	26.4	33.9	36.5
T9	17.1	21.2	24.3	31.1	33
T10	16.6	18	22.8	25	27
T11	16	16.8	17.3	17.8	19.6
T12	17.5	18.9	25.6	32	32.2
T13	17.2	18.2	24	28.7	29.3
T14	16	17	22	24.1	25
T15	15	15.3	15.2	15.5	15.8
T16	18.2	21.7	25.9	31.6	35.7
T17	17.8	18	23.1	28.5	31.9
T18	17	17.9	20	25	25.3
T19	16	16.7	17	20.1	22.5
T20	17.4	22.7	27.9	25.7	35.9
T21	17.2	20.6	24.7	23.9	32.9
T22	17	18.1	22.2	22.9	24.4
T 23	13.1	12	12.5	12.1	10.1
T 24	16.7	17	17.3	17.5	17

Table (A-6) Temperature measurement for case (2) : cylindrical obstacle , AR = 0.5

T(x, y, z)	Q=105.413 W T (^{o}C)	Q=220 W T (^{o}C)	Q=326.271 W T (^{o}C)	Q= 415.103 W T (^{o}C)	Q=435.423 W T (^{o}C)
T1	20.5	25.1	31.1	35.3	41.8
T2	19.2	24	27.8	30.3	35.5
T3	18.8	19.5	26	29.1	31
T4	20.3	25	30.1	34.9	40.3
T5	20.1	25	29.7	35	40
T6	19.7	25	30.5	35	40.1
T7	20	24.8	30	34.8	39.8
T8	19.2	23.9	28.4	31.2	36.8
T9	19	23	26.5	28.3	35.2
T10	18	21.7	24	26.1	30.3
T11	15.8	17.5	22.8	24.7	25.7
T12	20.3	22.1	24	24.5	25.9
T13	18.9	20	20.5	21.7	23
T14	17.9	18.3	19.3	20	20.7
T15	15	15.1	15.3	15.1	15.2
T16	19.6	23.3	27.5	32.2	37.2
T17	19	22.8	25.8	29.1	35.8
T18	18.5	22	23.7	26.5	29.5
T19	17.3	17.3	22.7	23.6	25.9
T20	18.5	18.9	19.8	20.7	22.5
T21	18.2	18.1	19.5	19.8	21.9
T22	17	17.8	19	19.3	20
T 23	13.5	12.1	11.6	11.3	10.8
T 24	19.8	16.8	18	18.3	18.7

Table (A-7) Temperature measurement for case (2) : cuboid obstacle, AR = 0.75

T(x, y, z)	Q=105.413 W T (^{o}C)	Q=220 W T (^{o}C)	Q=326.271 W T (^{o}C)	Q= 415.103 W T (^{o}C)	Q=435.423 W T (^{o}C)
T 1	20.6	25.3	30.1	35	40
T2	17.1	23.3	27.7	31.7	30.1
T 3	15.3	19.7	20.9	21	21.5
T4	20.1	25.1	30.5	35.1	40.2
T5	20.3	24.9	29.8	34.9	39.9
T6	20	24.9	30	35	39.4
T7	20	25	30	35	39.1
T 8	17	23.9	25.8	30.7	34.8
T 9	16.7	21.2	22.2	24.5	29
T10	15	16	16.5	16.7	169
T12	17	20.8	22.7	26.7	30.6
T13	16.8	18.9	20.9	21.3	22.4
T14	15.1	15.5	15.7	15.9	16
T15	15	15	15.1	15.1	15.5
T16	17.8	22.8	26	30.1	36
T17	16.9	18.7	19.4	27.8	34.3
T18	15	15.3	15.7	16	16.1
T20	17.4	19.1	22.6	25	32
T21	16.3	18.7	20.4	21	22.7
T22	15	15.4	15.5	15.7	16
T23	13.9	13.5	14	13	12
T 24	16.6	16.9	17.5	17.9	17.8

Table (A-8) Temperature measurement for case (2) : cylinder obstacle , AR = 0.75

T(x, y, z)	Q=105.413 W T (^{o}C)	Q=220 W T (^{o}C)	Q=326.271 W T (^{o}C)	Q= 415.103 W T (^{o}C)	Q=435.423 W T (^{o}C)
T 1	21	25.1	30.1	35.5	40.5
T2	19.2	24.1	26.8	30	35.5
T 3	17.8	18.3	19.2	19.7	20.5
T4	20.3	25	30.1	35	40.3
T5	20.5	24.9	30	35	40
T6	19.9	25	30	34.8	40.1
T7	20.5	24.8	30	35	39.8
T 8	19.2	23.9	27.4	31.8	37.8
T 9	19	23	25.5	27.5	33.2
T10	16.2	16.7	17	17.5	17.6
T12	19.3	21.5	25	28.4	28.9
T13	18.5	20.1	22	24.7	25.2
T14	15.3	15.8	16	16.1	16.2
T15	15	15	15.2	15.4	15.4
T16	19.6	23.7	27.5	30.3	37.2
T17	18.8	22.3	25.4	23.6	34.7
T18	16	16.3	16.5	16.9	17
T20	17.8	18	19.7	33.1	20.8
T21	16.2	17.2	18.5	18.8	18.9
T22	15.3	15.5	15.5	15.9	16
T23	11.5	11.1	11	10.5	10
T 24	16.8	17.8	16.6	18.7	19

Table (A-9) Temperature measurement for case (3): cuboid obstacle , AR = 0.5

T(x, y, z)	Q=105.413 W T (^{o}C)	Q=220 W T (^{o}C)	Q=326.271 W T (^{o}C)	Q= 415.103 W T (^{o}C)	Q=435.423 W T (^{o}C)
T1	20	25.1	30.4	35.3	40.9
T2	19.4	24	25	30.3	36.8
T3	17.3	19.5	22	29.1	29
T4	20.1	25	29.5	35	39
T5	19.5	25	30.1	34.9	40.1
T6	20	25	30	35	39.5
T7	20	24.8	29.9	34.8	40
T8	19.5	23.9	29.4	31.2	39
T9	19.6	23	28.1	28.7	36.6
T10	18	21.7	24.7	26.2	29
T11	17.7	17.5	22	24.7	26
T12	19.6	22.1	28	29	37
T13	17.5	20	25	26.7	31
T14	17.5	18.3	22	23.1	27
T15	15	15.1	15.5	15.1	15.7
T16	19.6	23.3	29	32.2	36.5
T17	19.2	22.8	28	29.1	34
T18	18.5	22	25.3	26.5	30.6
T19	16.9	17.3	21.2	22.6	24
T20	19.8	21.2	29	30.7	38
T21	18.5	18.7	25	27.8	32
T22	17.6	17.8	23	25	27
T 23	13	12.1	11.7	11	10
T 24	16.5	16.9	16.5	17	17.3

Table (A-10) Temperature measurement for case (3): cuboid obstacle, AR = 0.75

T(x, y, z)	Q=105.413 W T (^{o}C)	Q=220 W T (^{o}C)	Q=326.271 W T (^{o}C)	Q= 415.103 W T (^{o}C)	Q=435.423 W T (^{o}C)
T 1	20.6	25.3	30.8	35.5	40.9
T2	18.7	23.3	29.7	30	32.5
T 3	15.1	19.7	16	21.9	17
T4	20.5	25.1	30	35	40.2
T5	20	24.9	29.8	35	40
T6	20	24.9	30.1	35	39.2
T7	19.7	25	30	34.8	40
T 8	18.5	23.9	29	31.8	38
T 9	17.7	21.2	25.5	27.5	31.8
T10	15	15.5	15.9	16	16.5
T12	19	20.8	26	28.4	34
T13	16.6	18.9	20	20.7	24
T14	15.1	15.3	15.5	15.8	16
T15	15	15.1	15.2	15.4	15.7
T16	19.5	22.8	29	31.3	37.5
T17	18	18.7	30.3	27.6	35
T18	15	15.3	15.9	17	16.4
T20	19.2	20.5	28	23.7	36
T21	17.5	18.7	22	22.2	27
T22	15	15.4	16	16.2	16.9
T23	14.1	13.5	12.1	11	10.1
T 24	16	16.9	17.4	17.7	17.8

Table (A-11) Temperature measurement for case (2) : cylindrical obstacle , AR = 0.5

T(x, y, z)	Q=105.413 W T (^{o}C)	Q=220 W T (^{o}C)	Q=326.271 W T (^{o}C)	Q= 415.103 W T (^{o}C)	Q=435.423 W T (^{o}C)
T1	20.6	25.4	31.4	35.2	40.5
T2	19.9	22.1	28	31.1	38
T3	19	19	27	21.2	33
T4	20.1	25.1	29.9	35	40
T5	12.5	24.9	30.1	35.1	40.1
T6	20.3	24.9	30	34.9	39.9
T7	20	25	29.9	35	40.3
T8	19.6	23.9	29.8	33.9	38
T9	19.3	21.2	27	31.1	36.7
T10	18.4	18	25	26.4	30.7
T11	15.5	16.8	23.4	23.9	26
T12	18.6	20.9	25	32	33.7
T13	18.5	19.2	23.9	29.3	30.2
T14	17.5	18	22	24.1	25
T15	15	15.1	15.4	15.2	15.3
T16	19.8	21.7	28.9	31.6	38.3
T17	19.5	20.3	26.5	28.5	36.5
T18	18.9	19.2	25.3	26	30.1
T19	18	18.7	23.2	24.1	26.5
T20	18	18.7	19.6	25.7	28.8
T21	17	17.6	19	23.9	25
T22	16.6	17.1	17.3	22.2	22
T 23	13.5	12	12.3	11.5	10
T 24	16.8	17.3	18.7	18	18

Table (A-12) Temperature measurement for case (3) : cylinder obstacle, AR = 0.75

T(x, y, z)	Q=105.413 W T (^{o}C)	Q=220 W T (^{o}C)	Q=326.271 W T (^{o}C)	Q= 415.103 W T (^{o}C)	Q=435.423 W T (^{o}C)
T1	21.6	25.3	31.5	35.5	40.5
T2	19.5	23.3	27.9	30	36.8
T3	18.3	19.7	22.8	23.9	24.5
T4	20.5	25.1	30.5	35	40
T5	20.5	24.9	30.1	35	40.1
T6	20	24.9	30	35	39.9
T7	20	25	30.9	34.8	40.3
T8	19.7	23.9	29.4	31.8	38
T9	19.4	21.2	28.3	29.5	34.3
T10	17	17.5	17.7	18.5	18.9
T12	19.6	20.8	25	28.4	31.7
T13	18.9	18.9	23.9	20.7	29.2
T14	15.3	15.5	16	16.2	16.5
T15	15	15	15.5	15.4	15.7
T16	19.7	22.8	28.9	31.3	38.3
T17	19.7	21.7	27	27.6	35.5
T18	16.5	17.1	17.4	17.6	17.4
T20	18.3	19.1	19.6	23.7	28.8
T21	17.4	18.7	19	22.2	25
T22	16	16.2	16.3	16.7	16
T 23	13.6	13.3	13	11	10.5
T24	16.8	16.9	17.7	17.7	18

Appendix (B): tables of calculated values from the experimental analysis

Table (B-1) calculated values for case one : cylindrical obstacle

a- AR = 0.5

Q (W)	h (W/m^2.K)	Pr	Ra	Nu
105.413	109.291	213.72	2.33E+06	46.839
220.00	113.84		4.65E+06	48.79
326.27	117.73		6.98E+06	50.457
415.103	120.912		9.31E+06	51.819
435.42	125.695		1.16E+07	53.869

b- AR = 0.75

Q (W)	h (W/m^2.K)	Pr	Ra	Nu
105.413	95	213.72	86177	13.5782
220.00	94.673		1.72E+05	13.5248
326.27	193.7		2.59E+05	27.6761
415.103	200.745		3.45E+05	28.6779
435.42	214.149		4.31E+05	30.5928

Table (B-2) calculated values for case one : cuboid obstacle

a- AR = 0.5

Q (W)	h (W/m^2.K)	Pr	Ra	Nu
105.413	72.12	213.72	2.33E+06	30.91
220.00	79		4.65E+06	33.86
326.27	87.145		6.98E+06	37.347
415.103	76.42		9.31E+06	32.75
435.42	94.316		1.16E+07	40.42

b- AR = 0.75

Q (W)	h (W/m^2.K)	Pr	Ra	Nu
105.413	61	213.72	86177	8.714
220.00	60.768		1.72E+05	8.68
326.27	124.34		2.59E+05	17.763
415.103	128.84		3.45E+05	18.41
435.42	137.445		4.31E+05	19.635

Table (B-3) calculated values for case two : cuboid obstacle

a- AR = 0.5

Q (W)	h (W/m^2.K)	Pr	Ra	Nu
105.413	49	367.26	3.32E+07	29.752
220.00	48.25		6.63E+07	29.115
326.27	55.296		9.95E+07	33.07
415.103	61.33		1.33E+08	36.291
435.42	74.5		1.66E+08	43.4

b- AR = 0.75

Q (W)	h (W/m^2.K)	Pr	Ra	Nu
105.413	57.6	367.26	1.23E+06	11.63
220.00	57.36		2.46E+06	11.525
326.27	68.15		3.68E+06	13.559
415.103	68.26		4.91E+06	13.468
435.42	68.72		6.14E+06	13.4

Table (B-4) calculated values for case two : cylindrical obstacle

a- AR = 0.5

Q (W)	h (W/m^2.K)	Pr	Ra	Nu
105.413	103.46	367.26	3.32E+07	62.44
220.00	107.7		6.63E+07	64.4
326.27	110.68		9.95E+07	65.428
415.103	113.6		1.33E+08	66.554
435.42	134.9		1.66E+08	77.928

b- AR = 0.75

Q (W)	h (W/m^2.K)	Pr	Ra	Nu
105.413	89.73	367.26	1.23E+06	18.126
220.00	89.376		2.46E+06	17.957
326.27	106.19		3.68E+06	21.126
415.103	110		4.91E+06	21.69
435.42	107		6.14E+06	20.89

Table (B-5) calculated values for case three : cuboid obstacle

a- AR = 0.5

Q (W)	h (W/m^2.K)	Pr	Ra	Nu
105.413	111.76	6.81	2.36E+08	28.339
220.00	112		4.71E+08	28.07
326.27	113.85		7.07E+08	28.276
415.103	118		9.43E+08	29.08
435.42	116.29		9.76E+08	28.255

b- AR = 0.75

Q (W)	h (W/m^2.K)	Pr	Ra	Nu
105.413	115.99	6.81	8.73E+06	9.8
220.00	126.483		1.75E+07	10.573
326.27	177.63		2.62E+07	14.66
415.103	173.886		3.49E+07	14.194
435.42	170.09		4.36E+07	13.73

Table (B-6) calculated values for case three: cylindrical obstacle

a- AR = 0.5

Q (W)	h (W/m^2.K)	Pr	Ra	Nu
105.413	114.959	6.81	2.36E+08	29.1206
220.00	119.746		4.71E+08	30.0303
326.27	133.431		7.07E+08	33.1038
415.103	137.035		9.43E+08	33.6206
435.42	142.455		9.76E+08	34.4717

b- AR = 0.75

Q (W)	h (W/m^2.K)	Pr	Ra	Nu
105.413	180.724	6.81	8.73E+06	15.276
220.00	180.013		1.75E+07	15.059
326.27	276.761		2.62E+07	22.844
415.103	286.779		3.49E+07	23.398
435.42	278.958		4.36E+07	22.52

Appendix (C): Tables of standard temperature uncertainty results

Table (C-1) When the enclosure has filled carboxy methyl cellulose CMC 1%.

a- rectangular obstacle,AR=0.75

Description	S.D value	Description	S.D value
T1	0.346	T13	0.095
T2	0.23	T14	0.075
T3	0.12	T15	0.121
T4	0.161	T16	0.2
T5	0.135	T17	0.15
T6	0.147	T18	0.21
T7	0.073	T19	0.296
T8	0.152	T20	0.231
T9	0.115	T21	0.175
T10	0.233	T22	0.186
T11	0.26	T23	0.427
T12	0.18	T24	0.23

b- cylindrical obstacle, AR=O.75

Description	S.D value	Description	S.D value
T1	0.28	T13	0.115
T2	0.15	T14	0.14
T3	0.21	T15	0.176
T4	0.296	T16	0.145
T5	0.231	T17	0.147
T6	0.147	T18	0.09
T7	0.152	T19	0.152
T8	0.21	T20	0.115
T9	0.233	T21	0.233
T10	0.26	T22	0.346
T11	0.12	T23	0.115
T12	0.346	T24	0.14

c- cylindrical obstacle, AR=0.5

Description	S.D value	Description	S.D value
T1	0.115	T13	0.185
T2	0.273	T14	0.075
T3	0.26	T15	0.121
T4	0.12	T16	0.2
T5	0.36	T17	0.15
T6	0.147	T18	0.21
T7	0.08	T19	0.296
T8	0.152	T20	0.231
T9	0.145	T21	0.145
T10	0.233	T22	0.178
T11	0.26	T23	0.317
T12	0.12	T24	0.288

Table (C-2) When the enclosure filled carboxy methyl cellulose CMC 0.5%.

a- rectangular obstacle, AR=0.5

Description	S.D value	Description	S.D value
T1	0.346	T13	0.095
T2	0.23	T14	0.075
T3	0.12	T15	0.121
T4	0.161	T16	0.2
T5	0.135	T17	0.15
T6	0.147	T18	0.21
T7	0.073	T19	0.296
T8	0.152	T20	0.231
T9	0.115	T21	0.175
T10	0.233	T22	0.186
T11	0.26	T23	0.427
T12	0.18	T24	0.23

b- cylindrical obstacle, AR=0.5

Description	S.D value		
T1	0.28	T13	0.115
T2	0.15	T14	0.14
T3	0.21	T15	0.176
T4	0.296	T16	0.145
T5	0.231	T17	0.147
T6	0.147	T18	0.09
T7	0.152	T19	0.152
T8	0.21	T20	0.115
T9	0.233	T21	0.233
T10	0.26	T22	0.346
T11	0.12	T23	0.115
T12	0.346	T24	0.14

c- rectangular obstacle, AR=0.75

Description	S.D value		
T1	0.115	T13	0.185
T2	0.273	T14	0.075
T3	0.26	T15	0.121
T4	0.12	T16	0.2
T5	0.36	T17	0.15
T6	0.147	T18	0.21
T7	0.08	T19	0.296
T8	0.152	T20	0.231
T9	0.145	T21	0.145
T10	0.233	T22	0.178
T11	0.26	T23	0.317
T12	0.12	T24	0.288

d- ***cylindrical obstacle, AR=O.75***

Description	S.D value	Description	S.D value
T1	0.346	T13	0.095
T2	0.23	T14	0.075
T3	0.12	T15	0.121
T4	0.161	T16	0.2
T5	0.135	T17	0.15
T6	0.147	T18	0.21
T7	0.073	T19	0.296
T8	0.152	T20	0.231
T9	0.115	T21	0.175
T10	0.233	T22	0.186
T11	0.26	T23	0.427
T12	0.18	T24	0.23

Table (C-3) When the enclosure is filled with water

a- rectangular obstacle, AR=0.5

Description	S.D value		
T1	0.346	T13	0.095
T2	0.23	T14	0.075
T3	0.12	T15	0.121
T4	0.161	T16	0.2
T5	0.135	T17	0.15
T6	0.147	T18	0.21
T7	0.073	T19	0.296
T8	0.152	T20	0.231
T9	0.115	T21	0.175
T10	0.233	T22	0.186
T11	0.26	T23	0.427
T12	0.18	T24	0.23

b- cylindrical obstacle, AR=0.5

Description	**S.D value**	Description	S.D value
T1	0.28	T13	0.115
T2	0.15	T14	0.14
T3	0.21	T15	0.176
T4	0.296	T16	0.145
T5	0.231	T17	0.147
T6	0.147	T18	0.09
T7	0.152	T19	0.152
T8	0.21	T20	0.115
T9	0.233	T21	0.233
T10	0.26	T22	0.346
T11	0.12	T23	0.115
T12	0.346	T24	0.14

c- rectangular obstacle, AR=0.75

Description	**S.D value**	Description	S.D value
T1	0.3	T13	0.302
T2	0.19	T14	0.17
T3	0.11	T15	0.139
T4	0.179	T16	0.155
T5	0.253	T17	0.24
T6	0.14	T18	0.07
T7	0.09	T19	0.25
T8	0.71	T20	0.231
T9	0.31	T21	0.22
T10	0.096	T22	0.307
T11	0.18	T23	0.139
T12	0.41	T24	0.167

d- ***cylindrical obstacle, AR=O.75***

Description	**S.D value**	Description	S.D value
T1	0.115	T13	0.185
T2	0.273	T14	0.075
T3	0.26	T15	0.121
T4	0.12	T16	0.2
T5	0.36	T17	0.15
T6	0.147	T18	0.21
T7	0.08	T19	0.296
T8	0.152	T20	0.231
T9	0.145	T21	0.145
T10	0.233	T22	0.178
T11	0.26	T23	0.317
T12	0.12	T24	0.288

الملخص

في العمل الحالي ، تم دراسة انتقال الحرارة بالحمل الحراري الطبيعي عدديا" وتجريبيا" في حاوية مستطيلة تحتوي على عائق ساخن مثبت في قاعدتها ومملوئة بسائل غير نيوتوني.

تم استخدام كربوكسي ميثيل سلولوز CMC مع الماء المقطر كسائل غير نيوتوني بثلاث تراكيز[1٪ ، 0.5٪ ، و 0٪]. قيم مؤشر قانون القوة للتراكيز الثلاثة هي 0.5 ، 0.72 ، و 1 على التوالي. وقد تم استخدام قيمتين لنسب العرض إلى الارتفاع (AR) وهما 0.5 و0.75. كذلك تم استخدام شكلين للعائق الساخن أسطواني ومتوازي المستطيلات. وفي هذه الدراسة قيمة رقم رايلي للسائل الأساسي عند AR تساوي 0.75 هي $8.73E + 06 \leq Ra \leq 4.36E + 07$. وعندما تكون قيمة AR =0.5 يكون $2.36E + 08 \leq Ra \leq 9.76E + 08$.اضافة لذلك لقد استخدم 24 مزدوجًا حراريًا لقياس درجة حرارة سائل العمل داخل العلبة وضعت في أماكن مختلفة عند او قرب الجدران الساخنة والباردة للحاوية وعند قيمتي AR.

تم تمثيل العمل النظري باستخدام برنامج CFD COMSOL ثلاثي الأبعاد للتنبؤ بتوزيع درجة حرارة السائل داخل العلبة.

تم تحليل درجة الحرارة المقاسة من العمل التجريبي لحساب Ra ، h وكذلك Nu . وقد ظهرت زيادة في قيمة رقم Nu مع زيادة تركيز CMC ورقم Ra الذي يتأثر بخصائص المائع ودرجة حرارة العائق الساخن وكذلك نسبة العرض إلى الارتفاع. كما ان رقم نسلت (Nu) يتحسن من 40.46٪ عند (n=1) إلى 50.79٪ عند (n=0.59) وهذا يدل على أن انتقال الحرارة يتحسن بتخفيض قيمة مؤشر قانون القوة للسائل غير النيوتوني. كما لوحظ أن رقم Nu يتأثر بشكل العائق.

توافق العمل التجريبي بشكل جيد مع العمل النظري بمتوسط انحراف حوالي 8.9٪.

جمهورية العراق
وزارة التعليم العالي والبحث العلمي
جامعة بابل / كلية الهندسة
قسم الهندسة الميكانيكية

انتقال الحرارة بالحمل الحر لسائل غيرنيوتوني داخل حاوية تحتوي على عائق ساخن

رسالة

مقدمة لكلية الهندسة جامعة بابل استيفاء جزئي لمتطلبات درجة الماجستير في الهندسة \ الهندسة الميكانيكية \ قدرة

أعدت من قبل
زينب مهدي عاكول حسن

بأشراف

أ.م. د. رفل حكمت حميد

1442 هـ ***2021 م***